# Improving the Numerical Accuracy of Models of Sector-shaped and Cross-bonded Cable Systems

By

Anuradha Kariyawasam Kapuge Kariyawasam Mudalige

A thesis submitted to the Faculty of Graduate Studies of
The University of Manitoba
in partial fulfilment of the requirements for the degree of

Doctor of Philosophy

Department of Electrical and Computer Engineering
Faculty of Engineering
University of Manitoba
Winnipeg, MB, Canada

## Abstract

This thesis introduces a comprehensive methodology to improve electromagnetic transient (EMT) modelling of power cables systems. Several improved modelling and validation techniques are proposed at the parameter estimation, time domain simulation and validation stages of the EMT modelling of transmission lines.

A novel approach is developed to model sector-shaped cables in electromagnetic transient type programs. First, the applicability of elemental sub-conductor technique is extended to accurately calculate the frequency dependent impedances of sector-shaped cables. The derived admittance and propagation characteristics of the sector-shaped cable are fitted with rational functions using the method of vector fitting in an EMT-type program. The time domain simulations are validated with the numerical inverse Laplace transform method.

A novel frequency domain approach is presented to model cascaded transmission systems. The procedure is based on obtaining four composite propagation functions representing the cascaded system. The performance of the technique does not diminish with increased number of cascaded segments and it preserves the intrinsic details of each line segment. This method is capable of modelling cascaded overhead lines or cables with different

characteristic admittances and line lengths. This method can be used to validate EMT models of cascaded transmission systems.

An improved generalized transmission line model is introduced which is capable of accommodating time steps greater than the travel time of the line. The time step of the conventional EMT models of transmission lines is constrained by the smallest travel time of the line. When the high frequency transients at the line terminations are not of interest, inaccurate nominal $\pi$ equivalents are used with large time steps to reduce the computational burden. The proposed model not only is more accurate than the $\pi$ equivalents, but also degenerates to the conventional frequency dependent EMT model when used with time steps smaller than the travel time. Therefore, the proposed model is highly convenient as it can be used for all types of EMT simulations without resorting to nominal $\pi$ equivalents when the large simulation time steps must be used to reduce computational burden.

# Acknowledgments

I would like to extend my sincere gratitude to Dr. Aniruddha Gole for his continuous encouragement, guidance and valuable suggestions. I consider myself privileged to have had the opportunity to work under his supervision. I would also like to thank the advisory committee members for their comments and feedbacks throughout the course of this work.

I would like to express my sincere thanks to Dr. Jeewantha De Silva for his immense support and feedback given to me in understanding and developing transmission line models. Also, I owe my gratitude to Dr. Shengtao Fan for his invaluable support in my work.

The financial support received from the Natural Science and Engineering Research Council (NSERC) and the University of Manitoba is greatly appreciated. I would like to thankfully remind the staff and all of my friends in the Department of Electrical and Computer Engineering for their continuous encouragement and pleasant company throughout the years at the university.

This acknowledgement will not be complete without thanking my family. I extend my gratitude to my parents, and my brother. Finally, I would like to thank my wife, Chathuri for her patience, love and support during the hard times.

# Contents

# List of Tables

# List of Figures

# List of Principle Symbols

| | |
|---|---|
| $Z$ | Series impedance (matrix) |
| $Y$ | Shunt admittance (matrix) |
| $\omega$ | Angular Frequency (rad/s) |
| $f$ | Frequency (Hz) |
| $Z_c$ | Characteristic impedance (matrix) |
| $Y_c$ | Characteristic admittance (matrix) |
| $A$ | Propagation function (matrix) |
| $\gamma$ | Propagation constant |
| $\alpha$ | Attenuation coefficient |
| $\beta$ | Phase coefficient |
| $E_I$ | Eigen vector matrix of $Y.Z$ |
| * | Convolution |
| $\delta(t)$ | Unit impulse function |
| $\tau$ | Transmission time delay |
| $\mu$ | Permeability of a vacuum |
| $\rho$ | Resistivity |
| $d_e$ | Complex depth of penetration |
| $\Delta t$ | Simulation time step |

# List of Acronyms

| | |
|---|---|
| EMT | Electro-Magnetic Transient |
| FEM | Finite Element Method |
| FD | Frequency Domain |
| GMD | Geometric Mean Distance |
| IFFT | Inverse Fast Fourier Transform |
| MTL | Multi-conductor Transmission Line |
| NILT | Numerical Inverse Laplace Transform |
| TD | Time Domain |
| TEM | Transverse Electro-Magnetic |
| TL | Transmission Line |

# Chapter 1

# Introduction

## 1.1 Background

Transmission Line (TL) in general is a structure that guides electro-magnetic wave from one point to another [1]. With regard to power systems, there are two main categories of transmission lines, overhead power transmission lines and underground power transmission cables. In this thesis, the term "transmission line" will refer to both types of structures. Accurate models of these transmission lines are essential in the analysis of Electro-Magnetic Transients (EMT) in power systems. EMT models of transmission lines range from constant line parameter models (such as the Bergeron Model) to highly detailed frequency dependent models. Constant parameter models are accurate in the vicinity of a base frequency at which the parameters are calculated, while frequency dependent models maintain accuracy within a far broader range of frequencies.

Developing an accurate EMT model of a transmission line consists of three main steps. The first step is to calculate transmission line parameter matrices (resistances, inductances and capacitances) per unit length, depending on the geometry and the inherent properties such as resistivity, permeability, etc. Transmission line parameters are calculated at a single or multiple frequencies depending on the type of the model. Overhead transmission lines have been studied for many years and there are many EMT models available in literature [2][3][4]. Although underground cables have been widely used for more than half a century, accurate EMT models are available only for the most common and simple types of cables [5], [6] due to mainly, the difficulty of obtaining frequency dependent parameters for complex conductor shapes.

The second step of transmission line modelling is to obtain a time domain model using the frequency domain information. In all frequency dependent transmission line models, this step involves curve fitting of frequency domain information and transforming to a time domain model [7]. Transmission lines comprise of inherent time delays (governed by the speed of propagation of electromagnetic waves) which influences passing information from one end to the other. All conventional distributed parameter transmission line models consider these transmission delays. Simulation time-step used in the EMT study is constrained by the minimum delay of all the transmission lines in the study system [8]. This restriction introduces additional computational

burdens to the simulation, particularly, in the presence of short transmission lines.

Third and final step is the proper validation of transmission line model. In general, errors in transmission line models can occur at frequency domain parameter estimation and while transforming it to the time domain [9]. Therefore, cable models should be validated in both frequency domain and time domain. In general, frequency domain solutions are highly accurate and errors occur mostly at the curve fitting stage. These errors can be particularly high in the case of cascaded transmission systems such as transposed overhead lines and cross-bonded cables.

## 1.2 Motivation behind the research

Underground cables are increasingly being preferred instead of overhead lines in many countries due to both environmental and political pressures. Therefore, there is an increasing need for accurate models of these in power system analysis programs. Accurate representation of underground cables in EMT programs plays a major role in determining accurate transient behavior of modern power systems. Proper EMT modelling of non-conventional, yet commonly used cable types such as sector-shaped cables is hardly reported hitherto in literature. Similarly, underground cable cross-bonding is a common practice, yet the EMT modelling and validation of such cables is not

investigated sufficiently. Representation of overhead lines and cables in an EMT program confines the simulation time step to less than the smallest propagation delay. This imposes huge computational burden on the simulation, especially with short transmission lines.

These aforementioned factors have motivated this research to develop techniques to improve the accuracy of EMT modelling and validation of power cable systems.

## 1.3 Objective and the contributions of the research

The principle objective of this research is to propose accuracy improvements in EMT modelling and validation of power cable systems. This overall research goal is achieved with the following major contributions:

- Development and validation of an accurate technique to obtain frequency dependent parameters of sector-shaped cables
- Development of an accurate model of sector shaped cables suitable for EMT simulations
- Development of a detailed and an accurate frequency domain model for cascaded transmission systems capable of validating EMT models
- Propose a generalized transmission line model capable of handling large time steps (greater than the travel time of the line)

- Application of the generalized transmission line model to various EMT examples to demonstrate its applicability

## 1.4 Overview of the Thesis

This thesis consists of six chapters. Chapter 2 explains the findings of the literature survey on EMT modelling of overhead lines and underground cables. Chapter 3 describes the steps of the proposed modelling procedure of sector-shaped cables in EMT programs. Chapter 4 introduces a novel technique to model cascaded transmission lines or underground cables in the frequency domain, which can be used to verify EMT simulations. Chapter 5 details the proposed generalized transmission line model capable of accommodating simulation time steps greater than the travel time of the line. Finally, Chapter 6 discusses the conclusions and future direction of the research.

# Chapter 2

# Aspects of Transmission Line Modelling

## 2.1 Introduction

In this chapter, the basic theory of transmission line modelling and different models of transmission lines found in literature will be discussed. First, single-conductor transmission line modelling in frequency domain will be discussed and then it will be extended to the multi-conductor case. Frequency domain line parameter calculation methods will be discussed for different transmission lines and the time domain solution obtained directly via frequency response is discussed later in the chapter.

## 2.2 Historical advancements in EMT models of transmission lines

Initial theoretical basis for transient analysis of transmission lines dates back to late 1920s to early 1930s period where formulae for conductor internal impedance [10] and earth-return impedance [11], [12] (Carson's and Pollaczek's equations) were developed. This was followed by the development

of travelling wave theory [13] and lumped parameter models [14] in the early 1950s.

In 1960s, already established theory of travelling wave solution was implemented in computer simulations [15], [16] with the emergence of the digital computer. Implementation of the lossless transmission line in an EMT program as shown in Figure 2-1 was a crucial milestone in TL modelling [15]. Line losses were represented by the lumping them at both ends and the middle of the line.

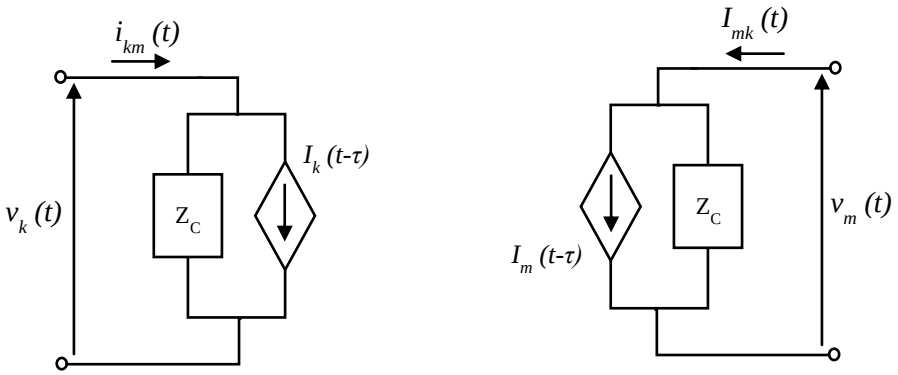


**Figure 2-1 – Constant parameter EMT model of lossless transmission line**

The Numerical Fourier Transform [17] and Fast Fourier Transform [18] were applied in the transmission line simulations in 1970s which vastly improved the accuracy and efficiency of computer simulations. Another important contribution in this era was the Wedepohl's impedance formulae for overhead lines and cables [19], [20]. One of the main advancements in 1980s and 1990s was the development of modal domain techniques [6], [21], [22]. Development of the Vector fitting technique [23] and the Universal Line Model (ULM) [24], have contributed greatly to shape the state of the art in the EMT modelling of transmission lines.

# 2.3 Single conductor transmission line

The simplest transmission line is one with a single conductor of uniform cross section. The following section will describe the method of modelling single conductor transmission line in frequency domain which forms the basis of multi-conductor transmission line modelling. Figure 2-2 shows a small segment of length $\Delta x$ within a single conductor transmission line having a total length of $l$.

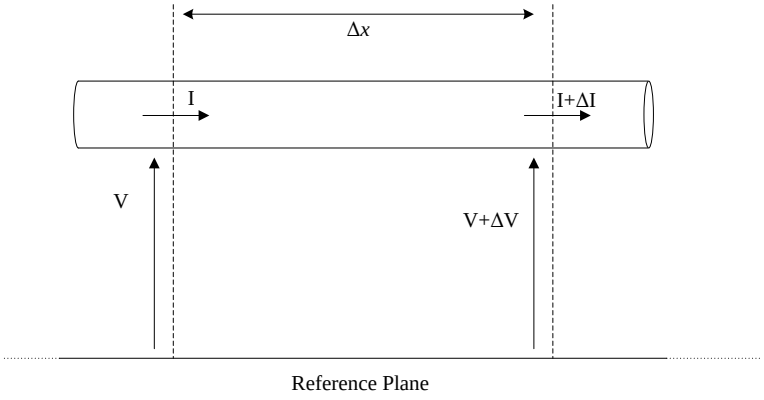


**Figure 2-2 - A section of a single conductor transmission line**

If $Z$ is the series impedance and $Y$ is the shunt admittance per unit length of the transmission line respectively, from Kirchhoff's current and voltage laws:

$$\Delta V = -(Z \cdot \Delta x) I \qquad \text{2-1}$$
$$\Delta I = -(Y \cdot \Delta x) V$$

Both parameters, $Z$ and $Y$ are frequency dependent and methods of obtaining them at a given frequency are discussed later in the chapter. Transmission line equations (or Telegrapher's equations) are derived using the famous

Maxwell's equations with the assumption that electric and magnetic fields surrounding the line are perpendicular to the line axis [1]. i.e., the electromagnetic waves in such a structure propagate in Transverse Electro-Magnetic (TEM) mode. With that, transmission line equations can be expressed in the frequency domain as follows:

$$\begin{aligned} -\frac{\partial}{\partial x}V(x,\omega) &= Z \cdot I(x,\omega) \\ -\frac{\partial}{\partial x}I(x,\omega) &= Y \cdot V(x,\omega) \end{aligned} \qquad \textbf{2-2}$$

Equations 2-3 and 2-4 show the solution to the above equation 2-2 obtained from partial differential equation theory [21].

$$I = \sqrt{\frac{Y}{Z}} \cdot e^{-\sqrt{YZ}(x)} \cdot V_f - \sqrt{\frac{Y}{Z}} \cdot e^{\sqrt{YZ}(x)} \cdot V_b \qquad \textbf{2-3}$$

$$V = e^{-\sqrt{YZ}(x)} \cdot V_f + e^{\sqrt{YZ}(x)} \cdot V_b \qquad \textbf{2-4}$$

Here, $V_f$ and $V_b$ are arbitrary constants which can be evaluated by applying boundary conditions at the sending-end (denoted by suffix '*k*') and receiving-end (denoted by suffix '*m*') of the TL as follows:

At the sending-end, $x$=0,

$$V_k = V_f + V_b \qquad \textbf{2-5}$$

$$I_k = \sqrt{\frac{Y}{Z}} \cdot V_f - \sqrt{\frac{Y}{Z}} \cdot V_b \qquad \textbf{2-6}$$

Similarly at the receiving-end, x = $l$ (length of the transmission line)

$$V_m = e^{-\sqrt{YZ}l} \cdot V_f + e^{\sqrt{YZ}l} \cdot V_b \quad \textbf{2-7}$$

$$I_m = \sqrt{\frac{Y}{Z}} \cdot e^{-\sqrt{YZ}l} \cdot V_f - \sqrt{\frac{Y}{Z}} \cdot e^{\sqrt{YZ}l} \cdot V_b \quad \textbf{2-8}$$

Characteristic admittance function, $Y_c$ and propagation function, $A$ can be defined as $Y_c = \sqrt{Y/Z}$ and $A = e^{-\sqrt{YZ}l}$. These two functions completely define the transmission line in frequency domain. Now, it is possible to exclude the unknowns $V_f$ and $V_b$ from equations 2-5 to 2-8. Then,

$$I_k = Y_c V_k - A(Y_c V_m + I_m) \quad \textbf{2-9}$$

$$I_m = Y_c V_m - A(Y_c V_k + I_k) \quad \textbf{2-10}$$

The equations 2-9 and 2-10 along with the equations written for the termination network can be used obtain currents and voltages ($V_k$, $V_m$, $I_k$ and $I_m$) of the transmission line at the sending and receiving ends.

### 2.3.1 Multi-conductor transmission line

Modelling multi-conductor transmission lines poses problems due to electromagnetic coupling between conductors. There are two main methods of tackling multi-conductor transmission lines, modal domain methods and direct phase domain methods.

## 2.3.2 Modal domain modelling

Equations 2-9 and 2-10 derived for single-conductor TL can be used to model multi-conductor transmission lines (MTL). However, $Y_c$ and $A$ become square ($n \times n$) matrices and $I_k$, $I_m$, $V_k$ and $V_m$ become n-dimensional vectors for the $n$-conductor system. Oscillatory behaviors can be observed [32] in the frequency response of the propagation matrix, $A$, both in magnitude and phase due to coupling effects. Although these do not pose any problems in the frequency domain, time domain modelling is difficult due to challenges in curve fitting and delay extractions when the frequency domain equations are transformed into time-domain form. However, these coupled frequency domain equations or direct phase equations can be decoupled using modal theory [6], [25].

A coupled set of equations of a model can be represented using the input vector, $u$, output vector, $v$ and a matrix, $H$ as below;

$$v = H \cdot u$$
$$\begin{bmatrix} v_1 \\ v_2 \end{bmatrix} = \begin{bmatrix} h_1 & h_2 \\ h_3 & h_4 \end{bmatrix} . \begin{bmatrix} u_1 \\ u_2 \end{bmatrix} \quad \textbf{2-11}$$

This coupled equation can be decoupled using the eigen-values and eigen vectors of $H$.

$$v_m = H_m \cdot u_m$$
$$\begin{bmatrix} v_{m1} \\ v_{m2} \end{bmatrix} = \begin{bmatrix} h_{m1} & 0 \\ 0 & h_{m2} \end{bmatrix} . \begin{bmatrix} u_{m1} \\ u_{m2} \end{bmatrix} \quad \textbf{2-12}$$

Where,

$$H_m = T^{-1} \cdot H \cdot T$$
$$v_m = T^{-1} \cdot v$$
$$u_m = T^{-1} \cdot u$$

$T$ is the right eigenvector matrix of $H$. $H_m$ is a diagonal matrix with eigenvalues of $H$ at its diagonal elements. Therefore, equation 2-12 decouples the model.

Using the same theory, equations 2-9 and 2-10 of the frequency domain transmission line model can be decoupled. Once the equations are transformed into modal domain, frequency responses of the functions (of each mode) are smooth and well behaved. They can be much easily approximated using low order rational functions and the delay extraction is also easier. For overhead transmission lines, the transformation matrices are real and relatively constant with frequency. These real constant transformation matrices result in efficient time domain modeling due the smaller number of iterations necessary in the convolution [26]. This real constant transformation matrix can be evaluated at the highest frequency point to be considered (usually 1 MHz). The Clark transformation can also be used for horizontally symmetrical transmission lines.

However, the transformation matrix from direct phase domain to modal domain is frequency dependent. Although for some overhead transmission lines (e.g. horizontally symmetrical overhead lines) this frequency dependency is insignificant and can be neglected. Constant transformation

matrix assumption is not valid for highly asymmetrical overhead line configurations and for many cable systems. In such cases, methods involving a frequency dependent transformation matrix should be used [21]. However, this procedure is computationally inefficient as the transformation matrix is calculated at each frequency and the number of additional convolutions. Eigenvalue calculation in such models should also be done with care due to the "eigen-value switching" phenomenon. Eigenvalues should be calculated so that their loci are smooth [22] to ensure accurate curve fitting.

### 2.3.3 Direct phase domain modelling

It has been shown in [7] that modal domain techniques cannot always avoid unstable poles when obtaining an accurate fitting for $A$. In contrast, direct phase domain models are inherently stable [47]. In direct phase domain models, the transmission line equations (equations 2-9 and 2-10) remain coupled therefore the problems associated with implementing frequency dependent transformation matrices do not arise. As discussed in section 2.3.2, $Y_c$ and $A$ are square (with dimension $n \times n$ for an $n$ conductor system) matrices and can be defined as follows:

$$Y_c = \sqrt{(YZ)^{-1}Y} \qquad \textbf{2-13}$$

$$A = e^{-\sqrt{YZ}\cdot l} \qquad \textbf{2-14}$$

It should be noted that the frequency dependence term ($\omega$) is omitted in each of these parameters for simplicity. Unlike the single conductor case, equations 2-13 and 2-14 are not directly used when obtaining $Y_c$ and $A$. First, the eigen-values and eigen-vectors of $YZ$ are computed. Let $\gamma_i$ be the $i^{\text{th}}$ eigenvalue of $YZ$ and $v_i$ be the $i^{th}$ eigen vector, then:

$$E_I = \left[v_1 \cdots v_i \cdots v_n\right] \tag{2-15}$$

$$\Lambda = \begin{bmatrix} e^{-\gamma_1 \cdot l} & 0 & \cdots & 0 \\ 0 & \ddots & & \vdots \\ \vdots & & e^{-\gamma_i \cdot l} & 0 \\ 0 & \cdots & 0 & e^{-\gamma_n \cdot l} \end{bmatrix} \tag{2-16}$$

$$\Pi = \begin{bmatrix} \sqrt{\frac{1}{\gamma_1}} & 0 & \cdots & 0 \\ 0 & \ddots & & \vdots \\ \vdots & & \sqrt{\frac{1}{\gamma_i}} & 0 \\ 0 & \cdots & 0 & \sqrt{\frac{1}{\gamma_n}} \end{bmatrix} \tag{2-17}$$

Now it is possible to find $Y_c$ and $A$.

$$Y_c = E_I \cdot \Pi \cdot E_I^{-1} \cdot Y \tag{2-18}$$

$$A = E_I \cdot \Lambda \cdot E_I^{-1} \tag{2-19}$$

Next step is to develop an equivalent circuit which can be used in time domain and it will be discussed next in section 2.4.

## 2.4 Time domain modelling

Time domain (TD) modelling can handle realistic system conditions such as nonlinearities whereas FD modelling is inherently linear. The objective of TD modelling is to develop an equivalent circuit by transforming original frequency domain equations (equations 2-9 and 2-10) to time domain. The time domain forms of those equations are as follows;

$$i_k(t) = y_c(t) * v_k(t) - a(t) * \left[ y_c(t) * v_m(t) + i_m(t) \right] \quad \textbf{2-20}$$

$$i_m(t) = y_c(t) * v_m(t) - a(t) * \left[ y_c(t) * v_k(t) + i_k(t) \right] \quad \textbf{2-21}$$

Here, the lower cases represent the time domain functions and the '$*$' denotes the convolution. Direct numerical integration of the convolution is not computationally efficient as it needs all the history terms for each calculation [2]. The mathematical technique called recursive convolution is a numerically efficient technique to evaluate the convolution. To perform recursive convolution, either one of the two functions should be expressed as a sum of exponentials in time domain. Recursive convolution is discussed in detail in section 2.4.2.

### 2.4.1 Curve fitting

Since the functions $Y_c$ and $A$ are originally formulated in the frequency domain (FD) numerical inverse Fourier transform methods (IFT) can be used

to get the corresponding discrete time domain functions. Then the time domain functions can be approximated by a summation of exponentials. However, a more convenient approach is to approximate the functions directly in the frequency domain using a least squares based curve fitting technique in the following form,

$$F(s) = \sum_{i=1}^{n} \frac{c_i}{s - a_i} + F_\infty \qquad \textbf{2-22}$$

The time domain form will then become,

$$f(t) = \sum_{i=1}^{n} c_i e^{a_i t} + F_\infty \delta(t) \qquad \textbf{2-23}$$

The direct frequency domain fitting has several advantages over time domain fitting. If the fitted function closely matches the actual function over a range of frequencies, then the corresponding steady state time domain simulation is usually accurate over that particular frequency range. Also the unknown coefficients in equation 2-22 can be efficiently evaluated using a robust curve fitting technique such as Vector Fitting [7], [23]. This method can be directly used to fit the elements of $Y_c$.

Since $Y_c$ is symmetric, only half of its off-diagonal elements need to be fitted. As $Y_c$ is the admittance seen by the sending-end for an infinite line, its diagonal elements are of minimum phase type. The off-diagonal elements are multiplied by (-1) before the rational function approximation, so that they too become minimum phase functions, whose angles lie in the first or fourth

quadrant. The minimum phase property of $Y_c$ allows it to be approximated only using real poles and zeros with a reasonable accuracy [4].

The propagation function (or entries of matrix *A*) cannot be directly approximated with low order rational functions. Instead, the time delay, $\tau$ is first extracted from the propagation function resulting in the form:

$$A_{unwound}(\omega) \cdot e^{-j\omega\tau} = A(\omega) \qquad \textbf{2-24}$$

The "unwound" function, $A_{unwound}$ has a smoother frequency response, therefore, can be fitted with low order rational functions. The accurate delay estimation for entries of *A* is a critical step in time domain modelling. Physically, time delay is the time required for travelling waves to reach the other end of the transmission line. A general time delay is difficult to define as each frequency in a waveform appear to have different travel times. However, it is necessary to consider a single delay (or series of modal delays in multi-conductor case) in order to develop a time domain equivalent circuit. In theory, a time delay in time domain means a phase shift in frequency domain. Frequency domain form can be written as:

$$a_{unwound}(t-\tau) = a(t) \qquad \textbf{2-25}$$

There are several methods of extracting delays from the propagation function. The simplest way is to use the velocity of light, *c* and the length of the line, *l* and the delay simply becomes $\tau = l/c$. Although this method is used with simple overhead line configurations, the assumption that there is a

single time delay breaks down in underground cable systems and complex overhead transmission systems. The velocities for each of the frequency components heavily depend upon the values of permittivity and permeability of the insulations. A more accurate and commonly used approach for estimating time delay is using Bode's Gain Phase formula which is described in [27]. When the time delays are extracted, the unwound $A$ matrix can be curve-fitted by low order rational functions. It is observed that the elements of $A$ are not always minimum phase functions, however, can be approximated using low order rational functions [24]. Complex poles and residues are required in curve-fitting to obtain a reasonable accuracy.

### 2.4.2 Recursive convolution

The recursive convolution is a numerically efficient technique used to compute convolutions [5]. The product of two frequency domain functions becomes convolution in the time domain:

$$F(s) = X(s) \cdot Y(s) \xrightarrow{\textit{In time domain}} f(t) = x(t) * y(t) \qquad \textbf{2-26}$$

Assume one of the frequency domain functions, say X can be written in the pole residue form as follows, so that in time domain, this function can be expressed as a summation of exponentials.

$$X(s) = \sum_{i=1}^{n} \frac{c_i \cdot e^{-s\tau}}{s - a_i} \xrightarrow{\textit{In time domain}} x(t) = \sum_{i=1}^{n} c_i \cdot e^{a_i (t-\tau)} \qquad \textbf{2-27}$$

Now, convolution can be written for a single exponential term (in integral form) in discrete time domain with a time step of $\Delta t$ as,

$$f(t) = \int_{\tau}^{\infty} y(t-u) \cdot ce^{a(u-\tau)}$$
$$= \int_{\tau}^{\tau+\Delta t} y(t-u) \cdot ce^{a(u-\tau)} + \int_{\tau+\Delta t}^{\infty} y(t-u) \cdot ce^{a(u-\tau)}$$

$$f(t) = \int_{\tau}^{\tau+\Delta t} y(t-u) \cdot ce^{a(u-\tau)} + e^{a\Delta t} \cdot f(t-\Delta t)$$

Trapezoidal integration can be used to evaluate the function in the $[\tau,\tau+\Delta t]$ period. Now, *f(t)* can be written in terms of past values of itself and present and past values of *y(t)*.

$$f(t) = k_1 \cdot y(t-\tau) + k_2 \cdot y(t-\Delta t-\tau) + k_3 \cdot f(t-\Delta t) \qquad \textbf{2-28}$$

The constants $k_1$, $k_2$, $k_3$ are derived based on the assumption that *y(t)* has a linear variation between $(t-\tau-\Delta t)$ and $(t-\tau)$:

$$k_1 = -\frac{c}{a} \cdot \left[ 1 + \frac{1-e^{a\Delta t}}{a\Delta t} \right]$$

$$k_2 = \frac{c}{a} \cdot \left[ e^{a\Delta t} + \frac{1-e^{a\Delta t}}{a\Delta t} \right]$$

$$k_3 = e^{a\Delta t}$$

The stability of the recursive convolution can be predicted using the z-transform. By applying the z-transform to the above equation:

$$F(z) = k_1 z^{-N} Y(z) + k_2 z^{-(N+1)} Y(z) + k_3 z^{-1} F(z) \xrightarrow{which\ gives} \frac{F(z)}{Y(z)} = \frac{z^{-N}(zk_1 + k_2)}{z - k_3}$$

The stability is guaranteed, if $k_3$ lies inside the unit circle in the complex plane. In recursive convolution, $k_3 = e^{a\Delta t}$. For stable poles, $a < 0$ which makes $k_3 < 1$, and therefore guarantees stability.

After expressing both $Y_c$ and $A$ using rational approximations, it is possible to use the recursive convolution to convert equations 2-20 and 2-21 into following time domain form;

$$i_k(t) = y_{eq}(t) \cdot v_k(t) + i_{history\_k} \quad \textbf{2-29}$$

$$i_m(t) = y_{eq}(t) \cdot v_m(t) + i_{history\_m} \quad \textbf{2-30}$$

The equations 2-29 and 2-30 corresponds to a time domain equivalent circuit having a shunt admittance and history current source as shown in Figure 2-3. This formulation is typical in admittance matrix based network solutions and it can be readily implemented in electromagnetic transient programs.

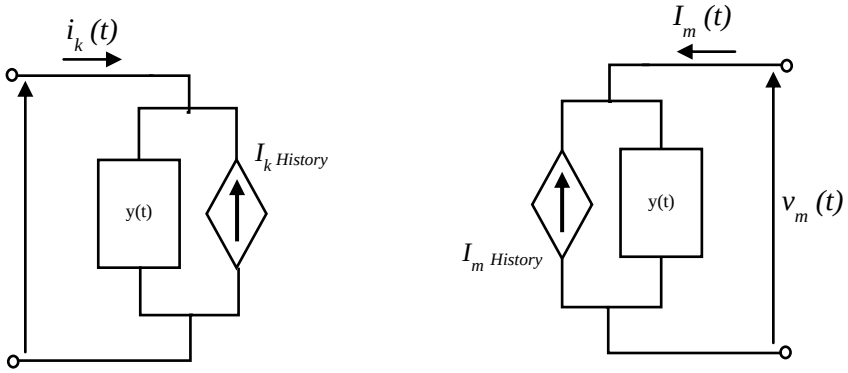


**Figure 2-3 – Time domain equivalent circuit of the transmission line model**

### 2.4.3 Passivity of transmission line models

Passivity in an electrical circuit means that a passive network must always absorb real power [28]. The transmission line is a passive network element i.e., the line itself cannot generate active power at any frequency. A recurring problem faced by all frequency dependent TL models is that the curve-fitted model of the (passive) transmission line cannot be guaranteed to be always passive.

In all frequency dependent transmission line models, transfer admittance *Y(s)* (where $s=j\omega$) relates the sending-end and receiving-end quantities as shown below:

$$\begin{bmatrix} I_k \\ I_m \end{bmatrix} = Y(s) \cdot \begin{bmatrix} V_k \\ V_m \end{bmatrix} \qquad \textbf{2-31}$$

It can be shown that the necessary and sufficient conditions for such a transmission line model to be passive are as follows [29]:

$$\begin{aligned} &1.\ Y(s)\ \textit{is analytic},\ \forall s : \mathrm{Re}(s) > 0 \\ &2.\ Y(s^*) = Y(s)^* \\ &3.\ H(s)\ \textit{is non-negative definite}, \\ &H(s)\ \textit{is given by}\ H(s) = Y(s) + \left\{Y(s)^*\right\}^T \end{aligned} \qquad \textbf{2-32}$$

Passivity enforcement methods introduced in [29]and [30] are applicable to many passivity violation issues observed in multi-conductor transmission line problems. Reference [32] provides a novel approach for guaranteeing an

asymptotic fit of the frequency domain characteristic of the transmission line as the frequency approaches zero.

### 2.4.4 Selection of time-step for time domain models

An inherent limitation in conventional EMT models of transmission lines is that the simulation time-step, $\Delta t$ must be smaller than the smallest propagation delay (or travel time), $\tau$ of the line [5]. All the distributed parameter models of transmission lines which take the travel time into account (i.e. Frequency dependent models as well as the simpler Bergeron model) have this restriction. Therefore, in an electromagnetic transient study, the minimum simulation time-step is limited by the transmission line having the shortest travel time (typically the shortest transmission line in length).

One common method of avoiding small simulation time-steps in EMT simulations is to represent short transmission lines in the study system with nominal π-equivalent circuits (as seen in Figure 2-4). Such lumped parameter models do not consider the transmission delay of the line and hence can be used with time-steps larger than travel time [47]. In a lossless line, the $Y$ and $Z$ parameters are constant with frequency and the π-equivalent model is unique. However, with lossy transmission, constancy of parameters is no longer valid. Then the π-equivalent can be constructed for maximum accuracy

at any given frequency by selecting the *Y* and *Z* in Figure 2-4 at that particular frequency.

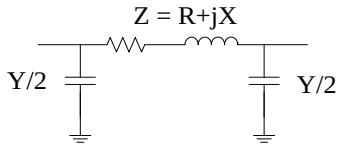


**Figure 2-4 – Typical $\pi$ equivalent circuit of a single conductor transmission line**

Although used commonly, nominal $\pi$ circuits pose many issues when used for transient solutions [47]. Lack of frequency dependency in the model parameters causes significant inaccuracies in the results. In addition, unwanted resonances may occur due to the lumped impendences in the model. The following example demonstrates the inadequacies in simulation with $\pi$ circuits. The example case shown in Figure 2-5 consists of a simple three phase cable system terminated with 10 Ω ($Z_L$) resistors. Phase 'a' is energized with a current ramp at 0.1 s (ramps from 0 to 1 kA in 0.02 s) and the ramp saturates at 0.12s.

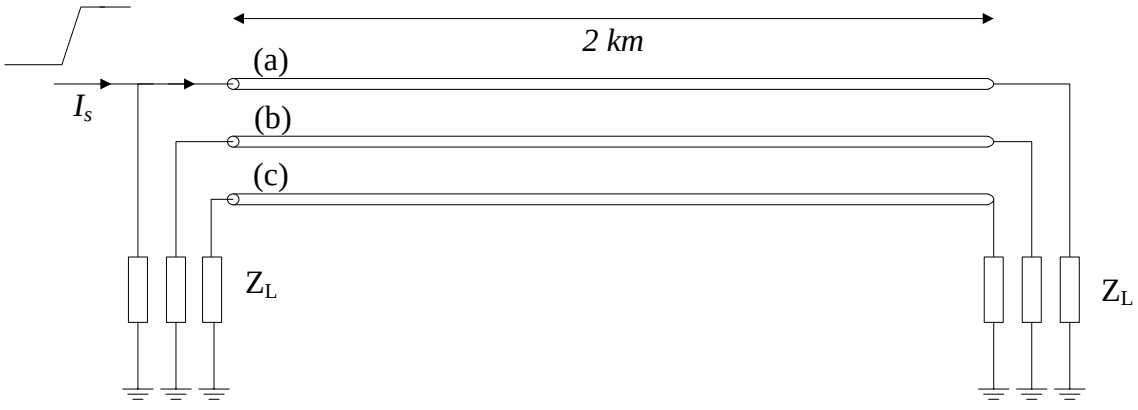


**Figure 2-5 – Three phase cable system energized with a ramp**

Simulations are carried out with detailed frequency dependent EMT model as well as π–equivalent circuits corresponding to impedances evaluated at 0.01 Hz (representing DC) and 50 Hz (ramping rate).These results are compared with numerical inverse Laplace transform (NILT) [48] of the frequency domain transmission line equation for accurate validation. Details of the NILT method are given in Appendix E. Comparisons of the receiving-end voltage of phase 'b' are shown in and Figure 2-6. The results indicate that EMT waveform and the waveform obtained by the numerical Laplace transform method agreed well, whereas both the π-equivalent circuits did not reproduce the same waveform. However, the π circuit corresponding to impedances evaluated at 0.01 Hz reached the correct steady state solution.

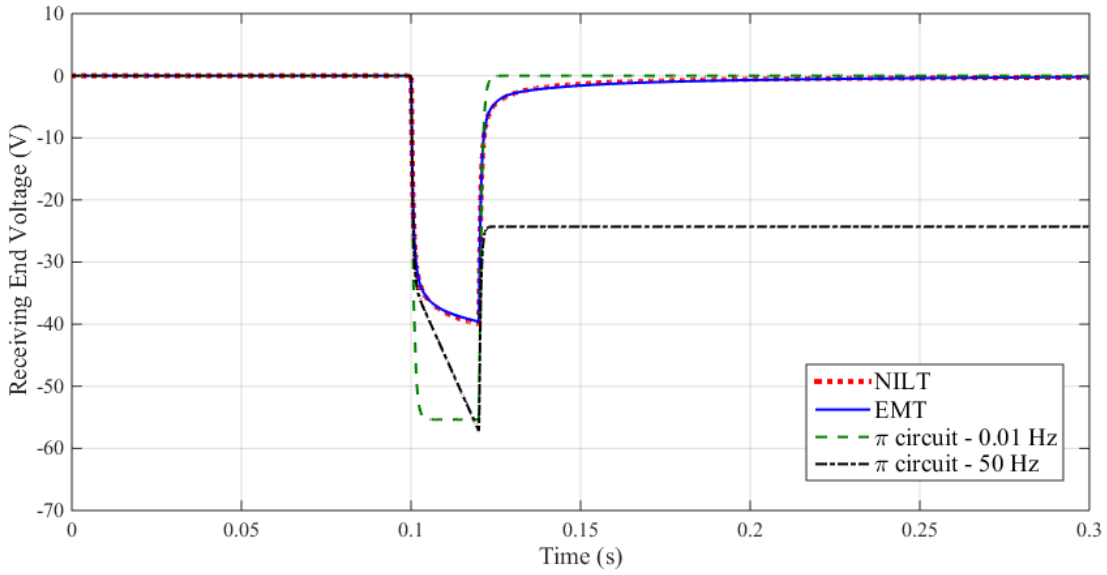


**Figure 2-6 – Receiving-end voltage – phase 'b' comparison**

As shown in the example, the use of nominal π-equivalent circuits to represent transmission lines may be inappropriate in some EMT simulations.

A novel generalized transmission line model which can accommodate all time-steps independent of the travel time is described in Chapter 5.

## 2.5 Computation of frequency dependent parameters

As discussed in sections 2.3 and 2.3.1, the terms, $Y_c$ and $A$ in frequency domain TL equations should be calculated at each frequency. To obtain those, it is essential to compute the series impedance matrix (per unit length), $Z$ and the shunt admittance matrix (per unit length), $Y$ of the transmission system (see equations 2-13 and 2-14). These two parameters depend on the applied frequency, configuration of the transmission system (shapes of conductors, distances between conductors, ground, etc.) as well as the inherent parameters (resistivity, permeability, etc.) of the conductors and the insulation layers, if any. Various methods developed for the computation of $Z$ and $Y$ with regard to overhead lines and underground cables are discussed in the following sections.

### 2.5.1 Skin and proximity effects

When alternating current flows in a conductor, its current distribution is not uniform over the cross-section, and more current tends to flow near the periphery of the conductor. This is called the skin effect [33]. Figure 2-7

illustrates the current density distribution along the diameter of a conductor at different frequencies.

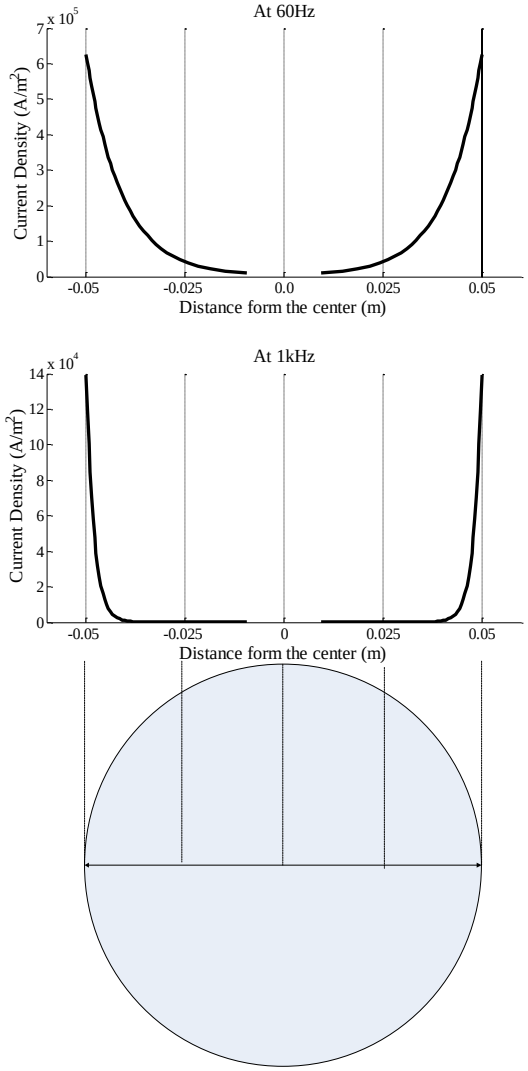


**Figure 2-7 – Current density variation due to skin effect at different frequencies**

If there are other current carrying conductors present in the vicinity, their alternating magnetic fields also contribute to the non-uniform distribution of current, giving rise to the so-called proximity effect [33]. Figure 2-8

demonstrates how the proximity effect influences the current distribution inside conductors.

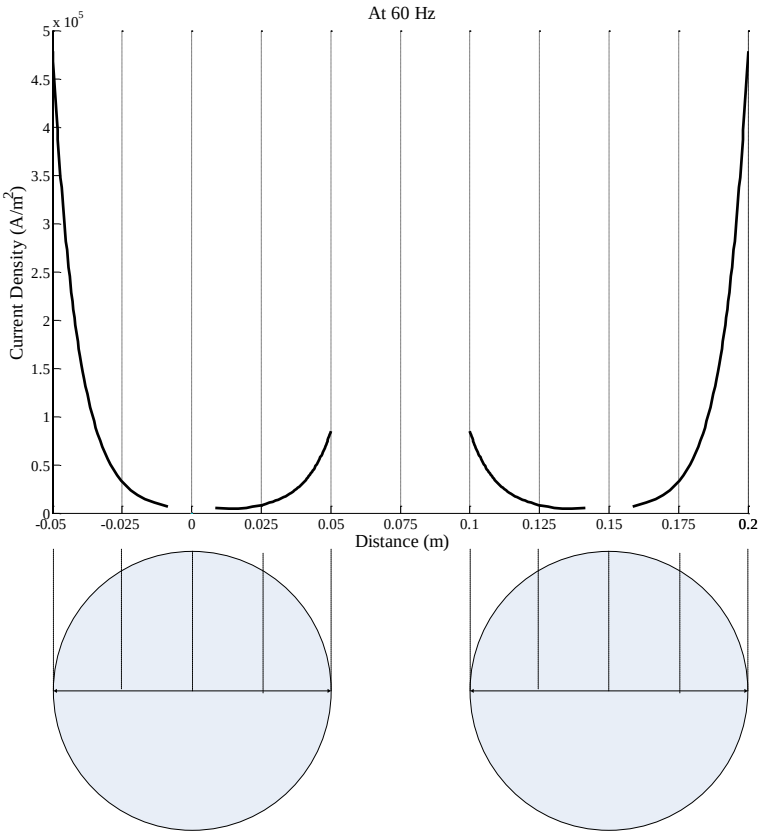


**Figure 2-8 – Current density variation due to proximity effect**

Both these effects become more severe as the frequency of the current increases. Therefore, the effective resistance and also the inductance of the conductor change with the frequency. These two effects are the main reasons for the transmission line parameters to be frequency dependent.

It can be observed that the current tends to concentrate near the outer layer at the higher frequency (1 kHz) more than the 60 Hz case. The current density distribution along the diameters of two adjacent conductors with the

same potential (1 V) is plotted in Figure 2-8. Both skin and proximity effects are visible in the plots and it can be observed that the proximity effect severely modify the current distribution of conductors which are close to each other. Therefore, when calculating impedances of transmission lines with closely positioned conductors, proximity effect should be taken into account. A general rule of thumb is to consider the proximity effect when the conductor radii and the distances between them are of the same order of magnitude.

### 2.5.2 Overhead transmission lines

In overhead lines, the cross-sectional distribution of conductors is relatively simple compared to power cables and the distances between conductors are at least one order of magnitude larger than conductor radii [5]. As discussed in section 2.5.1, the proximity effect can be neglected in such instances. This facilitates simpler models compared to power cables without a significant loss of accuracy. The impedances for the transmission lines over a finitely conducting ground plane were originally formulated by Carson [12] and the equation for self-impedance is as follows:

$$Z_{ii} = \frac{j\omega\mu}{2\pi}\left[\log_e\left(\frac{2h_{ii}}{r}\right) + 2\cdot C_{ii}\right] \qquad \textbf{2-33}$$

Where,

$Z_{ii}$ - Self impedance of conductor $i$
$\omega$ - angular frequency
$\mu$ - absolute permeability
$h_{ii}$ - height of the conductor $i$ above ground
$r$ - radius of the conductor
$C_{ii}$ - Carson's integral for self impedance

Carson's integral is defined as follows:

$$C_{ii} = \int_0^{\infty} \frac{e^{\alpha 2h_{ii}}}{\alpha + \sqrt{\alpha^2 + m^2}} d\alpha \qquad \textbf{2-34}$$

Where,

$m = \sqrt{\frac{j\omega\mu_e}{\rho_e}}$, $\rho_e$ is the ground resistivity and $\mu_e$ is the ground permitivity

Another expression can be written for the mutual impedance [12] which also includes a similar integral term, $C_{ij}$. Both these integrals are present due to the finite conductivity of ground and the difficulty is that these integrals cannot be evaluated analytically in their original form. There are many approximations proposed and a common closed form approximation [5], [34] for self and mutual impedances are as follows:

$$Z_{ii}(\text{int}) = \frac{\rho m \coth(0.777mr)}{2\pi r} + \frac{0.3565\rho}{\pi r^2} \qquad \textbf{2-35}$$

$$Z_{ii}(ext) = \frac{j\omega\mu}{2\pi} \log_e\left(\frac{2h_{ii} + d_e}{r}\right) \qquad \textbf{2-36}$$

$$Z_{ij} = \frac{j\omega\mu}{2\pi} \log_e\left(\frac{\sqrt{(y_i + y_j + 2d_e)^2 + (x_i - x_j)^2}}{d_{ij}}\right) \qquad \textbf{2-37}$$

Where,

$$m = \sqrt{\frac{j\omega\mu}{\rho}},\ d_e = \sqrt{\frac{\rho_e}{j\omega\mu_e}}$$

$\rho$ is the conductor resistivity and $\mu$ is the conductor permitivity

$\rho_e$ is the ground resistivity and $\mu_e$ is the ground permitivity

$(x_i, y_i)$ and $(x_j, y_j)$ are coordinates of $i^{th}$ and $j^{th}$ conductors

$r$ – radius of the conductor

$d_{ij}$ – distance between conductors

$\omega$ – angular frequency

Admittance matrix calculation is much simpler as air can be assumed to be lossless and ground can be of zero potential [5]. Therefore,

$$Y_{ij}^{-1} = \frac{1}{j2\pi\varepsilon\omega}\log_e\left(\frac{D_{ij}}{d_{ij}}\right) \qquad \textbf{2-38}$$

Where,

$$D_{ij} = \sqrt{(x_i - x_j)^2 + (y_i + y_j)^2},\ d_{ij} = \sqrt{(x_i - x_j)^2 + (y_i - y_j)^2}$$

$D_{ii} = 2.y_i,\ d_{ii} = r_i$

$(x_i, y_i)$ and $(x_j, y_j)$ are coordinates of $i^{th}$ and $j^{th}$ conductors

$r_i$ – radius of the conductor

## 2.5.3 Underground cables

Obtaining the frequency dependent parameters of underground cables is difficult compared to overhead lines due to the following reasons.

- Conductors are close to each other making proximity effect quite significant

- Standard formulae for impedance calculation of conductors cannot be used for cables with atypical conductor geometries such as sector shaped cables.
- The effect of the ground plane is more significant and therefore accurate evaluation of earth return impedances is necessary.

In case of coaxial type cables, the necessary equations to calculate the series impedance matrix are available in literature. The impedances of underground cables include first and second kind modified Bessel functions. Self and mutual earth impedances of buried cables include Bessel functions as well as integral terms which are first derived by Pollaczek [11]. Numerically efficient and accurate approximations of Pollaczek's equations are provided in [20], [35]. These along with the rest of the approximate equations necessary to calculate $Z$ and $Y$ matrices of a coaxial cable are given in Appendix A.

*Cables with non-concentric cross sections*

Certain types of cables used in transmission systems have cross-sections which pose problems when obtaining $Z$ and $Y$ matrices. Cross sections of pipe type and sector-shaped cables are shown in Figure 2-9. In pipe type cables, it can be seen that that the conducting surfaces are not concentric and proximity effect varies from one point to another in the surface. In addition, the pipe carrying the conductors can saturate as it is made of ferromagnetic

material. These effects make it difficult to obtain the parameters of the pipe type cables, however there are several methods proposed in literature [36], [37], [38] which tackles these problems.

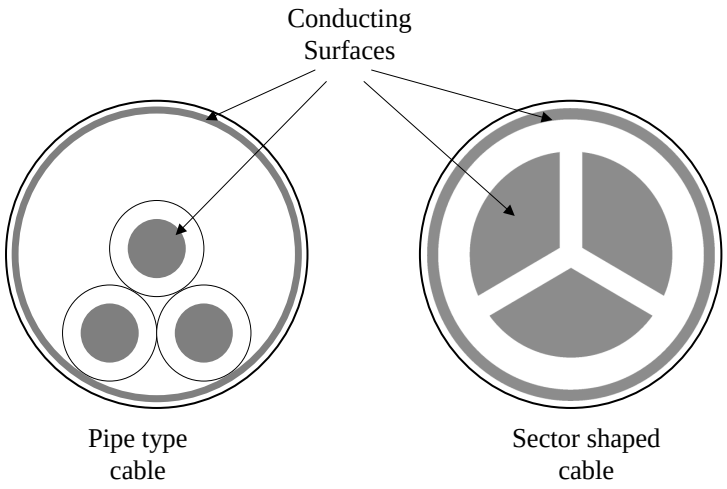


**Figure 2-9 – Cross sections of pipe type & sector shaped cables**

Sector shaped cables have a different conductor shape which makes it difficult to develop analytical formulae for impedance calculations. Numerical techniques such as finite element method (FEM) can be used to obtain these impedances accurately. However, they are computationally expensive and difficult to include in an electro-magnetic transient model. For sector shaped geometries, such as those considered in this thesis, the FEM formulation results in a system of equations in the order of tens to hundreds of thousands which has to be solved to obtain the parameters corresponding to a single frequency. Also the accuracy depends on the mesh selected, so it is always better to use other methods and compare for a sanity check.

The method of moments (MoM) technique has been used recently in [51] to calculate impedances of sector-shaped cables. This method seems to be promising and may need further investigation. Reference [39] provides a simple technique to transform any arbitrarily shaped cable into circular shape and then apply simple formulae. However, it is shown in [40], [41] that errors involved in this method when applied to sector-shaped cables can be as high as 40-50%, both at low and high frequency limits compared to FEM based techniques. Therefore, sector shaped cable modelling in EMT type programs using the state of the art poses many difficulties. A novel approach to model sector shaped cables in EMT programs is introduced in Chapter 3.

## 2.6 Frequency domain models for transmission line EMT model validation

### 2.6.1 Accuracy and validation of EMT models

When developing EMT models for transmission lines, accurately validating those models is essential before incorporating them with the other simulation models of the power system. In general, errors in line models can occur at three different stages of modelling:

- Due to assumptions and approximations in the computation of line parameters (series impedance and shunt admittance matrices per unit length)
- Errors in curve fitting the frequency dependent characteristic admittance, $Y_c$ and the propagation function, $A$
- Errors in time domain simulation due to interpolation, etc.

Therefore, transmission line models should be validated at all these stages of modelling.

Computing line parameters can be difficult for power cables with atypical cross sections. In addition, the accuracy in parameter estimation reduces at frequencies in the megahertz range as most line parameter computation techniques neglect the displacement current [1], which becomes significant at high frequencies. Finite element techniques are commonly used [41], [40] to validate transmission line constant estimation. Method of moments is preferred in reference [50]. The standard equations for impedance and admittance calculations of overhead lines and coaxial cables are derived and validated by multiple researchers [5], [19], [20], and they are widely accepted to be accurate.

Curve fitting errors can cause many inaccuracies in the EMT models of transmission lines. Comparing the actual values and the fitted function of $Y_c$ and $A$ at selected frequencies is commonly used to validate curve fitting [24]. As the comparisons can be done only at a finite number of frequencies, this

method does not guarantee an accurate fitting. Errors can occur due to poor asymptotic fitting as well as overfitting. Furthermore, passivity violations can result in unstable simulations even with fairly accurate fitting [32].

Errors introduced in time domain simulations of transmission lines are mainly due to the travel time interpolation. One of the methods to validate time domain models is by carrying out a field test for the overhead line or the cable, and comparing the results with the simulation [56]. However, field result data are not readily available for many types of transmission line configurations and carrying out such a test is not within the capability of many models developers.

If accurate frequency domain (FD) solutions are available for the transmission lines, these can be transformed into time domain and used for model verification. The numerical inverse Laplace transform (NILT) [48], [49] of the frequency domain transmission line equations can be used for the time domain transformation. The NILT method applies a modified discrete Fourier transform to the excitation function, and calculates the response of the system to each frequency component. It then recombines the individual frequency responses into a time domain response waveform. As superposition is used, it is obvious that NILT can only be used with linear terminations on the transmission line (e.g., resistors, inductors, etc.). A detailed description of the NILT method is given in Appendix E.

### 2.6.2 Modelling and validation of cascaded transmission systems

Two common examples of cascaded power transmission systems are transposed overhead lines and cross-bonded cables. Transposition of conductors is carried out in overhead lines to minimize the impedance unbalance created by the line geometry, therefore, reduce the voltage and current imbalances [53]. Cross-bonding in cable systems is becoming common in many European countries, where there is an increasing trend to replace overhead transmission lines with underground cables [54]. Many power cable systems are fully cross-bonded as it increases the ampacity of cables by lowering the circulating sheath currents and prevent sheath over-voltages [55]. With the increased number of cascaded power transmission lines in the modern power systems, proper EMT modelling and validation of these lines becomes increasingly important. In addition, there are several novel techniques developed recently to represent non-homogenous transmission lines in EMT programs using cascaded homogenous line segments [58], [59], which convert non-homogenous transmission lines into a series of homogenous lines.

When modelling transmission systems with a large number of transpositions, ideal transposition (ideal cross bonding for cables) can be used [5], [57]. However, in certain time domain simulations, individual transmission line

segments of cascaded power transmission systems need to be modelled separately [53]. Errors can be significant in time domain simulations of cascaded power transmission systems due to the complexity in modelling. Primarily, the fitting errors can be significant in cascaded transmission systems as they accumulate with the increased no. of transmission segments. It is essential to develop a technique capable of validating these EMT models in time domain. A novel accurate FD model for cascaded lines is presented in chapter 4 which can be used to verify the accuracy of EMT models.

# Chapter 3

# Electro-Magnetic Transient Modelling of Sector-Shaped Cables

## 3.1 Introduction

This Chapter introduces a new contribution to the state-of-the-art of the cable modelling by extending the elemental sub-conductor technique to model sector-shaped cables. The cables with non-concentric cross-sections can be categorized mainly into sector-shaped cables and pipe-type cables. As described in Chapter 2, both of these cable types are subjected to skin and proximity effects, which make the evaluation of frequency dependent impedances a formidable challenge. As mentioned in Section 2.5.3, several methods have been developed to model pipe type cables in EMT type programs with acceptable accuracy. However, there is little activity in modelling sector shaped cables in literature. Some of these models are in the frequency domain and do not transfer to the time domain simulations [42]. A

new method that can be used to model sector-shaped cables in EMT programs is presented in this chapter.

## 3.2 Sub-conductor technique [43], [44]

The sub-conductor technique is a simple, yet an accurate method, which can be used to find cable impedances. In this method, each conductor of the cable is partitioned into a number of small sub-conductors. The shape of the sub-conductor can be circular, square or elemental (a specialized sub-conductor shape which will be discussed in this section). However, circular and square shaped subdivision can cause errors as shown in Figure 3-1, as they do not cover the entire cross section. With square sub-conductors, the boundary of the conductor is not completely filled in, whereas with the circular ones, lacunae remain in the interior portion. Therefore, they require a large number of subdivisions to minimize those errors and to get accurate enough results, thus requiring significant computational effort and memory.

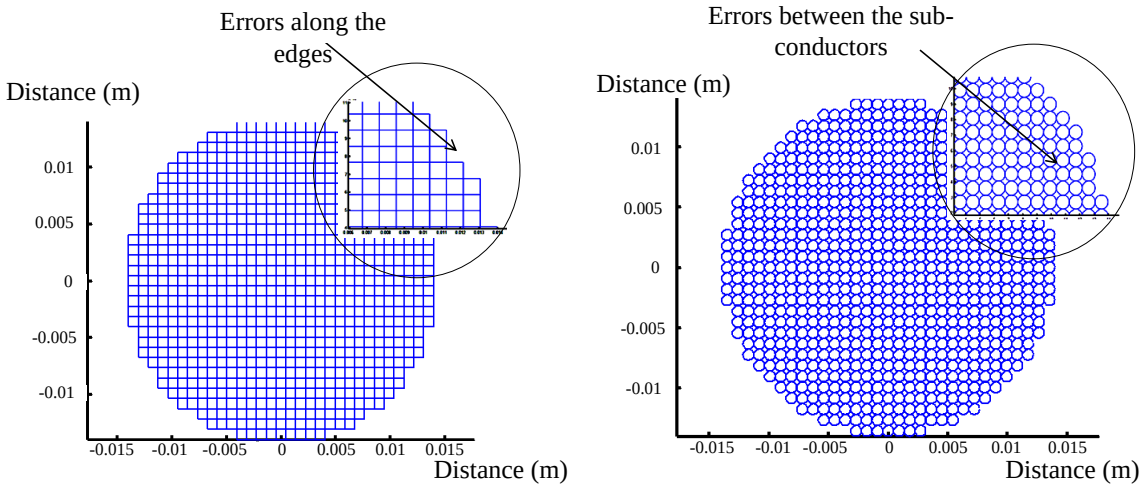


**Figure 3-1 – Errors in circular and square subdivision**

The elemental sub-conductor technique proposed in [43] has been used successfully for precisely circular conductor shapes and it is proven to provide better results than square and circular sub-conductor shapes in [43] and [44]. The elemental shape is shown in Figure 3-2 a).

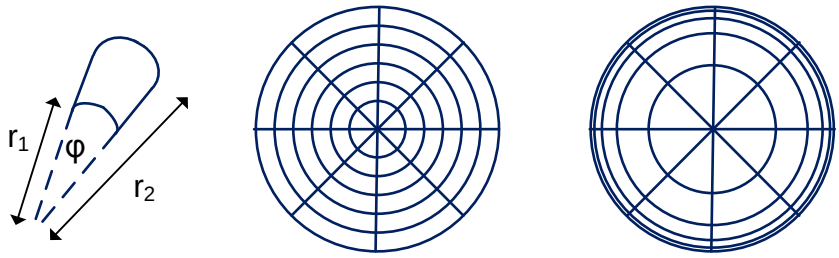


a) Elemental Shape b) Linear Subdivision c) Exponential Subdivision

**Figure 3-2 – Subdivision using elemental shaped sub-conductors**

There are several important aspects to be carefully considered in determining the number of sub-conductors required for each conductor of the cable. The

accuracy of the series impedance values can be improved by increasing the number of sub-conductors. The resistances obtained using the sub-conductor technique asymptotically reaches a certain "cut-off resistance", with the increase of frequency, which is slightly higher than the dc resistance of the outermost sub-conductors [43]. This is mainly due to the small penetration depth at high frequencies. Therefore, to include skin and proximity effects accurately, the outer sub-conductors should be selected to be smaller than the penetration depth of the maximum frequency of interest. Penetration depth, $\delta$, for a given conductor is as follows:

$$\delta = \sqrt{\frac{1}{\pi \cdot f \cdot \sigma \cdot \mu}} \qquad \textbf{3-1}$$

Where, $\sigma$ and $\mu$ are the conductivity and permeability of conductor respectively, and $f$ is the frequency in Hz.

Selecting smaller sub-conductor filaments increases the total number of sub-conductors significantly and thereby the computational effort and memory requirement. An exponential subdivision of the conductor as seen in Figure 3-2 c, reduces the size of the outer sub-conductors without affecting the total number of sub-conductors. This increases accuracy of calculation at the highest frequency of interest without an increase in the computational effort.

One of the limitations in the elemental sub-conductor method is that it can be directly used only with circular shaped conductors [43]. However, in this

chapter, its applicability is extended to sector shaped (non-circular) conductors.

## 3.3 Frequency domain cable model

Frequency domain model development requires accurate estimation of the series impedance and the shunt admittance matrices $Z$ and $Y$ for the cable system at a given frequency range (usually 1Hz to 1MHz). In this method, $Z$ matrix is computed by subdividing the conductors.

### 3.3.1 Subdivision of the cable

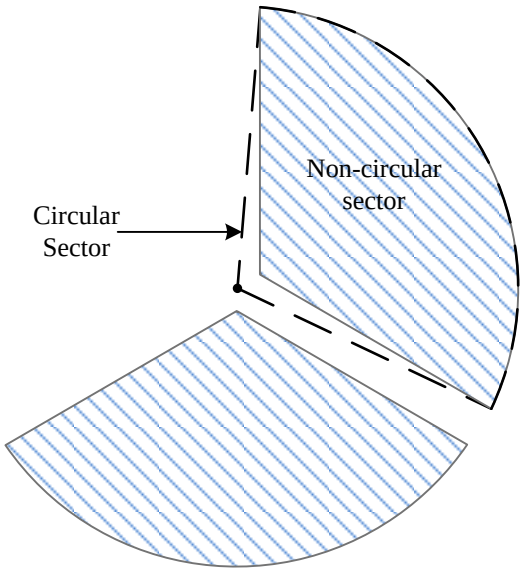


**Figure 3-3 - Conductor shape and geometry of a sector-shaped cable**

Figure 3-3 shows a main conductor cross-section of a sector-shaped cable with three sectors. It can be seen that the conductor cross-section is a non-circular sector. The vertex $C_1$ in Figure 3-4 is not the center of the conducting sector. The actual center of the arc in the conductor ($C_0$) lies outside the conducting area, which indicates that these are not circular sectors. In other words, the distance $r_1$ from conductor vertex ($C_1$) to the circumference (A) is not a constant. This calls for a novel subdivision procedure to effectively subdivide sector-shaped conductors.

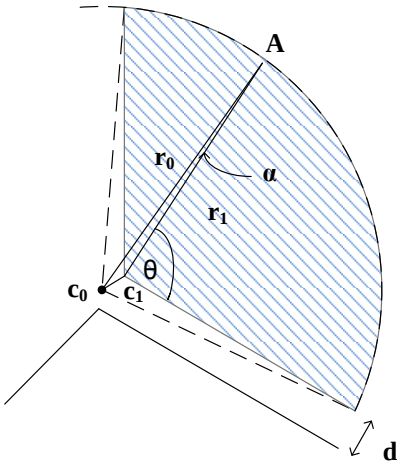


**Figure 3-4 - Conductor Shape of sector shaped cable**

The distance, $r_1$ (see Figure 3-4) is essential in subdividing the conductor. $r_1$ can be found using the following equation:

$$r_1 = \begin{cases} \dfrac{r_0}{\sin\left(120^0 + \theta\right)} \sin\left\{60^0 - \theta - \alpha\right\}, \; for\, \theta \neq 60^0 \\ \\ r_0 - \dfrac{d}{2}\cos\left(30^0\right), \; for\, \theta = 60^0 \end{cases} \qquad \textbf{3-2}$$

The derivation of equation (3-2) is given in Appendix B. First, each conductor is subdivided in the azimuth direction with an angle, φ. Figure 3-5 shows an arbitrary sub-sector with an angle, φ and radii at each side being $r'_1$ & $r''_1$, which can be found using equation 3-2. After that, this sub-sector is replaced with a circular sub-sector with the same angle, φ and a constant radius of $(r'_1 + r''_1)/2$, which is the average of the previous radii. This substituting sector can be subdivided in the radial direction using conventional "elemental" type sub-conductors.

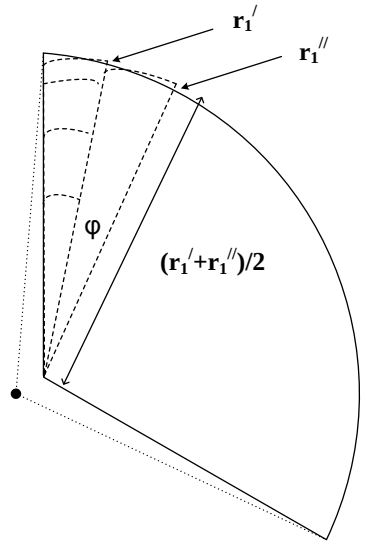


**Figure 3-5 - Subdivision of a single sector**

The sheath in which the conductors are encased has an annular cross-section, hence, the elemental sub-conductor method is straightforward and easy to apply as documented in [43].

### 3.3.2 Series Impedance Calculation

Inductance values of the series impedance matrix of the cable depend heavily on the return path selected. These inductances are functions of Geometric Mean Distances (GMDs), which are calculated with respect to the loops formed by cable conductors and the return conductor [43]. First, a fictitious, lossless circular ring with a large radius (much larger than that of the cable) enclosing the cable is chosen as the return path. At this stage, ground return is not considered due to two reasons. One of the reasons is that, ground resistance values at most frequencies are much larger the cable resistances; so that the total resistance terms will be dominated by them and make it hard to identify the errors in cable resistance calculation. The second reason is that the methods proposed in [40] and [41] neglect the ground effect, therefore using a fictitious, lossless return path facilitates comparisons.

*a) Resistance Calculation*

As a constant current density is assumed within a sub-conductor filament, resistance calculation of any sub-conductor, *i* can be performed using the

cross-sectional area of that sub-conductor, $A_i$ and the resistivity, $\rho$ of the corresponding conductor as shown below:

$$R_i(\textit{per unit length}) = \frac{\rho}{A_i} \quad \textbf{3-3}$$

$A_i$ is given by,

$$A_i = \frac{(r_{2i}^2 - r_{1i}^2)}{2}\varphi \quad \textbf{3-4}$$

Where, $r_{1i}$ and $r_{2i}$ are the minimum and maximum radii of the elemental sub-conductor, and $\varphi$ is the angle of the elemental sub-conductor in radians (see Figure 3-5).

*b) Inductance Calculation*

Before calculating the inductances, it is necessary to obtain self and mutual Geometric Mean Distances (GMDs) of sub-conductors. Formulae needed for GMD calculation are given in [43] and thus, not repeated. For the chosen return conductor (a ring with radius '*a*'), the self GMD of the $i^{th}$ sub-conductor is denoted by $GMD_i$ and the mutual GMD between the $i^{th}$ and $j^{th}$ sub-conductors is denoted by $GMD_{ij}$. The inductances can be found using the GMDs as follows [41]:

$$L_{ii} = \frac{\mu}{2\pi}\ln\left(\frac{a}{GMD_i}\right) \quad \textbf{3-5}$$

$$L_{ij} = \frac{\mu}{2\pi}\ln\left(\frac{a}{GMD_{ij}}\right) \quad \textbf{3-6}$$

*c) Formulation of the Impedance matrix*

If the total number of sub-conductors is assumed to be n, a diagonal resistance matrix, $R_{nxn}$ can be formed by using the equation 3-3 to form its diagonal elements. Similarly, inductance matrix, $L_{nxn}$ can be produced using equations 3-5 and 3-6. Then, the corresponding impedance matrix, $Z_{nxn}$ for a given frequency, $f$, becomes:

$$Z_{n\times n}(f)=\begin{bmatrix} R_1 & 0 & \cdots & 0 \\ 0 & R_2 & & \vdots \\ \vdots & & \ddots & \vdots \\ 0 & \cdots & \cdots & R_n \end{bmatrix} + j2\pi f \begin{bmatrix} L_{11} & L_{12} & \cdots & L_{1n} \\ L_{21} & L_{22} & & \vdots \\ \vdots & & \ddots & \vdots \\ L_{n1} & \cdots & \cdots & L_{nn} \end{bmatrix} \qquad \textbf{3-7}$$

However, this impedance matrix has to be reduced such that each element represents conductor impedances instead of the sub-conductor quantities. For example, a four conductor cable system should have a four-by-four impedance matrix.

If it is assumed that the total number of conductors in the cable system is $K$, and the number of sub-conductors in each conductor is $N_k$, then the number of total sub-conductors, $n=\sum_{k=1}^{K} N_k$ The number $N_k$ is taken to be constant ($N_k$=$N$) for all conductors in following analysis to simplify the discussion. However, the generalized procedure considers cases with different number of sub-conductors in each conductor. This sub-conductor impedance matrix relates to the voltage and the sub-conductor current as follows:

$$(-)\frac{d}{dx}[V_{n\times 1}] = Z_{n\times n}[I_{n\times 1}] \qquad \textbf{3-8}$$

By inverting $Z_{nxn}$, it is possible to rearrange the equation 3-8 to the form seen in Figure 3-6. The superscripted number represents the conductor number and the subscripted numbers represent sub-conductors. It can be observed that first $N$ voltages are the same ($V^{(1)}$) as they belong to the same conductor and the next $N$ to the second conductor ($V^{(2)}$). Therefore, the addition of currents $I_1^{(1)}$ to $I_N^{(1)}$ would give the conductor 1 current and the currents $I_{N+1}^{(2)}$ to $I_{2N}^{(2)}$ would give the conductor 2 current and so on. This would yield a reduced $Z^{-1}$ matrix of size $K\times K$:

$$(-)\begin{bmatrix} I_1^{(1)} \\ I_2^{(1)} \\ \vdots \\ I_N^{(1)} \\ I_{N+1}^{(2)} \\ \vdots \\ \vdots \\ I_{2N}^{(2)} \\ \vdots \\ \vdots \\ \vdots \\ I_n^K \end{bmatrix} = \underbrace{\begin{bmatrix} Y_{1,1} & Y_{1,2} & \cdots & Y_{1,N} & Y_{1,N+1} & \cdots\cdots & Y_{1,2N} & \cdots\cdots\cdots & Y_{1,k\times N} \\ Y_{2,1} & Y_{2,2} & & \vdots & \vdots & \ddots & \vdots & & \vdots \\ \vdots & & \ddots & \vdots & \vdots & & \ddots & \vdots & \vdots \\ Y_{N,1} & \cdots & \cdots & Y_{N,N} & Y_{N,N+1} & \cdots\cdots & Y_{N,2N} & & Y_{N,K\times N} \\ Y_{N+1,1} & \cdots & \cdots & Y_{N+1,N} & & & & & \\ \vdots & & \ddots & \vdots & & & & & \\ \vdots & & \ddots & \vdots & & & & & \\ Y_{N+1,N} & \cdots & \cdots & Y_{2N,N} & & & & & \\ \vdots & & & & & & & \vdots & \\ \vdots & & & & & & & \vdots & \\ \vdots & & & & & & & \vdots & \\ Y_{K\times N,1} & \cdots & \cdots & Y_{K\times N,N} & & \cdots\cdots & & \cdots\cdots & Y_{K\times N,K\times N} \end{bmatrix}}_{\text{Inverse of } Z_{nxn} \text{ matrix, } nxn=(K.N)x(K.N)} \frac{d}{dx}\begin{bmatrix} V^{(1)} \\ \vdots \\ \vdots \\ V^{(1)} \\ V^{(2)} \\ \vdots \\ \vdots \\ V^{(2)} \\ \vdots \\ \vdots \\ \vdots \\ V^{(K)} \end{bmatrix}$$

1st Conductor (N sub-conductors

2nd Conductor (N sub-conductors

**Figure 3-6 – Sub-conductor admittance matrix**

The reduced $Z^{-1}$ matrix of the cable system can be written as follows:

$$(-)\begin{bmatrix} I^{(1)} \\ I^{(2)} \\ \vdots \\ I^{(K)} \end{bmatrix} = \begin{bmatrix} Y_{sum\_11} & Y_{sum\_12} & \cdots & Y_{sum\_1K} \\ Y_{sum\_21} & Y_{sum\_22} & & Y_{sum\_2K} \\ \vdots & \vdots & \ddots & \vdots \\ Y_{sum\_K1} & Y_{sum\_K2} & \cdots & Y_{sum\_KK} \end{bmatrix} \frac{d}{dx} \begin{bmatrix} V^{(1)} \\ V^{(2)} \\ \vdots \\ V^{(K)} \end{bmatrix} \qquad \textbf{3-9}$$

Where the current vector and the elements of $Y$ matrix $(K\times K)$ are given by:

$$I_m = I^{(m)}_{(m-1)N+1} + I^{(m)}_{(m-1)N+2} + \cdots + I^{(m)}_{mN}$$

$$Y_{sum\_mm} = Y_{(m-1)N+1,(m-1)N+1} + \cdots + Y_{(m-1)N+1,mN} + \cdots + Y_{(m-1)N+2,(m-1)N+1} + \cdots + Y_{(m-1)N,2\times mN} + \cdots$$
$$\cdots + Y_{mN,(m-1)N+1} + \cdots + Y_{mN,mN}$$

$$Y_{sum\_mr} = Y_{(m-1)N+1,(r-1)N+1} + \cdots + Y_{(m-1)N+1,rN} + \cdots + Y_{(m-1)N+2,(r-1)N+1} + \cdots + Y_{(m-1)N+2,rN} + \cdots$$
$$\cdots + \left( Y_{mN,(r-1)N+1} + \cdots + Y_{mN,rN} \right)$$

The subscripts m and r denote $m^{\text{th}}$ and $r^{\text{th}}$ conductor of the cable. The series impedance matrix with the fictitious return path can be obtained by inverting the $Y$ matrix $(K\times K)$ in equation 3-9:

$$(-)\frac{d}{dx}[V_{K\times 1}] = Z_{K\times K}[I_{K\times K}] \qquad \textbf{3-10}$$

### 3.3.3 Performance enhancement of the algorithm

*Fast matrix reduction*

The proposed procedure requires the inversion of an $n\times n$ matrix, which may be difficult for large number of subdivisions. Therefore, the matrix reduction method [43] given in Appendix C is applied to improve computational efficiency. This reduces the problem to inverting $K$ number of $N$x$N$ matrices instead of one $n\times n$ matrix. For example, consider the case of a four conductor

cable sub-divided into 2000 filaments with each conductor having 500 filaments. Using the method in Appendix C, problem can be reduced to inverting four matrices of size 500x500 rather than inverting a single 2000x2000 matrix. This reduces the computational effort approximately by half [43].

*Reducing the number of sub-conductors*

Frequency domain fitting algorithms in EMT programs require the calculation of series impedance matrix at a number of frequency points (e.g. 100) spaced logarithmically. Therefore, the majority of the frequency points are distributed in the lower frequency range. If 100 frequency points are considered in the 1 Hz – 1 MHz range, 85 frequency points are less than 100 kHz. As the required number of sub-conductors is determined by the maximum frequency of interest, a smaller number of sub-conductors can be used for lower frequencies as shown in Figure 3-7. Therefore, the largest sub-conductor matrix of size $N_3$x$N_3$ has to be inverted only in the frequency range $f_2$-$f_3$, where the number of frequency points is small due to logarithmic spacing.

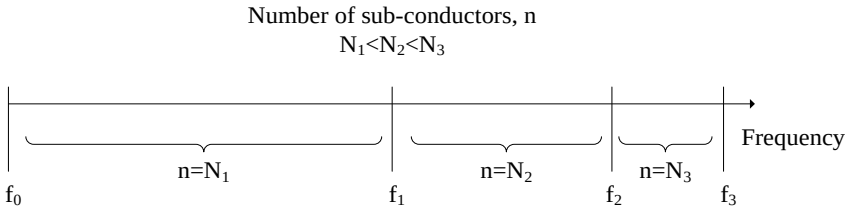


**Figure 3-7 – use of different no. of sub-conductors for different frequency ranges**

### 3.3.4 Inclusion of ground return path

In underground cable systems, return path is through neutral conductors (sheath, armour, etc.), or through ground or both [60]. If ground return is involved, it should be considered as a separate conductor. This can be accomplished by subdividing the surrounding ground in a manner similar to the subdivision of conductors. However, due to the relatively high resistivity of earth (typical 1-100 Ωm) compared to the conductors, skin depth can vary from 5m to 5000m in the frequency range of 1Hz-1MHz. Therefore, if a constant sub-conductor size is selected, the large skin depth of ground at low frequencies demands a large number of sub-conductors. To account for this, it is possible to subdivide the ground by considering the skin depth at each frequency. The number of total sub-conductors is kept constant and the sub-conductor size is varied depending on the frequency. Also, as high current density variation is expected near the earth surface and the cable, sub-conductor size is kept comparatively small and constant there (See Figure 3-8). Square sub-conductors are selected for subdivision as they are better suited for this shape. A square shaped area surrounding the cable with a side length of twice the skin depth is used for the ground subdivision. Initially, areas with larger side lengths were selected to represent the ground and the impedance results were compared. It is found empirically that the accuracy

gained by increasing the side length more than twice the skin depth is minimal.

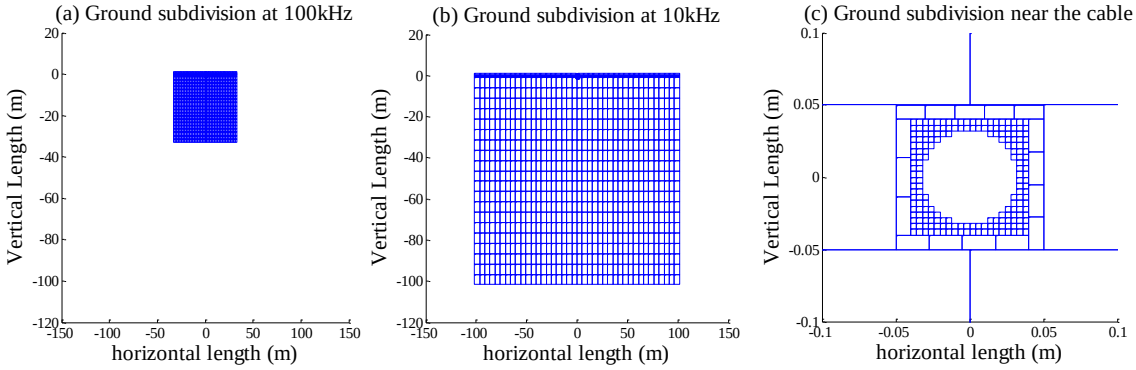


**Figure 3-8 – Subdivision of the surrounding ground**

In the above method, subdivision is needed to be done at every frequency point considered, which can be computationally inefficient if there are large number of frequencies of interest. The alternative is to use an approximate formula based on Pollaczek's equation [11] such as formulae presented in [20] and [35].

The formula proposed in [35] for the self-earth return impedance is shown in equation 3-11:

$$Z_s = \frac{\rho m^2}{2\pi}\left[K_0(mR) + \frac{2}{4+m^2R^2}e^{-2hm}\right] \qquad \textbf{3-11}$$

Where $\rho$ is resistivity of earth, $R$ is the outer radius of the cable, $h$ is the buried depth of the cable. $m$, is the intrinsic propagation constant of the earth, where: $m = \sqrt{\frac{j\omega\mu}{\rho}}$

The impedance matrix obtained in 3-10 can be modified to include the earth return impedance as follows:

$$Z_{ij\_new} = Z_{ij\_old} - Z_{ref} + Z_{ground} + Z_{insulation} \quad \textbf{3-12}$$

$Z_{ground}$ can be found from equation 3-11. $Z_{ref}$ is the impedance due to the fictitious return conductor used before. This is only an inductance value as a lossless ring is used as the return conductor. This value can be found by considering the entire cable as a single "elemental" and using the equation 3-5. The final term $Z_{insulation}$ is given as:

$$Z_{insulation} = \frac{j\omega\mu}{2\pi} \ln\left(\frac{Outer\ radius\ of\ insulation}{Inner\ radius\ of\ insulation}\right) \quad \textbf{3-13}$$

### 3.3.5 Shunt Admittance Calculation

The shunt admittance matrix for a cable system can be shown as follows:

$$Y_{cable} = [G] + j\omega[C] \quad \textbf{3-14}$$

*[G]* in equation 3-14 is the conductance matrix which can be neglected as the conductivity of the insulation material is very low. Therefore, using only the capacitance matrix *[C]*, is sufficient to form the shunt admittance matrix. A significant characteristic of the capacitance matrix is that its values remain essentially constant within the frequency range (up to 1 MHz) considered. In other words, it is possible to assume frequency independence and use

capacitance values obtained at a single frequency for all frequencies without loss of much accuracy. The approximate method of obtaining capacitances of sector-shaped cables shown in [61] is used here. For a cable with three sectors and a sheath, capacitance matrix is given as follows:

$$C = \begin{bmatrix} 2C_c + C_s & -C_c & -C_c & -C_s \\ -C_c & 2C_c + C_s & -C_c & -C_s \\ -C_c & -C_c & 2C_c + C_s & -C_s \\ -C_s & -C_s & -C_s & 3C_c + C_g \end{bmatrix} \quad \textbf{3-15}$$

Where,

$$C_c = \frac{\varepsilon r_1}{d} \quad C_s = \frac{2\pi\varepsilon}{3\ln\left(\frac{r_2}{r_1}\right)} \quad C_g = \frac{2\pi\varepsilon}{\ln\left(\frac{r_4}{r_3}\right)}$$

$r_1$ - distance from center to main conductor circumference
$r_2$ - inner radius of sheath
$r_3$ - outer radius of sheath
$r_4$ - outer radius of the cable
$d$ - distance between inner conductors
$\varepsilon$ - permitivity of the insulator

This calculation is later compared in Section 3.4.4 with the values obtained using the full-wave analysis method in [62].

## 3.4 Application Example

The method described in section 3.3 is applied to obtain the frequency dependent parameters of the cable shown in Figure 3-9. This cable example is

identical to the one reported in [39], so that the comparative results are available.

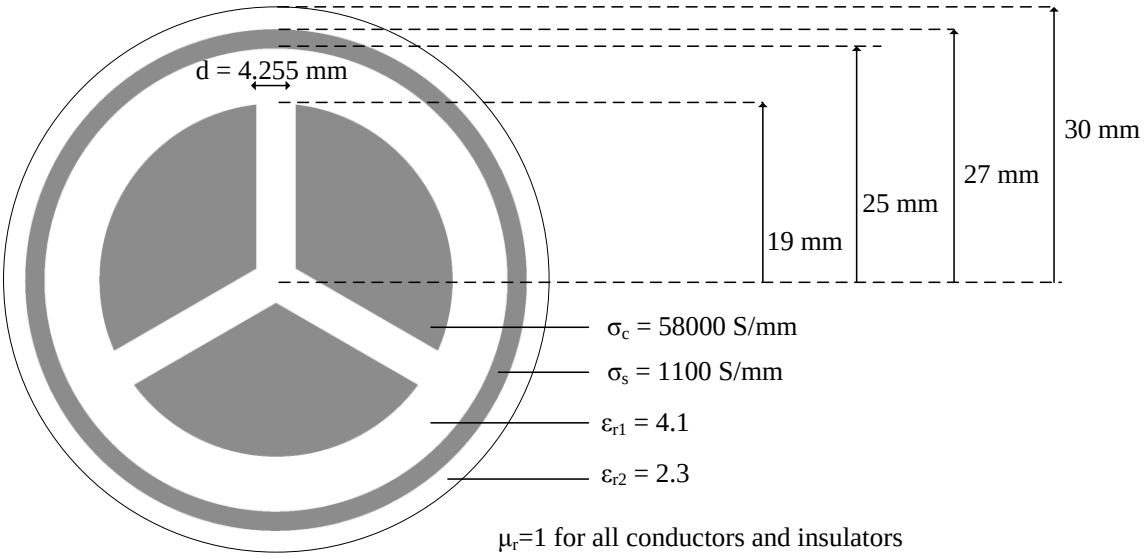


**Figure 3-9 – Geometry of the sector-shaped cable in example case**

### 3.4.1 Calculation of series impedance parameters using a fictitious return path

The series impedance parameters (resistances and inductances) calculated with respect to a fictitious return conductor are compared with the results of a Finite Element Method (FEM) analysis of the same cable provided in [40] for six different frequencies ranging from 6 to 600 kHz. As the finite element method uses a full electromagnetic solution, it is considered as the template for comparison. A total of 1920 sub-conductors are used for the calculation.

Self and mutual resistances are compared in Table 3-1 and inductances are compared in Table 3-2.

**Table 3-1 – Comparison of self and mutual resistances with finite element results**

| **Self-Resistance (Ω/km)** | | | |
|---|---|---|---|
| Frequency (Hz) | Finite Element Method | Sub-conductor Method | Error (%) |
| 6 | 2.8400 | 2.8400 | 0.000 |
| 60 | 2.8499 | 2.8496 | 0.009 |
| 600 | 2.9675 | 2.9661 | 0.047 |
| 6E+03 | 3.5250 | 3.5151 | 0.281 |
| 60E+03 | 5.1505 | 5.0095 | 2.738 |
| 600E+03 | 15.916 | 16.159 | 1.527 |
| **Mutual Resistance (Ω/km)** | | | |
| Frequency (Hz) | Finite Element Method | Sub-conductor Method | Error (%) |
| 6 | 2.7825 | 2.7824 | 0.003 |
| 60 | 2.7832 | 2.7833 | -0.003 |
| 600 | 2.7804 | 2.7871 | -0.241 |
| 6E+03 | 2.6946 | 2.7090 | -0.534 |
| 60E+03 | 2.8882 | 2.7693 | 4.110 |
| 600E+03 | 8.8231 | 7.9854 | 9.490 |

**Table 3-2 - Comparison of self and mutual inductances with finite element results**

| **Self-Inductance (µH/km)** | | | |
|---|---|---|---|
| Frequency (Hz) | Finite Element Method | Sub-conductor Method | Error (%) |
| 6 | 232.02 | 229.98 | 0.91 |
| 60 | 220.67 | 218.32 | 1.13 |
| 600 | 156.80 | 155.35 | 0.78 |
| 6E+03 | 120.40 | 121.61 | 1.19 |
| 60E+03 | 105.09 | 107.42 | -2.49 |
| 600E+03 | 99.003 | 102.42 | -4.60 |
| **Mutual Inductance (µH/km)** | | | |
| Frequency (Hz) | Finite Element Method | Sub-conductor Method | Error (%) |
| 6 | 40.445 | 40.833 | -0.959 |
| 60 | 40.191 | 40.207 | -0.039 |
| 600 | 35.722 | 34.627 | 3.060 |
| 6E+03 | 38.324 | 36.607 | 4.480 |
| 60E+03 | 40.692 | 37.524 | 7.780 |
| 600E+03 | 38.061 | 34.661 | 8.930 |

Parameters indicated in the tables match acceptably with the finite element results with an error less than 3% up to 6 kHz frequency and a maximum error of 9.4% at 600 kHz. It can be observed that the difference in the two methods increase with the frequency. This is due to the increase in sub-conductor width compared to the skin depth.

### 3.4.2 Performance analysis of the approach

Using the proposed approach, the cable in the example is subdivided into 1920 sub-conductors and comparisons with FEM results showed close agreement as shown in Table 3-1 and Table 3-2. In comparison, the PSEC (partial sub-conductor equivalent circuit) method proposed by Rivas [40], uses 5043 sub-conductors to model the same cable example. A maximum error of 12.5% is observed (compared to FEM results) using the PSEC method and comparatively high errors around 11% are observed at low frequencies such as 600 Hz. Therefore, it is possible to obtain higher accuracy with significantly lower number of sub-conductors with the proposed technique.

As discussed in 3.2, the selection of smaller sub-conductor sizes increases the accuracy at the cost of high computational effort. The conductors in the example are subdivided using three different numbers of sub-conductors and series impedance matrix is calculated at hundred (100) frequency points logarithmically spaced in the range 1 Hz to 1 MHz. The time required for the

calculation and the maximum difference with FEM calculation are compared in Table 3-3.

**Table 3-3 - Comparison of computation times with the proposed method**

| Total no. of sub-conductors | Time required for 100 frequency samples (Seconds) | Maximum Difference with FEM (%) |
|---|---|---|
| 1376 | 217 | 15.8 |
| 1920 | 559 | 9.5 |
| 2868 | 1391 | 6.9 |

It can be observed that the time required for the computation increases rapidly with the increase of the number of sub-conductors. However, the accuracy of the computation increases only marginally once a certain threshold number of conductors is used. For example, when number of conductors is increased from 1920 to 2868 the accuracy improvement is 3.6%, although the time consumed is more than doubled. In addition, it is observed that most of the errors occur at the high frequency extreme and the accuracy in frequencies less than 100 kHz is less than 5% for all three sub-conductor numbers (1376, 1920 and 2868) used.

When the performance enhancements discussed in Section 3.3.3 (fast matrix reduction and reduced number of sub-conductors for low frequencies) are applied to the algorithm, computation time is significantly improved as seen in Table 3-4. The number of sub-conductors used for frequencies less than 100 kHz is shown within brackets.

**Table 3-4 - Comparison of computation times with performance enhancements**

| Total no. of sub-conductors | Time required for 100 frequency samples (Seconds) | Maximum Difference with FEM (%) |
|---|---|---|
| 1376 (984)* | 82 | 15.8 |
| 1920 (1248)* | 207 | 9.5 |
| 2868 (1884)* | 542 | 6.9 |

* *The number of sub-conductors used for frequencies less than 100 kHz*

Calculation of the characteristic admittance and the propagation function at 100 frequency points is sufficient for frequency domain fitting in EMT programs such as PSCAD/EMTDC. These results indicate that this method can be used accurately and efficiently in EMT programs to model sector shaped cables.

### 3.4.3 Calculation of series impedance parameters using the non-ideal ground return

Impedances are computed considering the effect of ground using both ground subdivision and approximate formulae. Earth resistivity is assumed to be 100 Ωm. 1278 more sub-conductors are introduced in the ground subdivision method, therefore the total number of sub-conductors is increased to 3198. The corresponding plots of all parameters are shown in Figure 3-10 and Figure 3-11. It can be observed that the resistance and inductance values obtained from both the methods agree satisfactorily. The important conclusion is that the use of equation 3-11 gives an accurate value for the

ground impedance, which makes it possible to avoid the computational burden of ground subdivision.

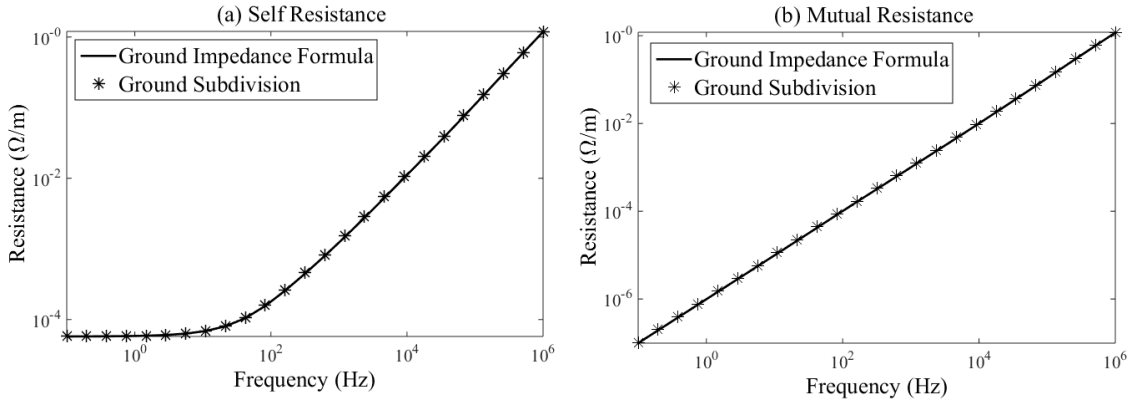


**Figure 3-10 – Comparison of resistances after the inclusion of ground**

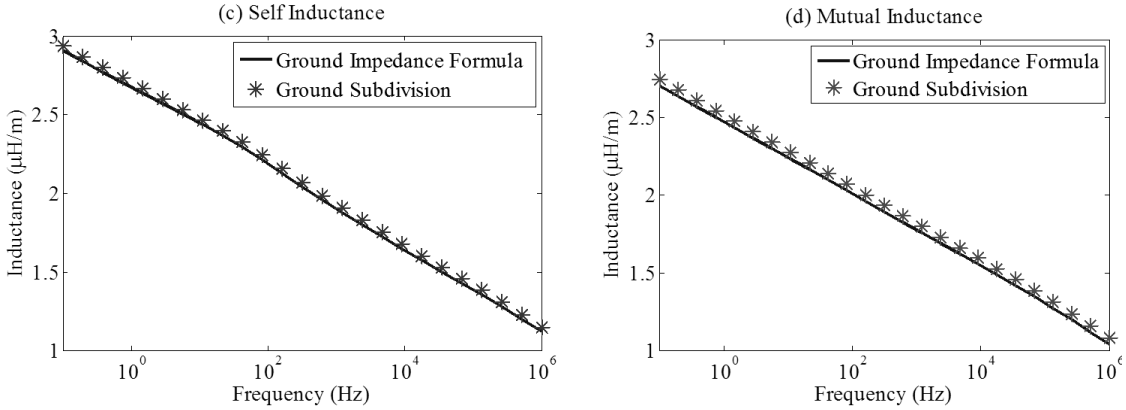


**Figure 3-11 – Comparison of inductances after the inclusion of ground**

## 3.4.4 Capacitance Calculation

As described in section 3.3.5, shunt admittance matrix can be obtained using the capacitance matrix. Simple capacitance calculation used in [61] is

compared with the more rigorous FEM based full wave analysis method in [62], which takes into account any frequency dependency. Results are shown in Table 3-5. It can be seen that the approximate capacitance values are in a close agreement with the values from full wave analysis method as the maximum difference between the values is 4.45%.

**Table 3-5 – Capacitance comparison**

| Elements of Capacitance Matrix | From Comsol at 800 kHz (nF) | From Comsol at 1 MHz (nF) | Approximate Method (nF) |
|---|---|---|---|
| $C_{11}$ | 603.73 | 595.91 | 601.23 |
| $C_{14}$ | -277.21 | -272.88 | -277.04 |
| $C_{23}$ | -160.68 | -159.79 | -162.10 |
| $C_{44}$ | 201.00 | 195.45 | 204.55 |

### 3.4.5 Frequency domain analysis of the cable using derived parameters

This section develops the frequency response characteristics of the cable based on the parameters obtained before. Similar analysis of the coaxial cable is described in [20]. The matrices *R, L* and *C* for the cable can be calculated according to the procedures mentioned in section 3.3. The influence of shunt conductance, *G* is assumed to be very small and therefore neglected. It is then possible to formulate *Z* and *Y* matrices for the cable at any given frequency up to 1 MHz. Once *Z* and *Y* are obtained, propagation coefficients of the four natural modes are computed using the eigenvalues of $\sqrt{(ZY)}$. Then, the attenuations and Mode Velocities for the modes can be found as follows:

$$\text{Attenuation Coefficient}, \alpha = \text{Re}\{\gamma\} \quad \textbf{3-16}$$

$$\text{Phase Coefficient}, \beta = \text{Im}\{\gamma\} \quad \textbf{3-17}$$

$$\text{Mode Velocity}, v = \frac{\omega}{\beta}$$

Where $\gamma$ is propagation coefficient and $\omega$ is angular velocity in rad/s.

*Mode identification*

Attenuation and mode velocity of all the nodes are plotted against frequency in Figure 3-12 and Figure 3-13. Mode 'a' in the two figures can be identified as a zero sequence mode with relatively high attenuation and very low velocity. The modes 'c' and 'd' can be identified as inter-conductor modes as their modal attenuation and velocity characteristics are almost identical. The remaining mode b should be a sheath-to-conductor mode (coaxial mode) and it is energized by injecting a current into sheath and extracting it from inner three conductors.

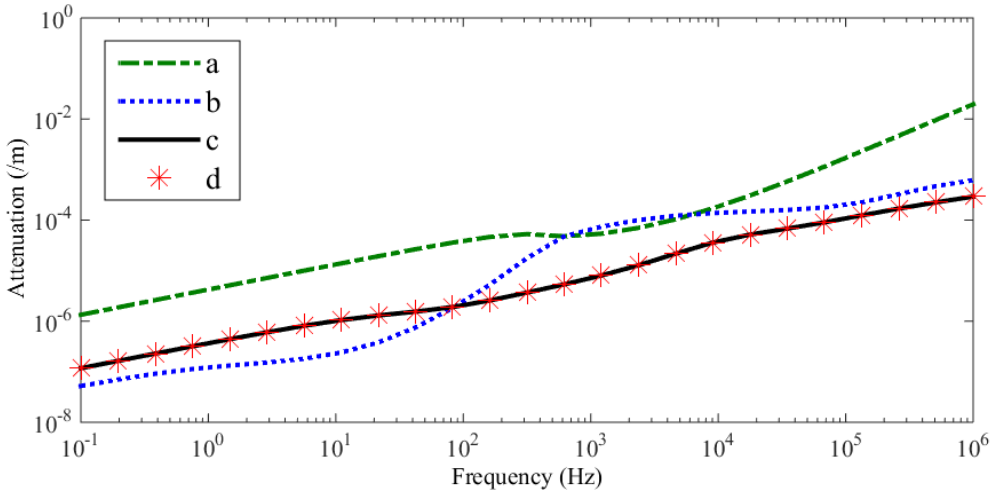


**Figure 3-12 – Mode attenuation characteristics**

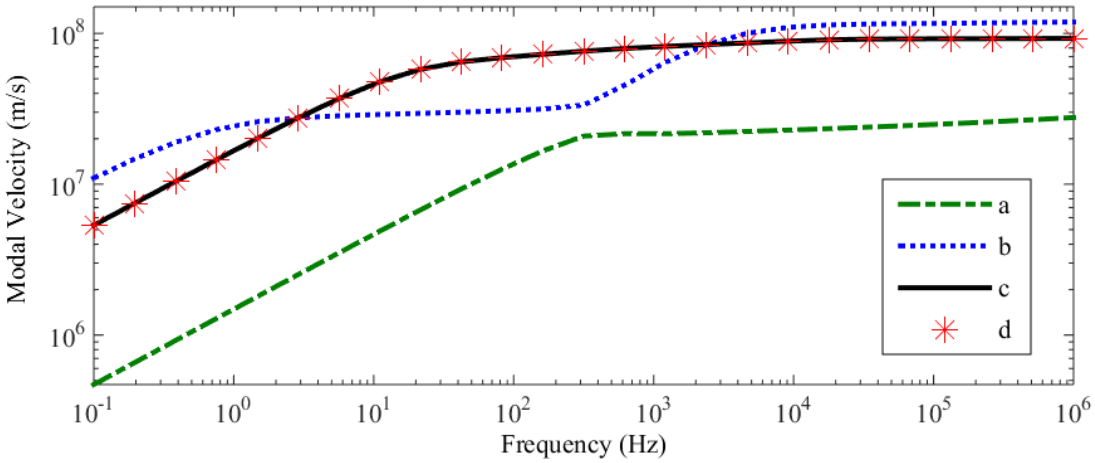


**Figure 3-13 – Modal velocity characteristics**

The mode distribution vectors for current at 1 MHz is shown in Table 3-6, which confirms the original identification of the modes. For example, mode 'a' in Table 3-6, has only a sheath current, for it is the ground mode. Modes 'c' and 'd' have currents distributed within inner conductors, while mode 'b' (coaxial mode) has equal currents in inner conductors and returning them through the sheath.

**Table 3-6 – Mode distribution vectors for current**

| Mode | | a | b | c | d |
|---|---|---|---|---|---|
| Attenuation (dB/m) | | 0.1739 | 0.0054 | 0.0025 | 0.0025 |
| Velocity (km/ms) | | 28.399 | 118.85 | 92.528 | 92.532 |
| Mode distribution vectors | Conductor 1 | 0.0000 | -0.2884 | 0.7776 | -0.2480 |
| | Conductor 2 | 0.0000 | -0.2886 | -0.6029 | -0.5494 |
| | Conductor 3 | 0.0000 | -0.2889 | -0.1744 | 0.7971 |
| | Sheath | 1.0000 | 0.8661 | -0.0003 | -0.0003 |

### 3.4.6 Time domain analysis of the cable

After the frequency domain model development, the admittance and propagation characteristics are fitted with rational functions using the method of vector fitting [63] in a EMT-type software (PSCAD/EMTDC) and a time domain simulation is carried out. Figure 3-14 shows the set up used to implement the proposed method in time domain. Termination resistance, $Z_L$ of 10 Ω is used. Inner conductors are denoted by $C_1$, $C_2$ and $C_3$ and sheath by $C_4$. Conductor $C_1$ is energized with a 1 kV voltage step.

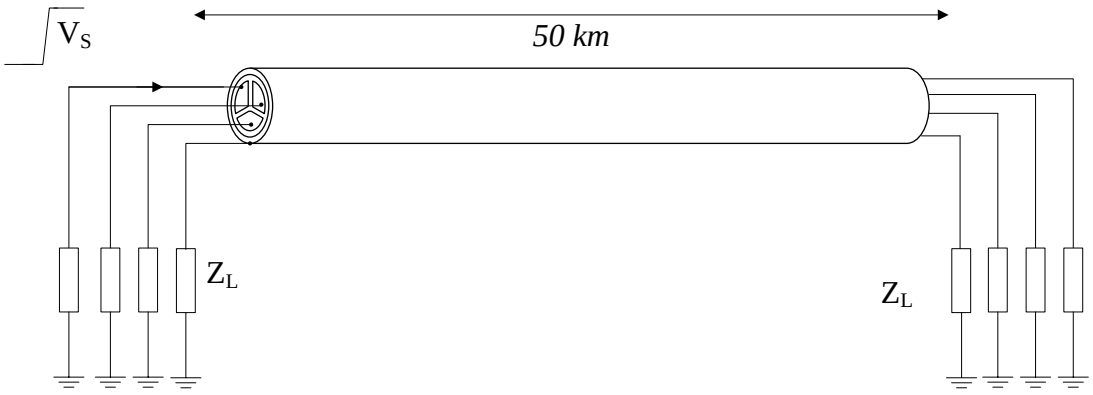


**Figure 3-14 – Cable termination network for time domain simulations**

Then, both the sending-end current and the receiving-end voltage of $C_1$ are observed and compared with the results obtained using Numerical Inverse Laplace Transform (NILT) of the frequency domain equations. Figure 3-15 and Figure 3-16 show the two methods are in close agreement, thereby confirming that the time domain model is accurate.

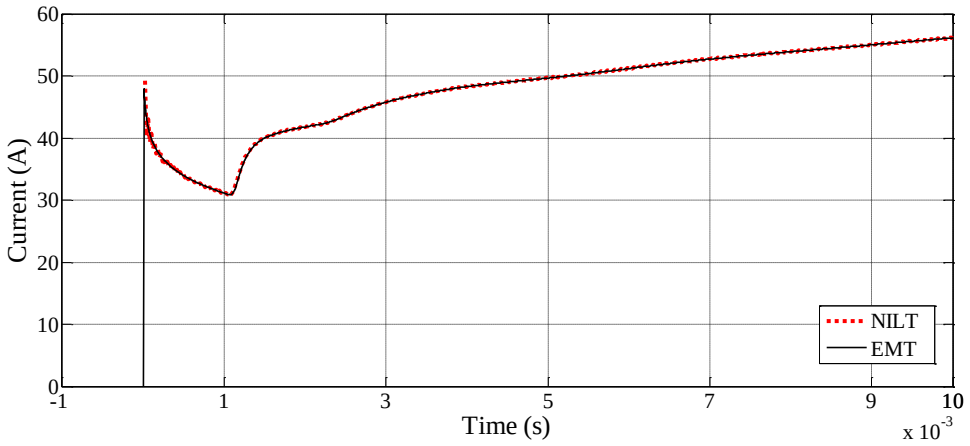


**Figure 3-15 – Sending-end current**

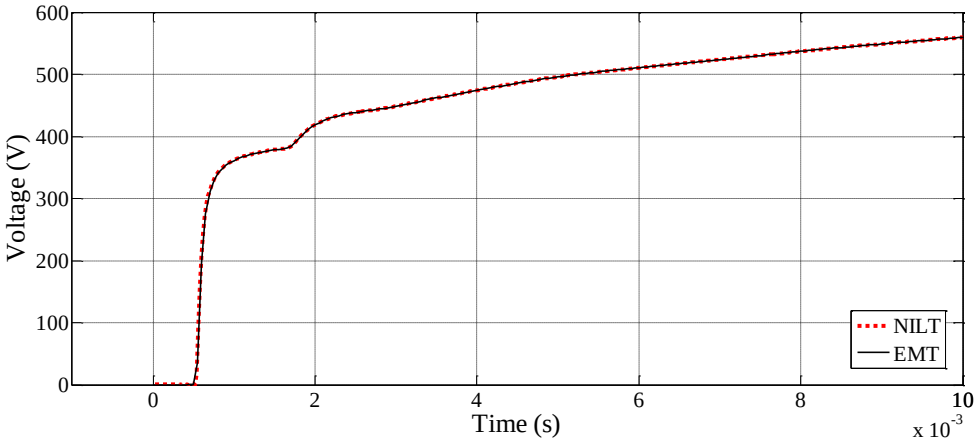


**Figure 3-16 – Receiving-end voltage**

This chapter introduces a novel technique to model sector-shaped cables in EMT programs. The introduced parameter calculation method extends the applicability of the elemental sub-conductor technique, which is hitherto used for circular conductor shapes. This method is validated with accurate FEM results for a range of frequencies. This technique is then implemented in an EMT type program and time domain results are validated using NILT method.

# Chapter 4

# Accurate Frequency Domain modelling of Cascaded Transmission Systems

## 4.1 Introduction

Cascaded power transmission systems such as cross-bonded cables (shown in Figure 4-1) are increasingly being used in modern power systems [54]. In many time domain simulations, each transmission line segment of a cascaded power transmission system needs to be modelled separately [53].

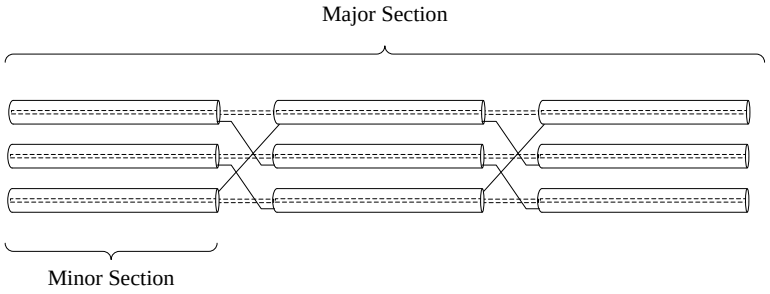


**Figure 4-1 - Segment of a fully cross-bonded cable system**

Fitting errors can be significant in the models of such transmission systems as they accumulate with the increased number of segments. Therefore, these

transmission line models should be properly validated before using them in time domain simulations. Field measurements can be used as an accurate validation method [56]. However, field measurements are not available for most scenarios and the frequency domain (FD) solution based techniques have to be adopted for EMT model validation.

For simple uniform transmission lines, the FD solution can be readily obtained using the characteristic admittance, *Yc* and the propagation function, *A*. To obtain the FD solution of cascaded transmission systems, ABCD parameter matrix (chain parameters) based frequency domain techniques have been used in [54]. This technique shows numerical inaccuracies when used with high number of cascaded segments and some simplified frequency domain solutions are available in literature [66], [67]. This chapter introduces an approach for improving the FD models for cross-bonded cables and transposed T-lines. This model can be converted to time domain and use to validate EMT models of cascaded transmission lines.

## 4.2 Frequency domain modelling using ABCD parameters

The ABCD parameter matrix is commonly used to represent cascaded systems. As shown in equation 4-1, the ABCD parameter matrix is used to

relate the voltage and current at terminal *k* to those of terminal *m*, in a two port network with terminals *k* and *m*:

$$\begin{bmatrix} V_m \\ I_m \end{bmatrix} = \begin{bmatrix} A & B \\ C & D \end{bmatrix} . \begin{bmatrix} V_k \\ I_k \end{bmatrix} \quad \textbf{4-1}$$

ABCD parameters of *n* cascaded systems can be easily derived as in 4-2, when the ABCD parameters of each system are known.

$$\begin{bmatrix} A & B \\ C & D \end{bmatrix}_{TOTAL} = \prod_{i=n}^{1} \begin{bmatrix} A & B \\ C & D \end{bmatrix}_{sys,i} \quad \textbf{4-2}$$

The chain parameter matrix provides the ABCD parameters of a homogenous transmission line segment its [66] as in 4-3:

$$\begin{bmatrix} A & B \\ C & D \end{bmatrix}_{tline} = \begin{bmatrix} Cosh(\gamma L) & Z_c Sinh(\gamma L) \\ Y_c Sinh(\gamma L) & \{Cosh(\gamma L)\}^T \end{bmatrix} \quad \textbf{4-3}$$

Where $Y_c$ is the characteristic admittance and $Z_c$ is the characteristic impedance; $\gamma$ is the propagation constant and $L$ the line length. When evaluating the ABCD parameters of a cascaded transmission system, each transmission line segment as well as the transpositions has to be taken into consideration. Figure 4-2 shows the types of sheath transpositions, T1 and T2 of a cross-bonded cable system.

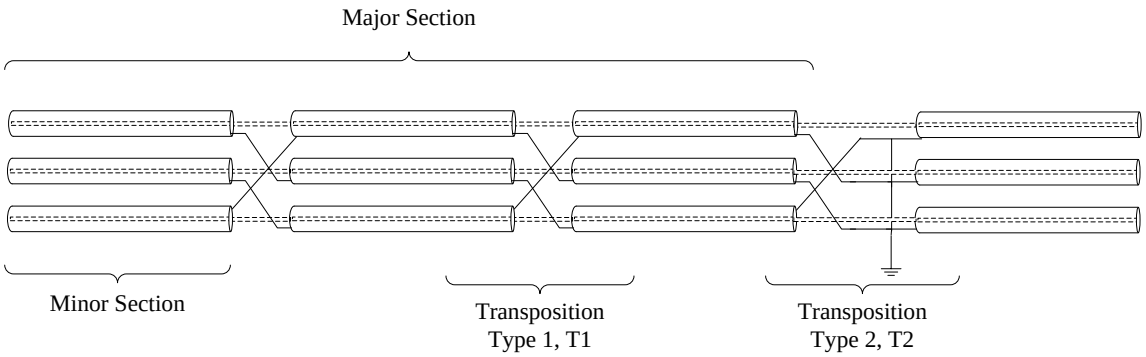


**Figure 4-2 – Sheath transposition types of a fully cross-bonded cable system**

The ABCD parameters of the transposition type 1 (T1) can be evaluated in terms of a transposition matrix and an impedance of the lead (wire). For transposition type 2 (T2) a grounding admittance is also included in its ABCD parameters. The FD solution can be obtained from the composite ABCD matrix for the cascaded transmission system. Equation 4-4 is used to obtain the ABCD matrix for a major section in terms of the ABCD matrices of the minor sections and transposition locations.

$$\begin{bmatrix} A & B \\ C & D \end{bmatrix}_{maj} = \begin{bmatrix} A & B \\ C & D \end{bmatrix}_{T2} \cdot \begin{bmatrix} A & B \\ C & D \end{bmatrix}_{\min} \cdot \begin{bmatrix} A & B \\ C & D \end{bmatrix}_{T1} \cdot \begin{bmatrix} A & B \\ C & D \end{bmatrix}_{\min} \cdot \begin{bmatrix} A & B \\ C & D \end{bmatrix}_{T1} \cdot \begin{bmatrix} A & B \\ C & D \end{bmatrix}_{\min} \quad \textbf{4-4}$$

It has been observed that the use of chain parameters to obtain the FD solution of cross bonded cables poses numerical inaccuracies due to the poor eigen structure [66]. The reason for this is that the A, D sub-matrices are ratios while B and C are impedances and admittances respectively. With a large number of cascaded systems, the ratio between the largest and the smallest element grow rapidly resulting in an ill-conditioned matrix.

A simple two conductor system example in Figure 4-3 is used to demonstrate the numerical issues related to the ABCD parameter method.

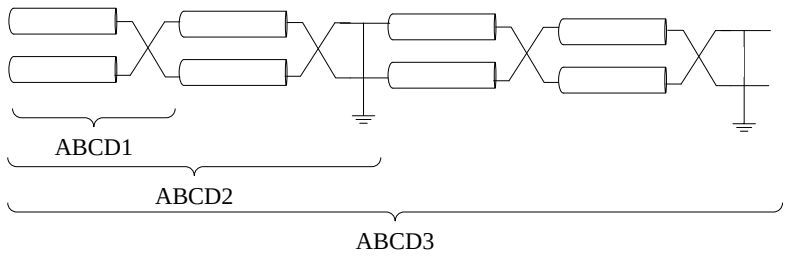


**Figure 4-3 – ABCD parameters of different cascaded segments of a simple cable system**

ABCD1, ABCD2 and ABCD3 represent the ABCD parameters of the three cable sections. The magnitude ratio of the largest eigenvalue to the smallest eigenvalue is calculated for ABCD1, ABCD2 and ABCD3 and listed in Table 4-1.

**Table 4-1 – Eigenvalue ratios for each cascaded segment**

| Cascaded Cable section | Ratio of largest and the smallest eigenvalues |
|---|---|
| ABCD1 | 1.0144 |
| ABCD2 | $6.8556 \times 10^{8}$ |
| ABCD3 | $1.5388 \times 10^{17}$ |

It can be seen that even with four cascaded segments, ratio of the largest eigenvalue to the smallest eigenvalue gets extremely high. This behaviour is the reason for the poor numerical performance of ABCD parameter method.

There are several reduced order solutions [66], [67] to validate cross bonded cables based on the simplifying the *Y* parameter matrix of a major section to have an equivalent sheath. Unlike the ABCD parameter method, these are numerically stable; however, the identity of minor sections is lost as they derive a simplified representation for a major section. These methods are not capable of obtaining individual sheath currents and voltages, due to the reduction in matrix order. In addition, these techniques require each transmission line segment to have the same characteristic admittance and same length. The proposed approach does not have the above constraints. Also it will be shown in the following sections that the numerical accuracy of the approach is maintained even with high number of cascaded segments.

## 4.3 The proposed approach

In the proposed approach, an equivalent two-terminal frequency domain representation for the cascaded transmission system is generated, whose form is similar to that of a two-terminal transmission line without any cross bonding or transpositions.

### 4.3.1 Frequency domain model of the homogenous transmission system

The FD model of a homogenous transmission line [4] is given in 4-5, in terms of voltages and currents at sending (*k*) and receiving end (*m*) terminals *($V_k$, $V_m$, $I_k$* and *$I_m$)*, characteristic admittance *($Y_c$)* and propagation function *(A)*.

$$\begin{aligned} I_k &= Y_c V_k - A\left(I_m + Y_c V_m\right) \\ I_m &= Y_c V_m - A\left(I_k + Y_c V_k\right) \end{aligned} \qquad \textbf{4-5}$$

Where,

$$\begin{aligned} Y_c &= \sqrt{(Y \cdot Z)^{-1}} \cdot Y \\ A &= e^{-\sqrt{Y \cdot Z} \cdot l} \end{aligned} \qquad \textbf{4-6}$$

*Y* and *Z* are the shunt admittance and series impedance matrices per unit length. *l* is the line length. It should be noted that these are matrix functions and they are calculated using standard spectral decomposition techniques [70]. This model can be represented using forward and backward travelling waves [71] at the terminals as in equations 4-7 and 4-8;

$$\begin{aligned} I_k^b &= A \cdot I_m^b \\ I_m^f &= A \cdot I_k^f \end{aligned} \qquad \textbf{4-7}$$

Where,

$$
\begin{aligned}
I_k^f &= \frac{1}{2}\left(I_k + Y_c V_k\right) \\
I_m^f &= \frac{1}{2}\left(-I_m + Y_c V_m\right) \\
I_k^b &= \frac{1}{2}\left(I_k - Y_c V_k\right) \\
I_m^b &= -\frac{1}{2}\left(I_m + Y_c V_m\right)
\end{aligned}
\qquad \textbf{4-8}
$$

## 4.3.2 Proposed model of a cascaded transmission system

The Figure 4-4 shows a cascaded transmission system with *N* segments.

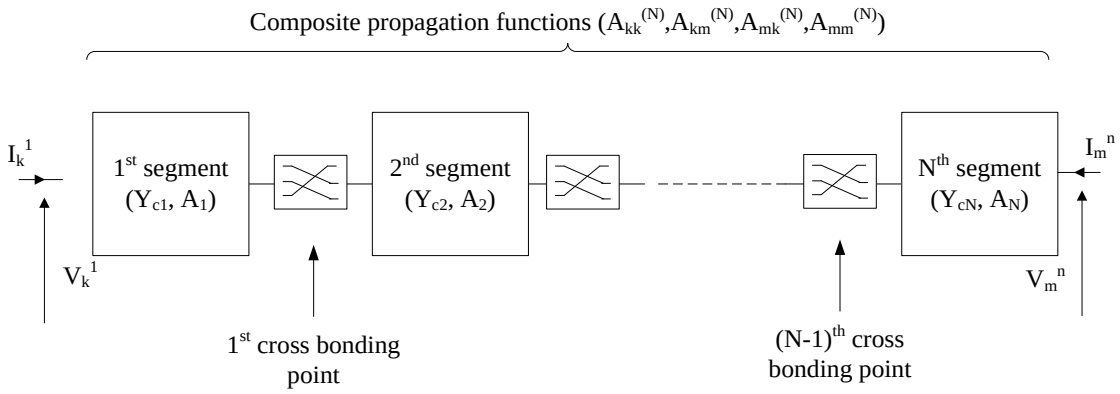


**Figure 4-4 - Cascaded transmission systems with *N* segments**

The proposed FD model consists of the characteristic admittances ($Y_{c1}$, $Y_{cN}$) of the first and N$^{th}$ cascaded segments and four composite propagation functions ($A_{kk}, A_{km}, A_{mk}, A_{mm}$) as in 4-9.

$$
\begin{aligned}
I_k &= Y_{c1}V_k - A_{kk}\left(I_k + Y_{c1}V_k\right) - A_{km}\left(I_m + Y_{cN}V_m\right) \\
I_m &= Y_{cN}V_m - A_{mk}\left(I_k + Y_{c1}V_k\right) - A_{mm}\left(I_m + Y_{cN}V_m\right)
\end{aligned}
\qquad \textbf{4-9}
$$

The proposed method develops the composite propagation matrices given in 4-9 and 4-11 in sequential steps by adding one section at a time. These

propagation functions can be assembled in an iterative manner as shown below.

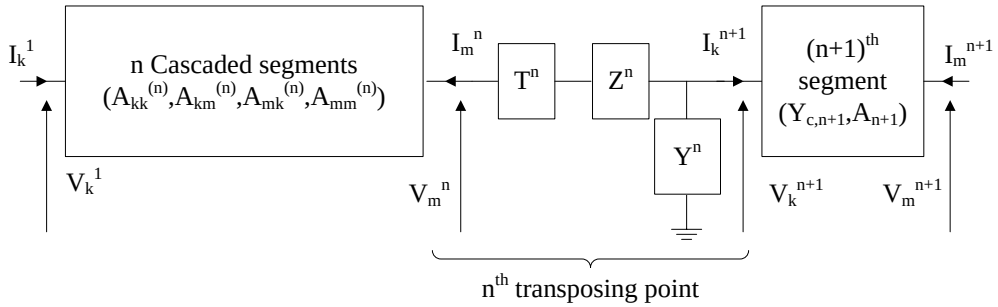


**Figure 4-5 - Connection of (n+1) cascaded transmission systems**

Figure 4-5 illustrates the connection of $(n+1)^{th}$ transmission segment to a cascaded transmission system with n segments. The $n^{th}$ transposing point is represented by the transposing matrix, $T^n$, the lead impedance, $Z^n$ and the grounding admittance $Y^n$. If the composite propagation functions, $A_{kk}^{(n)}, A_{mk}^{(n)}, A_{km}^{(n)}$ and $A_{mm}^{(n)}$ are known for n cascaded transmission segments, the composite propagation functions for n+1 cascaded segment are given as follows:

$$\begin{bmatrix} A_{kk}^{(n+1)} & A_{km}^{(n+1)} \\ A_{mk}^{(n+1)} & A_{mm}^{(n+1)} \end{bmatrix} = \begin{bmatrix} A_{kk}^{(n)} - Q_{11}Q_{21}^{-1}A_{mk}^{(n)} & Q_{12}A_{n+1} - Q_{11}Q_{21}^{-1}Q_{22}A_{n+1} \\ A_{n+1}Q_{21}^{-1}A_{mk}^{(n)} & A_{n+1}Q_{21}^{-1}Q_{22}A_{n+1} \end{bmatrix} \quad \textbf{4-10}$$

Where,

$$\begin{bmatrix} Q_{11} & Q_{12} \\ Q_{21} & Q_{22} \end{bmatrix} = \begin{bmatrix} 0 & A_{km}^{(n)} \\ I & -A_{mm}^{(n)} \end{bmatrix} \cdot Tr^{-1} \cdot \begin{bmatrix} I + Y^n Y_c^{-1} & I - Y^n Y_c^{-1} \\ Y_c^{-1} & -Y_c^{-1} \end{bmatrix}$$

$$Tr = \begin{bmatrix} T^n & T^n{}_1 \\ T^n Y_c^{-1} - Z^n T^n & -T^n Y_c^{-1} - Z^n T^n \end{bmatrix}$$

The procedure of obtaining the four composite propagation functions $A_{kk}, A_{mk}, A_{km}, A_{mm}$ is described in the proof of the approach given in the following section (Section 4.4). The forward and backward travelling wave notation (given in 4-8) can be used to represent this model as follows:

$$\begin{aligned} I_k^b &= -A_{kk} I_k^f + A_{km} I_m^b \\ I_m^f &= -A_{mk} I_k^f - A_{mm} I_m^b \end{aligned} \qquad \textbf{4-11}$$

This formation is similar to the equations 4-5 and 4-7 which describes the model of a homogenous transmission line. However, this formulation utilizes four composite propagation functions and it can handle separate characteristic admittances for each transmission line segment and. If this model is applied to a homogenous line, the propagation functions, $A_{kk}$ and $A_{mm}$ become zero and $A_{km}$ equals to $A_{mk.}$ Therefore, the model degenerates to equation 4-7 of the homogenous line.

## 4.4 Proof of the approach

The proposed FD model can be proved using mathematical induction. First, the model is proved to be accurate for one transmission line segment. Then, it is assumed that the model is correct for $n$ cascaded segments and using that a model for ($n$+*1*) segments is derived.

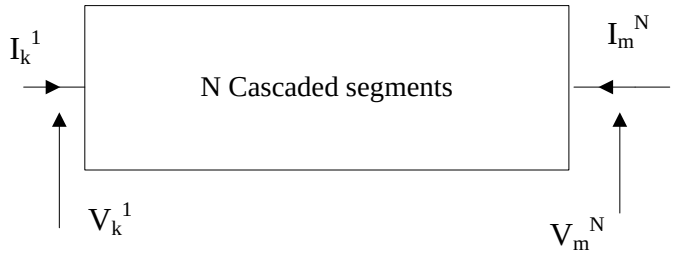


**Figure 4-6 - Terminal currents and voltages of N cascaded transmission line segments**

*Theorem*

Given a cable with N number of cascaded transmission segments, the FD equations can be represented in the form:

$$\begin{aligned} I_k^1 &= Y_{c1}V_k^1 - A_{kk}^{(N)}\left(I_k^1 + Y_{c1}V_k^1\right) - A_{km}^{(N)}\left(I_m^N + Y_{cN}V_m^N\right) \\ I_m^N &= Y_{cN}V_m^N - A_{mk}^{(N)}\left(I_k^1 + Y_{cN}V_k^1\right) - A_{kk}^{(N)}\left(I_m^N + Y_{cN}V_m^N\right) \end{aligned} \qquad \textbf{4-12}$$

Alternatively, similar to the homogenous line (equation 4-7), the equivalent form of this is given in terms of forward and backward travelling waves as:

$$\begin{bmatrix} I_k^{b,1} \\ I_m^{f,N} \end{bmatrix} = \begin{bmatrix} -A_{kk}^{(N)} & A_{km}^{(N)} \\ A_{mk}^{(N)} & -A_{mm}^{(N)} \end{bmatrix} \begin{bmatrix} I_k^{f,1} \\ I_m^{b,N} \end{bmatrix} \qquad \textbf{4-13}$$

Where,

$$I_k^{f,1} = \frac{1}{2}\left(I_k^1 + Y_{c1}V_k^1\right), \quad I_k^{b,1} = \frac{1}{2}\left(I_k^1 - Y_{c1}V_k^1\right)$$
$$I_m^{f,N} = \frac{1}{2}\left(-I_m^N + Y_{cN}V_k^N\right) \quad I_m^{b,N} = -\frac{1}{2}\left(I_m^N + Y_{cN}V_k^N\right)$$

$I_k^{f,1}$ and $I_m^{f,N}$ are the forward travelling waves at the sending and receiving-end terminals of the entire line. Similarly, $I_b^{f,1}$ and $I_b^{f,N}$ are the backward travelling waves at the sending and receiving-end terminals.

*The proof by mathematical induction*

*Proof for N=1*

For N = 1, the cascaded transmission system consists of only one section. Hence, the statement of the theorem 4-13 becomes:

$$\begin{bmatrix} I_k^{b,1} \\ I_m^{f,1} \end{bmatrix} = \begin{bmatrix} \bar{0} & A \\ A & \bar{0} \end{bmatrix} . \begin{bmatrix} I_k^{f,1} \\ I_m^{b,1} \end{bmatrix} \qquad \textbf{4-14}$$

As the single section is a homogenous transmission line by itself, equation 4-14 follows directly from the model of homogenous transmission line given in 4-5 and 4-7 can be applied. This is a special case of 4-13 where,

$$Y_{c1} = Y_{cN} = Y_c, A_{kk}^{(N)} = A_{mm}^{(N)} = 0 \; and \; A_{km}^{(N)} = A_{mk}^{(N)} = A$$

Therefore, the theorem is true for N=1.

*Inductive Step*

In this step, the theorem is assumed true for N = n, which means that it holds true for the cascaded transmission line system with n sections. With a new segment appended as shown in Figure 4-7, the theorem is proven to be true for N = n+1.

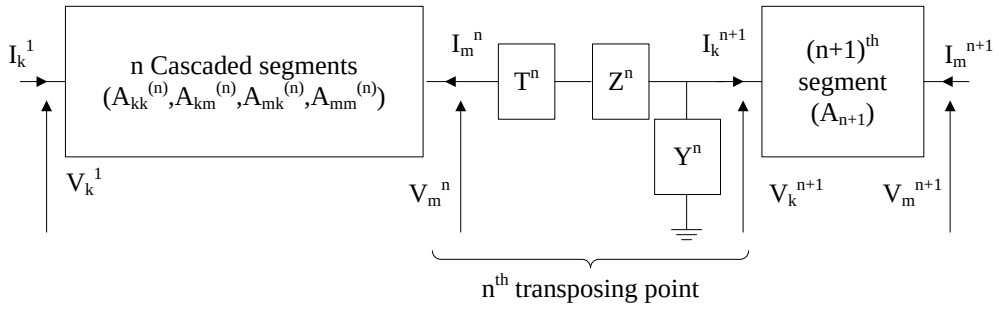


**Figure 4-7 - $(n+1)^{th}$ segment connection to cascaded system with n segments**

As the theorem is assumed to be correct for N = n, equation 4-13 is valid and can be written as follows:

$$\begin{bmatrix} I_k^{b,1} \\ I_m^{f,n} \end{bmatrix} = \begin{bmatrix} -A_{kk}^{(n)} & A_{km}^{(n)} \\ A_{mk}^{(n)} & -A_{mm}^{(n)} \end{bmatrix} \begin{bmatrix} I_k^{f,1} \\ I_m^{b,n} \end{bmatrix} \quad \textbf{4-15}$$

This can be rearranged for convenience as follows:

$$\begin{bmatrix} I_k^{b,1} \\ 0 \end{bmatrix} = \begin{bmatrix} -A_{kk}^{(n)} & 0 \\ -A_{mk}^{(n)} & 0 \end{bmatrix} \begin{bmatrix} I_k^{f,1} \\ 0 \end{bmatrix} + \begin{bmatrix} 0 & A_{km}^{(n)} \\ I & A_{mm}^{(n)} \end{bmatrix} \begin{bmatrix} I_m^{f,n} \\ I_m^{b,n} \end{bmatrix} \quad \textbf{4-16}$$

As the appended segment ((n+1)$^{th}$ segment) is a single homogenous line, it can be represented with equation 4-7. This can be rearranged and written in matrix form as follows:

$$\begin{bmatrix} I_k^{f,n+1} \\ I_k^{b,n+1} \end{bmatrix} = \begin{bmatrix} (A_{n+1})^{-1} & 0 \\ 0 & A_{n+1} \end{bmatrix} \begin{bmatrix} I_m^{f,n+1} \\ I_m^{b,n+1} \end{bmatrix} \quad \textbf{4-17}$$

The voltages and currents of the n cascaded segments and the (n+1)$^{th}$ segment are related in terms of the matrix, $T^n$ which represents transpositions, lead impedance, $Z^n$ and grounding admittance $Y^n$ as shown in equation 4-18:

$$\begin{aligned} T^n I_m^n + I_k^{n+1} + Y^n V_k^{n+1} &= 0 \\ V_k^n - T^n V_m^n &= Z^n T^n I_m^n \end{aligned} \quad \textbf{4-18}$$

The above follows directly from Kirchhoff's current law and Kirchhoff's voltage law. The terminal voltages and currents in 4-18 can be substituted

from forward and backward travelling waves at the terminals, given in 4-16 as follows:

$$\begin{aligned} &-T^n\left(I_m^{f,n}+I_m^{b,n}\right)+\left(I_k^{f,n+1}+I_k^{b,n+1}\right)+Y^nY_{c,n+1}^{-1}\left(I_k^{f,n+1}-I_k^{b,n+1}\right)=0 \\ &Y_{c,n+1}^{-1}\left(I_k^{f,n+1}-I_k^{b,n+1}\right)-T^nY_{c,n}^{-1}\left(I_m^{f,n}-I_m^{b,n}\right)=-Z^nT^n\left(I_m^{f,n}+I_m^{b,n}\right) \end{aligned} \quad \textbf{4-19}$$

Equation 4-19 can be rearranged and written in matrix form,

$$\begin{bmatrix} T^n & T^n \\ T^nY_{c,n}^{-1}-Z^nT^n & -T^nY_{c,n}^{-1}-Z^nT^n \end{bmatrix}\begin{bmatrix} I_m^{f,n} \\ I_m^{b,n} \end{bmatrix}=\begin{bmatrix} I+Y^nY_{c,n+1}^{-1} & I-Y^nY_{c,n+1}^{-1} \\ Y_{c,n+1}^{-1} & -Y_{c,n+1}^{-1} \end{bmatrix}\begin{bmatrix} I_k^{f,n+1} \\ I_k^{b,n+1} \end{bmatrix} \quad \textbf{4-20}$$

To get the relationship between the forward and backward travelling waves at terminal k of 1st segment and terminal m of (n+1)th segment, 4-16, 4-17 and 4-20 can be combined:

$$\begin{bmatrix} I_k^{b,1} \\ 0 \end{bmatrix}=\begin{bmatrix} -A_{kk}^{(n)} & 0 \\ -A_{mk}^{(n)} & 0 \end{bmatrix}\begin{bmatrix} I_k^{f,1} \\ 0 \end{bmatrix}+[Q]\begin{bmatrix} (A_{n+1})^{-1} & 0 \\ 0 & A_{n+1} \end{bmatrix}\begin{bmatrix} I_m^{f,n+1} \\ I_m^{b,n+1} \end{bmatrix} \quad \textbf{4-21}$$

Where,

$$\begin{bmatrix} Q_{11} & Q_{12} \\ Q_{21} & Q_{22} \end{bmatrix}=\begin{bmatrix} 0 & A_{km}^{(n)} \\ I & -A_{mm}^{(n)} \end{bmatrix}\cdot Tr^{-1}\cdot\begin{bmatrix} I+Y^nY_c^{-1} & I-Y^nY_c^{-1} \\ Y_c^{-1} & -Y_c^{-1} \end{bmatrix}$$

$$Tr=\begin{bmatrix} T^n & T^n{}_1 \\ T^nY_c^{-1}-Z^nT^n & -T^nY_c^{-1}-Z^nT^n \end{bmatrix}$$

Equation 4-21 can be rearranged to get the following form:

$$\begin{bmatrix} I_k^{b,1} \\ I_m^{f,n+1} \end{bmatrix}=\begin{bmatrix} Q_{11}Q_{21}^{-1}A_{mk}^{(n)}-A_{kk}^{(n)} & Q_{12}A_{n+1}-Q_{11}Q_{21}^{-1}Q_{22}A_{n+1} \\ A_{n+1}Q_{21}^{-1}A_{mk}^{(n)} & -A_{n+1}Q_{21}^{-1}Q_{22}A_{n+1} \end{bmatrix}\begin{bmatrix} I_k^{f,1} \\ I_m^{b,n+1} \end{bmatrix} \quad \textbf{4-22}$$

Therefore, for $N = n+1$;

$$\begin{bmatrix} I_k^{b,1} \\ I_m^{f,n+1} \end{bmatrix} = \begin{bmatrix} -A_{kk}^{(n+1)} & A_{km}^{(n+1)} \\ A_{mk}^{(n+1)} & -A_{mm}^{(n+1)} \end{bmatrix} \begin{bmatrix} I_k^{f,1} \\ I_m^{b,n+1} \end{bmatrix} \quad \textbf{4-23}$$

Where,

$$\begin{bmatrix} A_{kk}^{(n+1)} & A_{km}^{(n+1)} \\ A_{mk}^{(n+1)} & A_{mm}^{(n+1)} \end{bmatrix} = \begin{bmatrix} A_{kk}^{(n)} - Q_{11}Q_{21}^{-1}A_{mk}^{(n)} & Q_{12}A_{n+1} - Q_{11}Q_{21}^{-1}Q_{22}A_{n+1} \\ A_{n+1}Q_{21}^{-1}A_{mk}^{(n)} & A_{n+1}Q_{21}^{-1}Q_{22}A_{n+1} \end{bmatrix}$$

The composite propagation functions given in the equation 4-23 are corresponding to entire (*n+1*) cascaded segments. Therefore, if the theorem holds true for the cascaded transmission line system with n sections, it is true for (n+1) sections. This proves the Theorem for all n greater than zero.

## 4.5 Voltage and current calculation of individual segments

The proposed method provides a relationship between the voltages and currents of the sending-end and receiving-end terminals of the cascaded system, as described in sections 4.3 and 4.4. In addition, this method can be used to obtain the voltages and currents of each individual segment of the cascaded system. Let us assume the voltages and currents are to be calculated at the $p^{th}$ segment of the cascaded system in addition to the overall terminal quantities. Figure 4-8 shows the $p^{th}$ segment of a cascaded system of N segments.

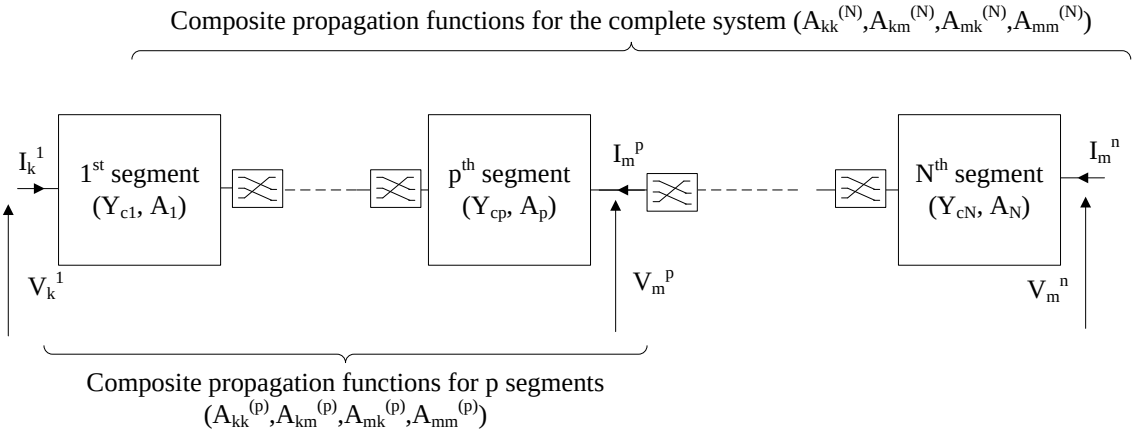


**Figure 4-8 – voltages and currents at the p$^{th}$ segment of the cascaded system**

As the propagation functions are calculated iteratively starting from a single segment as in equation 4-9, the composite propagation functions for the first p segments can be given as follows:

$$\begin{aligned} I_k^1 &= Y_{c1}V_k^1 - A_{kk}^{(p)}\left(I_k^1 + Y_{c1}V_k^1\right) - A_{km}^{(p)}\left(I_m^p + Y_{cp}V_m^p\right) \\ I_m^p &= Y_{cp}V_m^p - A_{mk}^{(p)}\left(I_k^1 + Y_{c1}V_k^1\right) - A_{mm}^{(p)}\left(I_m^p + Y_{cp}V_m^p\right) \end{aligned} \quad \textbf{4-24}$$

Similarly, the composite propagation functions for the complete system with N segments can be given as,

$$\begin{aligned} I_k^1 &= Y_{c1}V_k^1 - A_{kk}^{(N)}\left(I_k^1 + Y_{c1}V_k^1\right) - A_{km}^{(N)}\left(I_m^N + Y_{cp}V_m^N\right) \\ I_m^N &= Y_{cN}V_m^N - A_{mk}^{(N)}\left(I_k^1 + Y_{c1}V_k^1\right) - A_{mm}^{(N)}\left(I_m^N + Y_{cp}V_m^N\right) \end{aligned} \quad \textbf{4-25}$$

Equations 4-24 and 4-25 can be solved with the two additional equations for the terminal conditions to obtain the terminal voltages and currents as well as those of the p$^{th}$ segment.

This demonstrates that all intrinsic quantities of the individual segments are preserved in this method, and those can be readily obtained if the requirement arises.

## 4.6 Conversion to ABCD parameter representation

This method also provides an efficient and numerically accurate alternate method to obtain the ABCD parameter representation of the complete system. The ABCD parameters of the cascaded system can be obtained using the composite propagation functions of the entire system. Equation 4-9 which represents the proposed FD model can be written with all terms in the right hand side as follows:

$$\begin{aligned}\bar{0} &= Y_{c1}V_k - A_{kk}\left(I_k + Y_{c1}V_k\right) - A_{km}\left(I_m + Y_{cN}V_m\right) - I_k \\ \bar{0} &= Y_{cN}V_m - A_{mk}\left(I_k + Y_{c1}V_k\right) - A_{mm}\left(I_m + Y_{cN}V_m\right) - I_m\end{aligned} \qquad \textbf{4-26}$$

This can be written in matrix form,

$$\begin{bmatrix}\bar{0}\\ \bar{0}\end{bmatrix} = \begin{bmatrix}Y_{c1} - A_{kk}\cdot Y_{c1} & I - A_{kk}\\ -A_{mk}Y_{c1} & -A_{mk}\end{bmatrix}\cdot\begin{bmatrix}V_k\\ I_k\end{bmatrix} - \begin{bmatrix}A_{km}Y_{cN} & A_{km}\\ -\left(Y_{cN} - A_{mm}\cdot Y_{cN}\right) & I + A_{mm}\end{bmatrix}\cdot\begin{bmatrix}V_m\\ I_m\end{bmatrix} \qquad \textbf{4-27}$$

Bringing the right hand term to the left hand side and inverting we get:

$$\begin{bmatrix}V_k\\ I_k\end{bmatrix} = \begin{bmatrix}A_{km}Y_{cN} & A_{km}\\ -\left(I - A_{mm}\right)Y_{cN} & I + A_{mm}\end{bmatrix}^{-1}\begin{bmatrix}\left(I - A_{kk}\right)Y_{c1} & \left(I - A_{kk}\right)\\ -A_{mk}Y_{c1} & -A_{mk}\end{bmatrix}\cdot\begin{bmatrix}V_m\\ I_m\end{bmatrix} \qquad \textbf{4-28}$$

Equation 4-28 is in the ABCD-parameter form: Therefore, ABCD parameters of the complete system can be given as in equation 4-29:

$$\begin{bmatrix} A & B \\ C & D \end{bmatrix} = \begin{bmatrix} A_{km}Y_{cN} & A_{km} \\ -(I - A_{mm})Y_{cN} & I + A_{mm} \end{bmatrix}^{-1} \begin{bmatrix} (I - A_{kk})Y_{c1} & (I - A_{kk}) \\ -A_{mk}Y_{c1} & -A_{mk} \end{bmatrix} \quad \textbf{4-29}$$

It should be noted that, the ABCD parameters of the complete system is derived here, by converting the composite propagation functions of the system, unlike the conventional method of multiplying ABCD matrices of individual segments.

## 4.7 Verification of the proposed approach

The following case study is used to demonstrate the proposed approach. The conventional ABCD parameter method is also implemented for comparison and it will be shown that this method cannot be used with a large number of cascaded segments. A cross bonded cable with N minor sections; each having the configuration given in Figure 4-9 is used in the case study. The sheaths are transposed at each minor section. A combination of three cascaded minor sections forms a major section at which the sheaths are grounded.

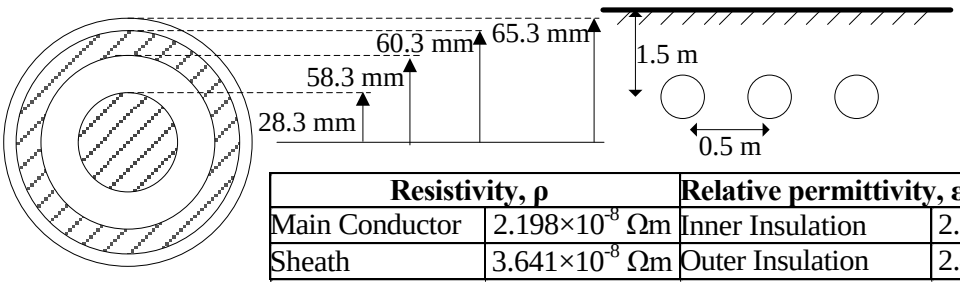


| Resistivity, ρ | | Relative permittivity, ε | |
|---|---|---|---|
| Main Conductor | $2.198\times10^{-8}$ Ωm | Inner Insulation | 2.8 |
| Sheath | $3.641\times10^{-8}$ Ωm | Outer Insulation | 2.4 |

**Figure 4-9 - Properties of a single cable section**

At each sheath transposition location, there is a series lead inductance of 0.02 mH. The grounding impedance of 1 Ω is assumed between major sections. The termination shown in Figure 4-10 is adopted for the case study. The sheaths are grounded at both terminals. On the sending-end, phase "a" is energized with a voltage step, with phases "b" and "c" grounded. On the receiving-end, all phases open circuited.

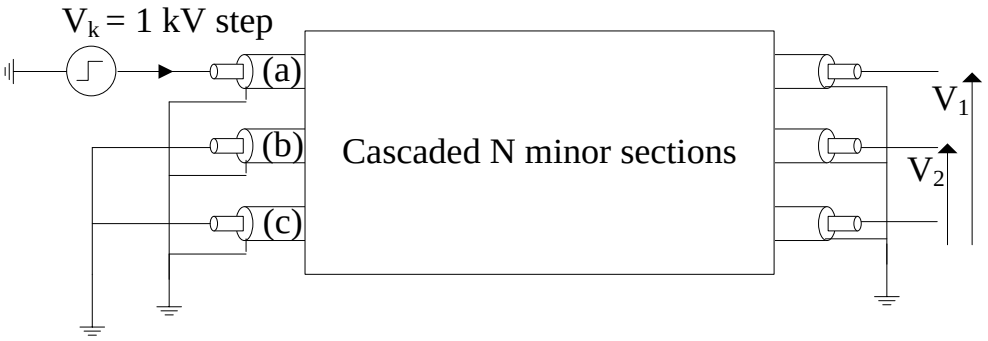


**Figure 4-10 - Termination network of the cross bonded cable**

The above configuration is used to perform detailed EMT simulations for different number of minor sections (N) with each section separately modeled. The waveforms obtained from this simulation which models the entire cable in full detail are considered as the template for comparison.

### 4.7.1 Rationale for using EMT simulation for FD model verification

The purpose of developing the FD Model is to have a model for validating EMT models which may have fitting errors. Here we seem to be doing the

opposite, i.e., EMT simulation is used to verify the proposed FD model for cascaded transmission systems. This is possible due to the difference in the types of errors in the FD models and the EMT models. The FD models such as the ABCD parameter based model are hampered by the cumulative numerical errors because of the repeated matrix multiplications. On the other hand, errors in the EMT models are of a completely different type than the numerical multiplication error and are associated with fitting a frequency domain characteristics to given data. Therefore, although this is a bit like the blind leading the blind [68], [69], we argue that the possibility of two different types of errors in the EMT and FD formulations still producing essentially the same result is highly improbable. We are therefore confident that the FD and EMT are concurrently validated.

### 4.7.2 Comparison of results

The frequency domain composite propagation functions are evaluated using the proposed technique implemented in MATLAB/SIMULINK. In addition, the conventional ABCD parameter method is also implemented to compare the numerical accuracy. The numerical inverse Laplace transform (NILT) method [48] is used to obtain time domain results from the FD solution (in both the proposed approach and the ABCD parameter approach). Figure 4-11, Figure 4-12 and Figure 4-13 show a comparison of the phase 'a' sending-end

current calculated using the EMT simulation, the proposed method and the ABCD parameters, for 6, 9 and 18 cascaded minor sections (N=6, 9 and 18), respectively.

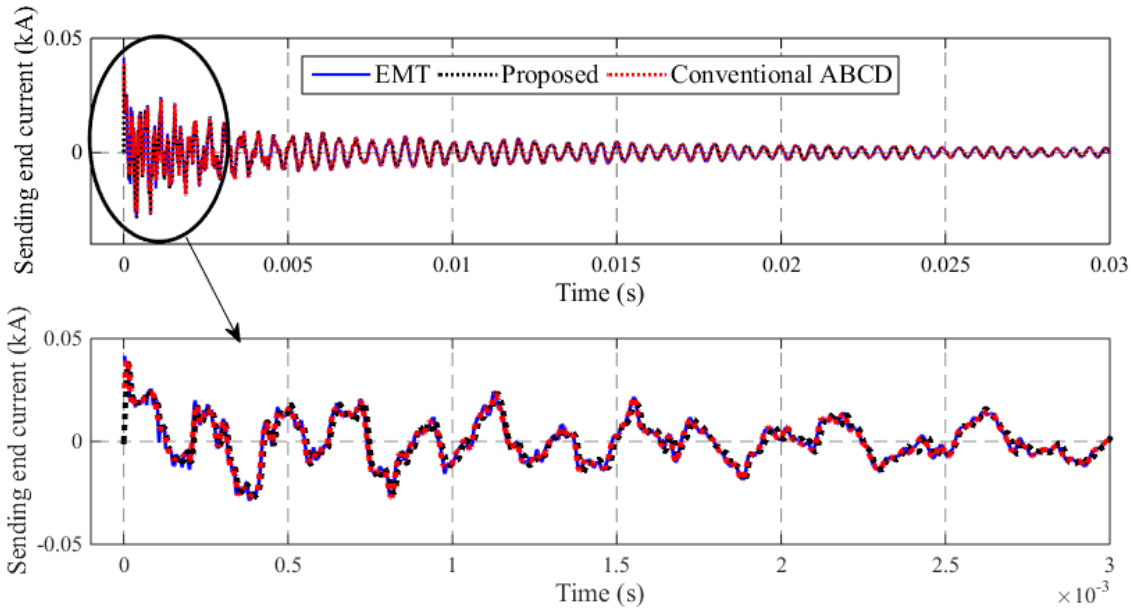


**Figure 4-11 - Comparison of sending-end current (phase 'a') N=6**

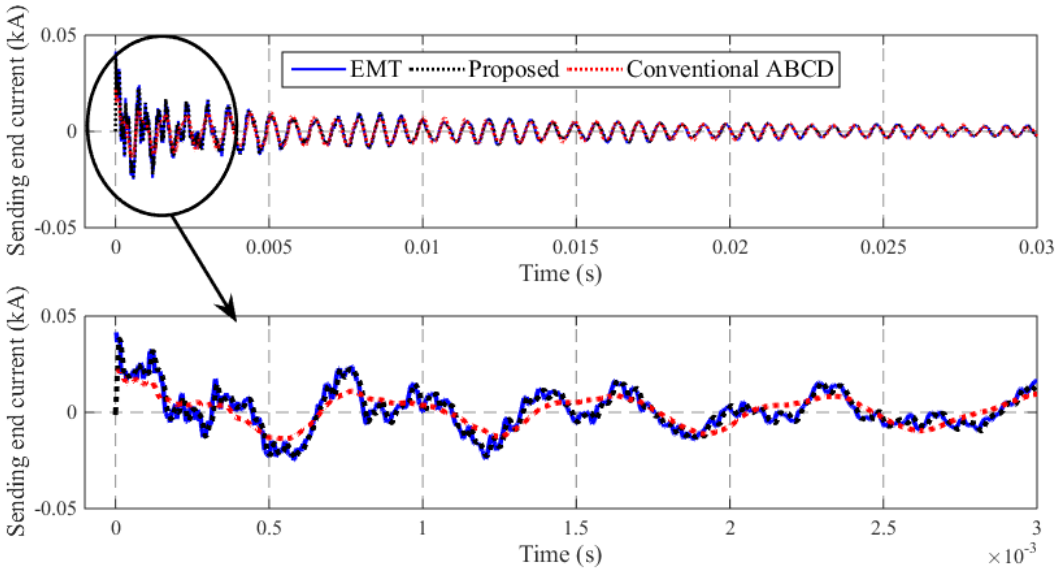


**Figure 4-12 - Comparison of sending-end current (phase 'a') N=9**

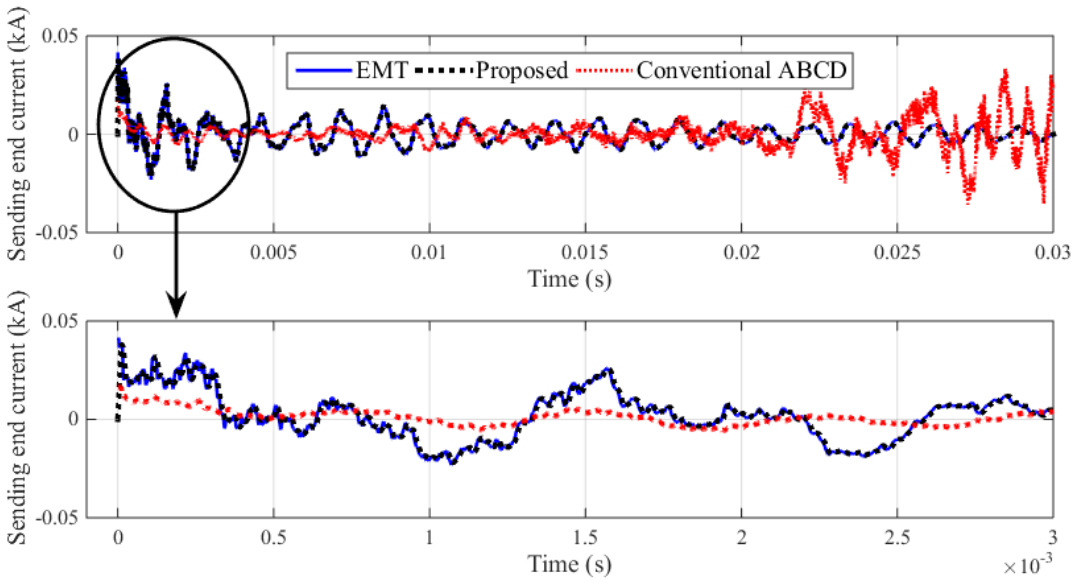


**Figure 4-13 - Comparison of sending-end current (phase 'a') N=18**

All methods agree well for N=6. When N is increased to 9, the ABCD parameter based result starts to show deviations while the proposed technique agrees with the detailed EMT results. The ABCD parameter based results become highly inaccurate with 18 minor sections whereas the proposed technique shows no such problems. This is consistent with the numerical inaccuracies of conventional ABCD based technique described in [66].

Sending-end current and receiving-end voltage comparisons with EMT results are shown for N=36 in Figure 4-14. It can be seen that the proposed technique performs well even with a high number of minor sections. Results from the conventional ABCD parameter method deviate significantly and are therefore not presented.

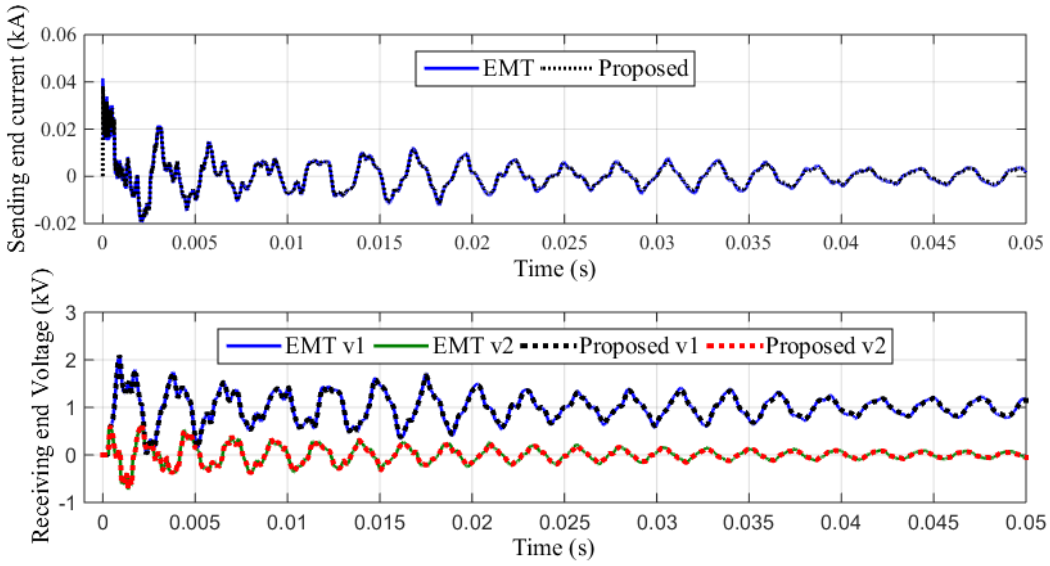


**Figure 4-14 - Comparison of sending-end current (phase 'a') and receiving-end voltages (phases 'a' and 'b') for N=36**

The composite propagation functions obtained from the proposed technique are converted to ABCD parameters in the alternate direct method introduced in section 4.6 which does not use cascaded ABCD matrix multiplications. The numerical inverse Laplace transform (NILT) method is used to obtain time domain results from the alternate ABCD based FD solution. The comparison of sending-end current with EMT results are shown for N=36 in Figure 4-15.

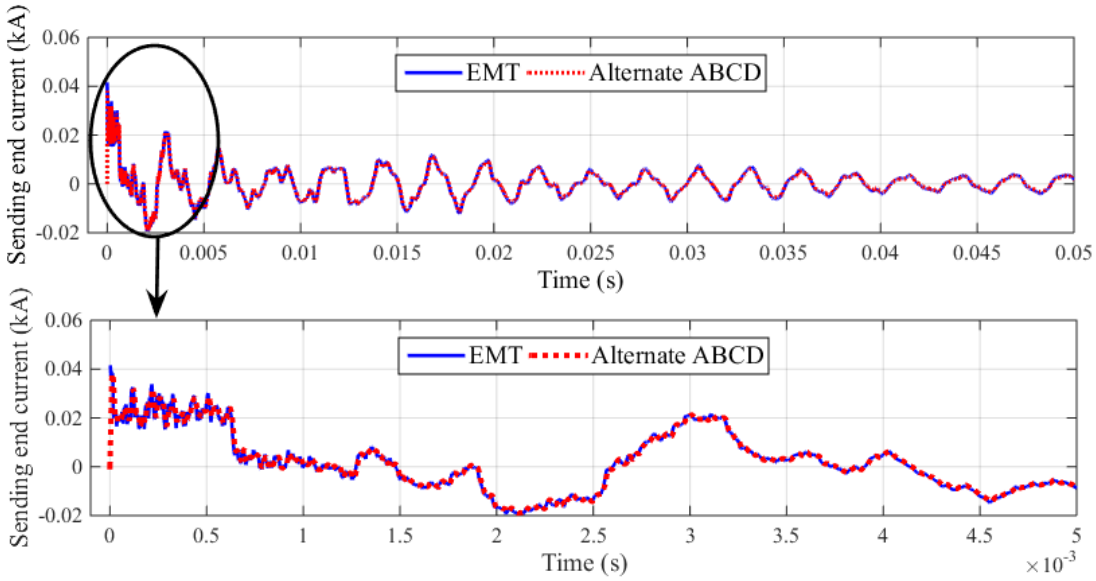


**Figure 4-15 - Comparison of sending-end current (phase 'a') with alternate ABCD parameters for N=36**

It can be seen that, the alternate method of calculating ABCD parameters based on the proposed approach maintains numerical accuracy at even large number of cascaded segments, unlike the conventional ABCD parameter method.

## 4.8 Case study - Cross bonded cable fitting error demonstration

Once an accurate FD model is developed as shown in this chapter, it can be used to verify EMT models of cascaded transmission lines .The following case study is used to demonstrate the applicability of the proposed approach to identify the EMT simulation inaccuracies due to the accumulation of fitting

errors. A cross bonded cable with 6 minor sections; each having the configuration given in Figure 4-16 is used. At each sheath transposition location, there is a series lead inductance of 0.02 mH. The grounding impedance of 1 Ω is assumed between major sections.

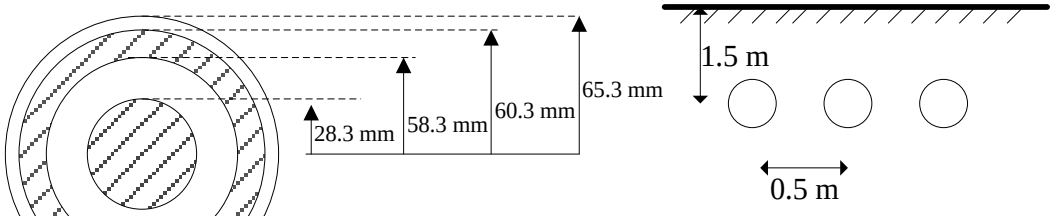


| Resistivity, ρ | | Relative permittivity, ε | |
|---|---|---|---|
| Main Conductor | $2.198\times10^{-8}$ Ωm | Inner Insulation Layer | 2.8 |
| Sheath | $3.641\times10^{-8}$ Ωm | Outer Insulation Layer | 2.4 |

**Figure 4-16 – Properties of a single cable section**

An open circuit termination is used at both sending and receiving-end as shown in Figure 4-17. The phase 'a' inner conductor of the cable system is energized at 0.1 s with a current source (having a 1 Ω shunt admittance) which ramps from 0 to 1 kA within 200 μs and then saturates.

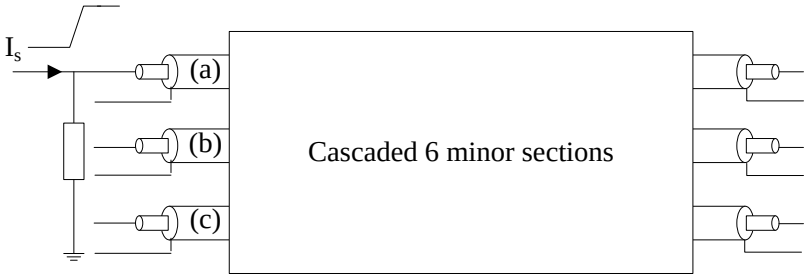


**Figure 4-17 – open circuit termination of the cross bonded cable**

The above configuration is used to perform detailed EMT simulations in PSCAD/EMTDC with each cable section separately modeled with frequency

dependent (phase) model. The fitting parameters used for the cable sections are given in Table 4-2. The frequency domain fitting resulted in maximum errors of 0.6761% and 0.8616% for characteristic admittance, *Yc* and propagation function, *A* respectively.

**Table 4-2 – Fitting parameters used to model each minor section**

| | |
|---|---|
| Curve fitting starting frequency | 0.5 Hz |
| Curve fitting ending frequency | 1 MHz |
| Total number of frequency increments | 100 |
| Maximum order of fitting for Yc | 20 |
| Maximum fitting error for Yc | 1% |
| Maximum order of fitting for each delay group of A | 20 |
| Maximum fitting error for A | 1% |

The proposed technique is used to obtain the FD solution and the numerical inverse Laplace transform (NILT) method is used to convert the FD solution into time domain. The receiving-end voltage of phase 'b' main conductor with the EMT simulations and the proposed approach are compared in Figure 4-18.

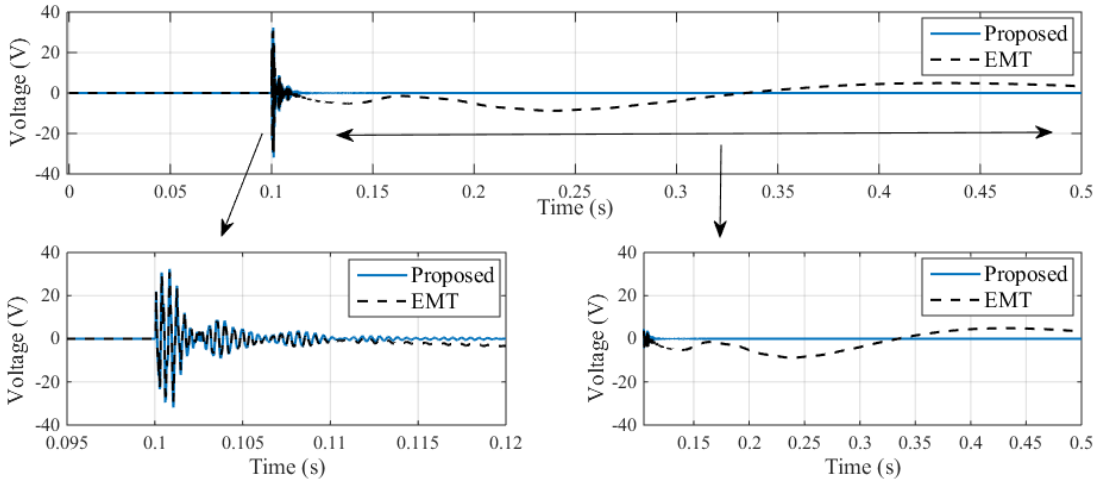


**Figure 4-18 – Receiving-end Voltage of phase 'b' main conductor**

It can be seen that although the initial transient agrees well, the EMT results show a slow oscillation which is absent in the proposed method. Therefore, the fitting parameters of the EMT model are tightened by selecting the maximum fitting error limits for *Yc* and *A* to be 0.1%. This resulted in a fitting where maximum fitting errors are 0.081% and 0.099% for characteristic admittance, *Yc* and propagation function, *A* respectively. The receiving-end voltage of phase 'b' main conductor with the modified EMT model and the proposed approach are compared in Figure 4-19. The EMT results with the modified fitting parameters agree well with the proposed validation method. Therefore, this approach can be used successfully to verify EMT simulations of cascaded power transmission systems.

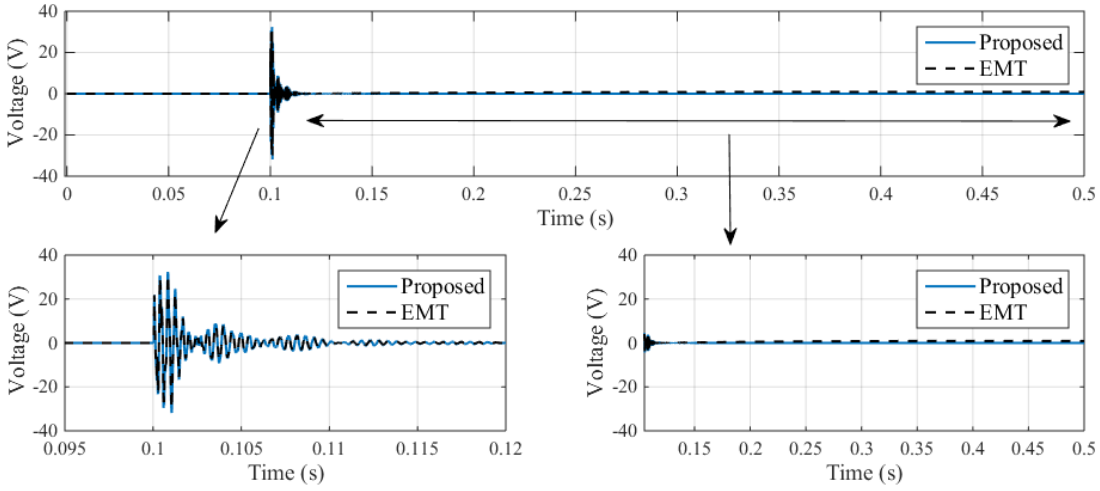


**Figure 4-19 – Receiving-end Voltage of phase 'a' main conductor (modified fitting)**

A novel approach to improve FD modelling of transposed transmission lines or cross-bonded underground cables is introduced in this chapter. The

performance of the technique does not reduce with increased number of cascaded segments as happens with the conventional ABCD parameter method. As this method preserves the intrinsic details of each line segment, it can be used to model cascaded overhead line or cable segments with different characteristic admittances and lengths. The proposed improved FD method can be used in a stand-alone FD program, or even to get TD solutions for linear systems using NILT method. It can also then be used to validate EMT models which may have fitting errors.

# Chapter 5

# Generalized, time delay independent model for transmission line simulations

## 5.1 Introduction

Conventional EMT models of transmission lines must be used with time-steps smaller than the smallest travel time (τ) of the line [45]; even when the resulting high frequency reflections at line terminations are not of interest to the user. When modelling large networks in EMTP type programs, the time-step ($\Delta t$) restriction can introduce a heavy computational burden. It is common in EMT simulations to represent the short transmission lines in the study system with nominal π-equivalent circuits to avoid $\Delta t$ constraints. As described in section 2.4.4, nominal π-equivalent circuits can cause significant inaccuracies due to the disregard of the frequency dependency in transmission line parameters and unwanted resonances introduced by the lumping of impendences.

In this chapter, we present a novel generalized transmission line model for EMTP type programs, which can accommodate all time-steps independent of the travel time. This model can be incorporated with simulation time steps greater than the transmission line travel time with high accuracy, although high frequency transients are attenuated due to high interpolation error. When small time-steps (less than the travel time) are used, the model degenerates to the conventional frequency dependent model of the transmission line.

There have been several previous attempts in literature to model transmission lines with large time-steps. The method proposed in [45], modifies the conventional Bergeron model to accommodate large time-steps, where transmission line frequency dependency is not considered. Reference [52] presents a single conductor transmission line model for large time-step EMT simulations. A multi-conductor frequency dependent transmission line model, which can accommodate time-steps greater than the maximum travel time is not hitherto developed. In addition, existing large time-step models require that the time step chosen to be greater than the largest travel time of the line.

# 5.2 Characteristics of large time-step simulation of transmission lines

Some inherent characteristics of large time-step modelling of transmission lines will be discussed in this section.

## 5.2.1 Elimination of network isolation

In conventional transmission line models (both frequency dependent and Bergeron type), sending and receiving-end networks are isolated due to the travel time (transportation time delay). An obvious consequence of modelling of transmission lines with large time-steps greater than the travel time is the elimination of network isolation. This can be observed (as shown in Figure 5-1) in the model proposed in [45], where sending-end, *k* and receiving-end, *m* are connected through an impedance. This is to be expected, as the time-step is greater than the travel time, sending-end quantities of the current time-step affect the receiving-end.

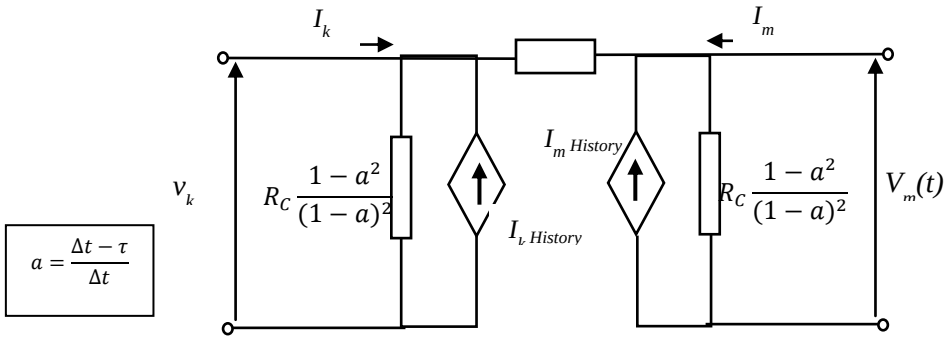


**Figure 5-1 –Equivalent circuit of a Bergeron type large time-step model [45]**

### 5.2.2 Attenuation of high frequency transients

When modelling transmission lines with large time steps, transients due to reflections at the line terminals are not accurately captured. This is mainly due to the high interpolation error associated with large time-steps, when obtaining quantities at $t$-$\tau$. However, the models may still be able to follow the average behaviour of such transients. Therefore, these types of models are not suited for line energization, lightning type studies, etc. Also, such studies are generally focused on a single transmission line and, detailed network representation after a few nearby busses is not required as the studied fast transients attenuate quickly [46]. Therefore, those studies generally require modelling of a small electrical network, thus using large time-steps is not required.

Large time-step models are most suitable for simulating an electrical network having a mixture of long transmission lines and as well as very short transmission lines. It should be noted that the time-step, $\Delta t$ must be small enough to handle the maximum frequency of excitation applied to the circuit and the other inherent time constants of the network.

## 5.3 Generalized model derivation

The proposed generalized transmission line model is derived starting with the conventional frequency domain equations of the transmission line.

## 5.3.1 Initial set up

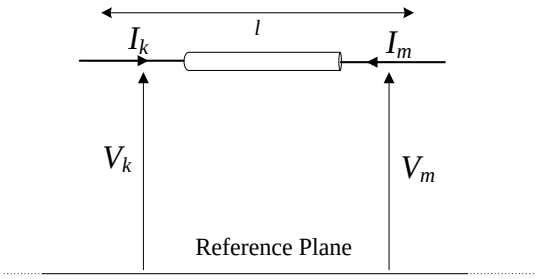


**Figure 5-2 – Sending-end and receiving-end quantities of a transmission line**

Transmission line sending-end, *k* and receiving-end, *m* quantities are defined as shown in Figure 5-2. Frequency domain transmission line equations can be re-written as shown in equations 5-1 and 5-2.

$$I_k = Y_c V_k - A\left(Y_c V_m + I_m\right) \qquad \textbf{5-1}$$
$$I_k = Y_c V_k - A \cdot F_m$$

$$I_m = Y_c V_m - A\left(Y_c V_k + I_k\right) \qquad \textbf{5-2}$$
$$I_m = Y_c V_m - A \cdot F_k$$

Where,

$F_m = \left(Y_c V_m + I_m\right)$ and $F_k = \left(Y_c V_k + I_k\right)$

Each multiplication in 5-1 and 5-2 becomes a convolution in the time domain. This process transforms each function into its time domain counterpart. There are two types of convolutions in the equations.

Convolution type 1: $Y_c \cdot V \rightarrow y_c(t) * v(t)$

As the characteristic admittance, $Y_c$ does not contain time delays, general

recursive convolution algorithm (section 2.4.2) with $\tau$ =0, can be used similar to the conventional transmission line model:

$$y_c(t) * v(t) = y_{eq} \cdot v(t) + i_{history}(t - \Delta t) \quad \textbf{5-3}$$

Convolution type 2: $A \cdot F \rightarrow a(t) * f(t)$

In order to achieve the generalized time step model proposed, a modification to the manner in which the convolution of type 2 is usually carried out is introduced, as is now described.

The propagation function, *a(t)* consists of multiple transportation delay groups, with some delays potentially less than *Δt*. If *a(t)* consists of *n* number of delay groups, it can be written as a summation of *n* "sub-propagation functions", each with a unique delay, as seen in 5-4 and 5-5.

$$\textit{In time domain, } a(t) = a_1(t) + a_2(t) + \cdots + a_n(t) = \sum_{i=1}^{n} a_i(t) \quad \textbf{5-4}$$

$$\textit{In frequency domain, } A = A_1 \cdot e^{-s \cdot \tau_1} + A_2 \cdot e^{-s \cdot \tau_2} + \cdots + A_n \cdot e^{-s \cdot \tau_n} = \sum_{i=1}^{n} A_i \cdot e^{-s \cdot \tau_i} \quad \textbf{5-5}$$

Now, the convolution type 2 can be written as follows:

$$a(t) * f(t) = \sum_{i=1}^{n} a_i(t) * f(t) \quad \textbf{5-6}$$

Each sub-propagation function will be handled separately depending on whether its inherent transportation delay is greater or less than the time-step, as will be explained next.

## 5.3.2 Time delay less than time-step ($\tau < \Delta t$)

Consider the case where the first *p* terms of *a(t)* have time delays less than *Δt*,

*i.e.* $\forall i \in (1,\ldots,p),\ \tau_i < \Delta t$

Therefore, at a given time, *t* time delay of a sub-propagation function can be shown as in Figure 5-3.

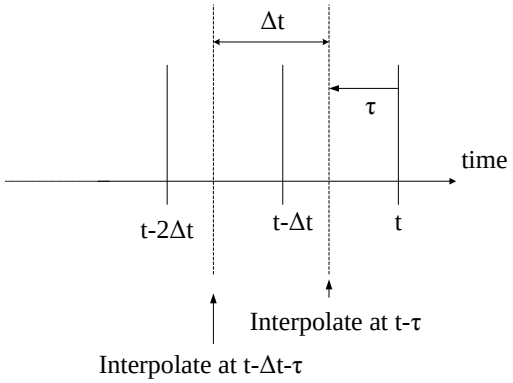


**Figure 5-3 – time delay when τ<Δt**

It can be shown that the $i^{th}$ term of the convolution (type 2), $s_i(t)$ can be written as a function of quantities in the current time-step, t and the previous two time-steps, $t-\Delta t$ and $t-2\Delta t$. The term, $s_i(t)$ can be written similar to equation 2-28 as follows:

$$s_i(t) = a_i(t) * f(t) = k_1' \cdot f(t-\tau) + k_2' \cdot f(t-\Delta t-\tau) + k_3' \cdot s_i(t-\Delta t) \qquad \textbf{5-7}$$

As the time, $t-\tau$ occurs within the last time-step period i.e. $(t, t-\Delta t)$, travel time interpolation can be applied to obtain the estimate of $f(t-\tau)$:

$$\frac{f(t)-f(t-\tau)}{\tau} = \frac{f(t)-f(t-\Delta t)}{\Delta t} \qquad \textbf{5-8}$$
$$f(t-\tau) = \left(\frac{\Delta t-\tau}{\Delta t}\right)\cdot f(t) + \left(\frac{\tau}{\Delta t}\right)\cdot f(t-\Delta t)$$

Similarly, $f(t-\Delta t-\tau)$:

$$f(t-\Delta t-\tau) = \left(\frac{\Delta t-\tau}{\Delta t}\right)\cdot f(t-\Delta t) + \left(\frac{\tau}{\Delta t}\right)\cdot f(t-2\Delta t) \qquad \textbf{5-9}$$

Therefore, $f(t-\tau)$ and $f(t-\Delta t-\tau)$ of equation 5-7 can be substituted with 5-8 and

5-9:

$$s_i(t) = a_i(t) * f(t) = c_1^i \cdot f(t) + c_2^i \cdot f(t-\Delta t) + c_3^i \cdot f(t-2\Delta t) + c_4^i \cdot s_i(t-\Delta t) \qquad \textbf{5-10}$$

Where,

$$c_1^i = k_1'\left(\frac{\Delta t-\tau}{\Delta t}\right), \quad c_2^i = k_1'\left(\frac{\tau}{\Delta t}\right) + k_2'\left(\frac{\Delta t-\tau}{\Delta t}\right), \quad c_3^i = k_2'\left(\frac{\tau}{\Delta t}\right) \quad \textit{and} \quad c_4^i = k_3'$$

It can be observed in 5-10 that the convolution is not completely a history term and it contains terms evaluated at present time-step.

## 5.3.3 Time delay greater than time-step (τ>Δt)

Here, the $(p+1)^{th}$ to $n^{\text{th}}$ terms of $a(t)$ have time delays greater than $\Delta t$,

*i.e.* $\forall i \in (p+1,\ldots,n),\ \tau_i > \Delta t$

Therefore, at a given time, $t$, the time delay of a sub-propagation function can be shown as of Figure 5-4.

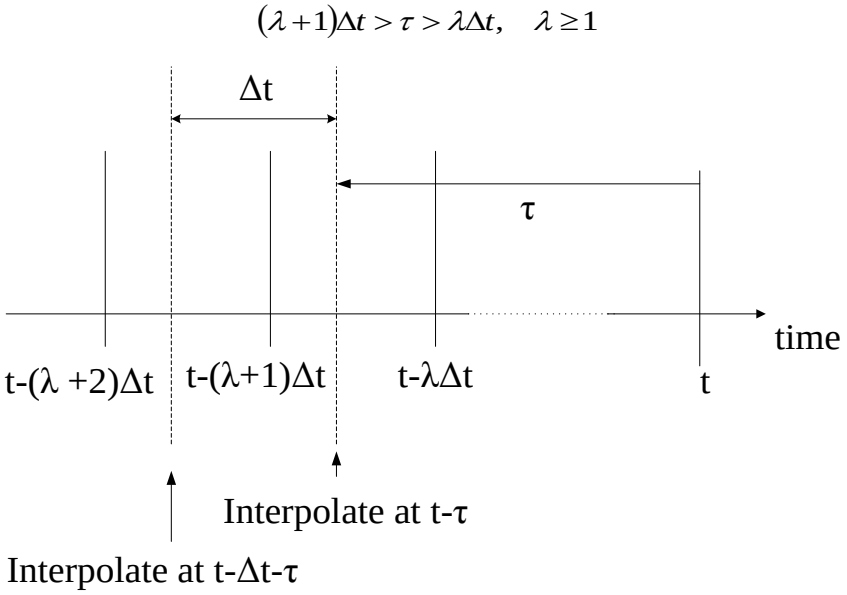


**Figure 5-4 - time delay when τ>Δt**

When $\tau > \Delta t$, the $i^{\text{th}}$ term of the convolution (type 2) can be evaluated in a

manner similar to the conventional transmission line model (Equation 2-28) as follows:

$$s_i(t) = a_i(t) * f(t) = k_1^{/} \cdot f(t-\tau) + k_2^{/} \cdot f(t-\Delta t-\tau) + k_3^{/} \cdot s_i(t-\Delta t) \qquad \textbf{5-11}$$

However, interpolation is still needed to obtain the sample values at ($t$-$\tau$) and ($t$-$\tau$-$\Delta t$) as shown in Figure 5-4. After incorporating the time delay interpolation,

$$s_i(t) = \left(k_1^{/}\mu_1\right) \cdot f(t-\lambda\Delta t) + \left(k_1^{/}\mu_2 + k_2^{/}\mu_1\right) \cdot f(t-(\lambda+1)\Delta t) + k_2^{/}\mu_2 \cdot f(t-(\lambda+1)\Delta t) + k_3^{/} \cdot s_i(t-\Delta t)$$

Where,

$$\mu_1 = \frac{\tau - \lambda \cdot \Delta t}{\Delta t} \text{ and } \mu_2 = 1 - \mu_1$$

Therefore, the $i^{\text{th}}$ term of the convolution type 2 can be written as,

$$s_i(t) = k_1^i \cdot f(t-\lambda\Delta t) + k_2^i \cdot f(t-(\lambda+1)\Delta t) + k_3^i \cdot f(t-(\lambda+2)\Delta t) + k_4^i \cdot s_i(t-\Delta t) \qquad \textbf{5-12}$$

Where,

$$k_1^i = k_1^{/}\mu_1, \quad k_2^i = k_1^{/}\mu_2 + k_2^{/}\mu_1, \quad k_3^i = k_2^{/}\mu_2 \quad \text{and} \quad k_4^i = k_3^{/}$$

## 5.3.4 Time domain model development

The time domain model can be generated from the frequency domain model by using recursive convolution as described in section 2.4.2. Frequency domain transmission line equation for $I_k$, can be written in the time domain form as,

$$i_k(t) = y_c(t) * v_k(t) - a(t) * f_m(t) \qquad \textbf{5-13}$$

The convolution, $y_c(t)*v_k(t)$ is of type 1 (equation 5-3) and given as follows:

$$y_c(t)*v_k(t)=y_{eq}\cdot v_k(t)+i_{hist,k}(t-\Delta t) \quad \textbf{5-14}$$

Similarly, $f_m(t)$ can be evaluated as:

$$f_m(t)=y_c(t)*v_m(t)+i_m(t)=y_{eq}\cdot v_m(t)+i_m(t)+i_{hist,m}(t-\Delta t) \quad \textbf{5-15}$$

$a(t)*f_m(t)$ Convolution can be written as follows;

$$a(t)*f_m(t)=\sum_{i=1}^{n}a_i(t)*f_m(t)=\sum_{i=1}^{p}\underbrace{a_i(t)*f_m(t)}_{S_1^i}+\sum_{i=p+1}^{n}\underbrace{a_i(t)*f_m(t)}_{S_2^i} \quad \textbf{5-16}$$

Let us assume convolutions in the first p terms of *a(t)* are *S1* (i.e. convolution of the i$^{th}$ term is $S_1^i$). Similarly, assume convolutions in the (*p+1, n*) terms of *a(t)* are *S2* (i.e. convolution of the *i*$^{th}$ term is $S_2^i$). Now it is possible to evaluate $a(t)*f_m(t)$ using the equations developed in sections 5.3.2 and 5.3.3.

$$a(t)*f_m(t)=\sum_{i=1}^{p}s_1^i(t)+\sum_{i=p+1}^{n}s_2^i(t) \quad \textbf{5-17}$$

$$a(t)*f_m(t)=T_1\cdot v_m(t)+T_2\cdot i_m(t)+i_{hist,Ak}$$

Where,

$$T_1=\left(\sum_{i=1}^{p}c_1^i\right)\cdot y_{eq}$$

$$T_2=\left(\sum_{i=1}^{p}c_1^i\right)$$

$$i_{hist,Ak}=\left(\sum_{i=1}^{p}c_2^i\right)\cdot f_m(t-\Delta t)+\left(\sum_{i=1}^{p}c_3^i\right)\cdot f_m(t-2\Delta t)+\sum_{i=1}^{p}c_4^i\cdot s_1^i(t-\Delta t)+\left(\sum_{i=p+1}^{n}k_1^i\right)\cdot f_m(t-\lambda\Delta t)$$
$$+\left(\sum_{i=p+1}^{n}k_2^i\right)\cdot f_m(t-(\lambda+1)\Delta t)+\left(\sum_{i=p+1}^{n}k_3^i\right)\cdot f_m(t-(\lambda+2)\Delta t)+\sum_{i=p+1}^{n}k_4^i\cdot s_2^i(t-\Delta t)$$

The complete time domain equation for sending-end current, $i_k(t)$ can be

written by assembling equations 5-14 and 5-17.

$$i_k(t) = y_{eq} \cdot v_k(t) + i_{hist,k} - T_1 \cdot v_m(t) - T_2 \cdot i_m(t) - i_{hist,Ak} \quad \textbf{5-18}$$

Similarly, $i_m(t)$

$$i_m(t) = y_{eq} \cdot v_m(t) + i_{hist,m} - T_1 \cdot v_k(t) - T_2 \cdot i_k(t) - i_{hist,Am} \quad \textbf{5-19}$$

Substituting 5-19 in 5-18 gives:

$$\begin{aligned} i_k(t) = {} & y_{eq} \cdot v_k(t) + i_{hist,k} - T_1 \cdot v_m(t) - \\ & T_2 \cdot \left\{ y_{eq} \cdot v_m(t) + i_{hist,m} - T_1 \cdot v_k(t) - T_2 \cdot i_k(t) - i_{hist,Am} \right\} - i_{hist,Ak} \end{aligned}$$

By rearranging the equation,

$$\begin{aligned} i_k(t) = {} & \left(I_n - T_2^2\right)^{-1} \cdot \left(y_{eq} + T_2 \cdot T_1\right) \cdot v_k(t) - \left(I_n - T_2^2\right)^{-1} \cdot \left(T_1 + T_2 \cdot y_{eq}\right) \cdot v_m(t) + \\ & \left(I_n - T_{2\,2}^2\right)^{-1} \cdot \left\{ i_{hist,k} - T_2 \cdot i_{hist,m} + T_2 \cdot i_{hist,Am} - i_{hist,Ak} \right\} \end{aligned} \quad \textbf{5-20}$$

Where, $I_n$ denotes the identity matrix. Therefore, $i_k(t)$ and $i_m(t)$ can be written in matrix form,

$$\begin{bmatrix} i_k(t) \\ i_m(t) \end{bmatrix} = \begin{bmatrix} Y_k & Y_{km} \\ Y_{km} & Y_m \end{bmatrix} . \begin{bmatrix} v_k(t) \\ v_m(t) \end{bmatrix} + \begin{bmatrix} history\_k \\ history\_m \end{bmatrix} \quad \textbf{5-21}$$

Equation 5-21 corresponds to a time domain equivalent circuit having shunt and series admittances and history current sources as shown in Figure 5-5. This formulation can be readily implemented in electromagnetic transient programs [5].

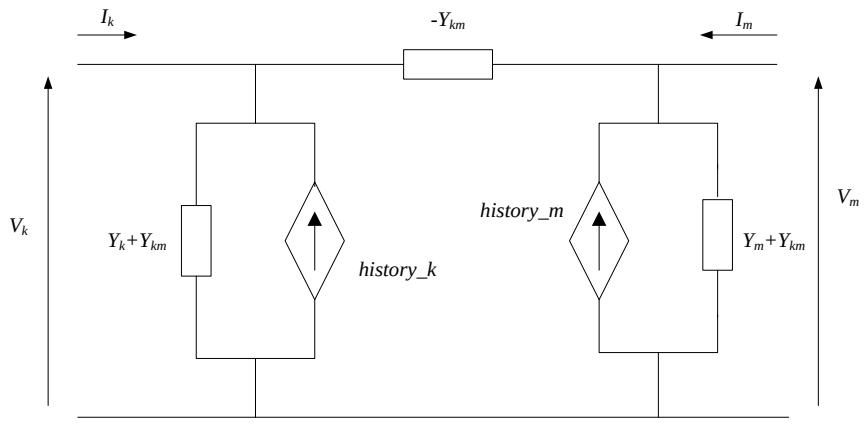


**Figure 5-5 - Time domain equivalent circuit of the proposed transmission line model**

If all time delays are less than the time-step, all $c_1$, $c_2$, $c_3$ and $c_4$ terms calculated in section 5.3.2 become zero. Therefore:

$$T_1 = \left( \sum_{i=1}^{p} c_1^i \right) \cdot y_{eq} = 0$$

$$T_2 = \left( \sum_{i=1}^{p} c_1^i \right) = 0$$

Therefore, $i_k(t)$ and $i_m(t)$ can be written in matrix form:

$$\begin{bmatrix} i_k(t) \\ i_m(t) \end{bmatrix} = \begin{bmatrix} y_{eq} & 0 \\ 0 & y_{eq} \end{bmatrix} \cdot \begin{bmatrix} v_k(t) \\ v_m(t) \end{bmatrix} + \begin{bmatrix} history\_k' \\ history\_m' \end{bmatrix} \quad \textbf{5-22}$$

This is the conventional transmission line model (shown in Figure 2-3) discussed in 2-29 and 2-30. Therefore, the proposed generalized model degenerates to the conventional frequency dependent (phase) transmission line model when the time step is less than the travel time. This is a very useful feature in the model as the user does not have to rely on multiple line models for different types of studies.

# 5.4 Application example

The proposed generalized model is implemented in MATLAB/SIMULINK as a standalone program. The proposed model can be validated by comparing the results of a time domain simulation with those of a conventional EMT model, where a small time step is used to ensure high accuracy. The geometry and the internal parameters of the cable system used in time domain simulations are given in Figure 5-6.

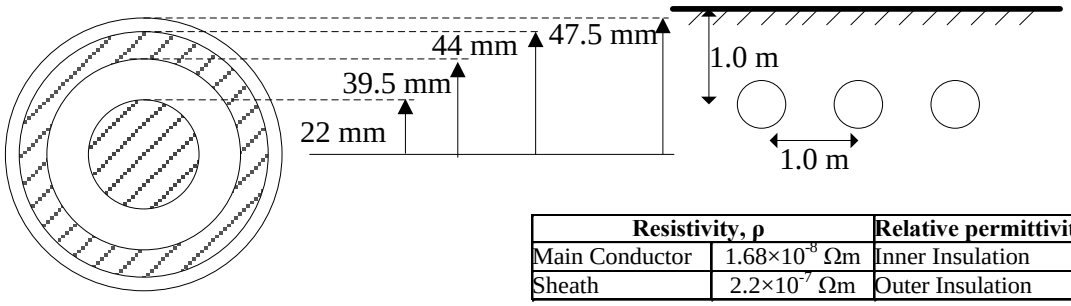


| Resistivity, ρ | | Relative permittivity, ε | |
|---|---|---|---|
| Main Conductor | $1.68\times10^{-8}$ Ωm | Inner Insulation | 4.1 |
| Sheath | $2.2\times10^{-7}$ Ωm | Outer Insulation | 2.3 |

**Figure 5-6 – Cable system geometry and parameters**

## 5.4.1 Impedance termination

The three phase cable system given in Figure 5-6 is implemented in PSCAD/EMTDC using the conventional EMT model in the configuration shown in Figure 5-7.

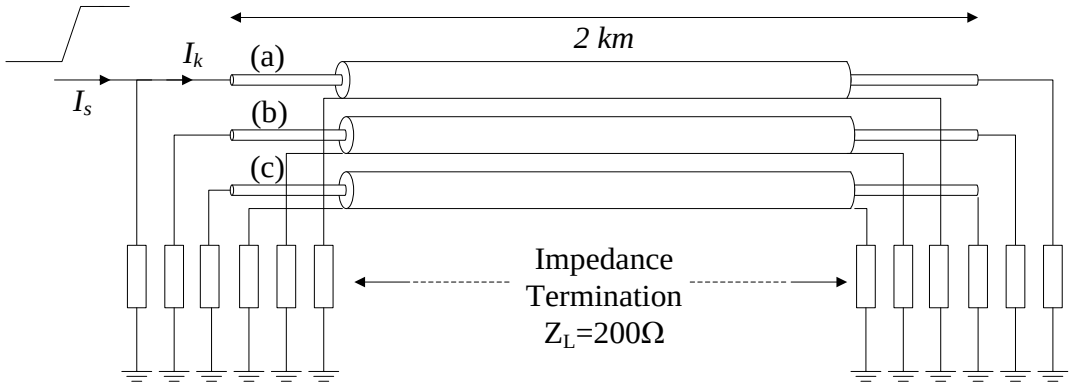


**Figure 5-7 –Cable configuration for impedance termination**

Phase 'a' inner conductor of the cable system is energized at 0.1 s with a current, which ramps from 0 to 1 kA within 20ms and then saturates. The maximum and minimum propagation delays extracted at the curve fitting stage are 116.7 μs and 13.5 μs, respectively. This restricts the time-step of the conventional EMT model to less than 13.5 μs. A time-step of 2.5 μs is selected for the conventional EMT model to minimize the attenuation of high frequencies due to time-step interpolation. This is not a large time-step (propagation delays are 13.5 ms or more), and the purpose here is to establish a base case which is accurate. The EMT results are validated using numerical inverse Laplace Transform (NILT), [48] of the frequency domain transmission line. Receiving-end and sending-end voltages of phase 'b' inner conductor obtained from EMT simulations are plotted in Figure 5-8 and Figure 5-9. Both waveforms agree well.

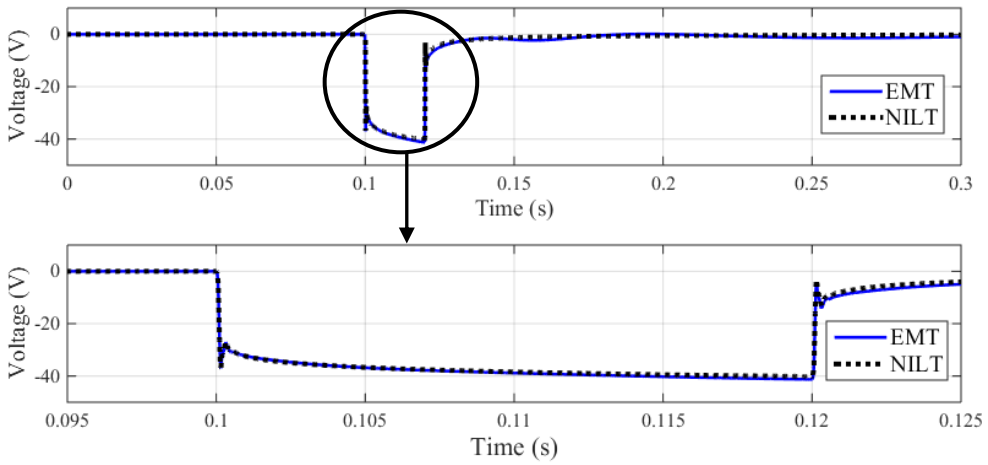


**Figure 5-8 – Receiving-end voltage, phase 'b' – EMT validation**

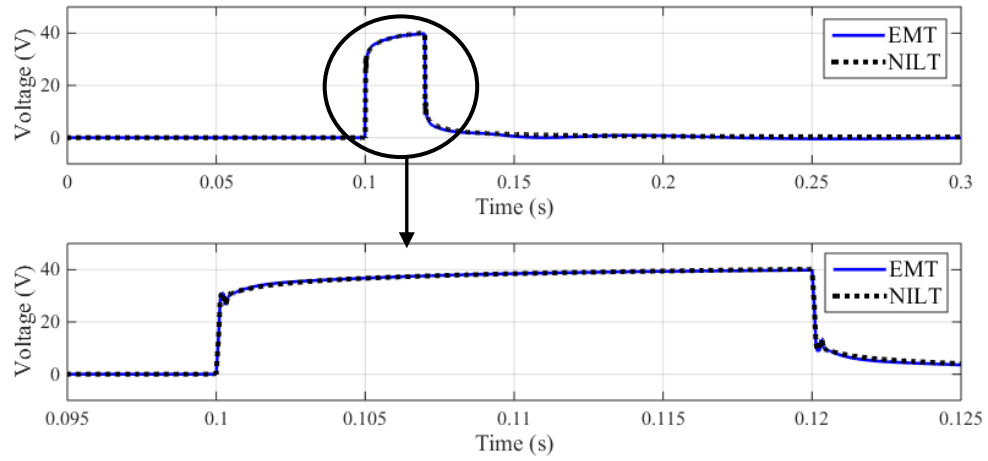


**Figure 5-9 – Sending-end voltage, phase 'b' – EMT validation**

The same cable configuration is modelled using the proposed generalized model and time domain simulations are carried out with various time-steps. The induced voltages of phase 'b' at sending and receiving-end are compared with the conventional EMT results.

#### 4.4.1.1. Time-step, Δt = 2.5 μs (less than the minimum delay)

Sending and receiving-end voltages of phase 'b' are compared in Figure 5-10 and Figure 5-11.

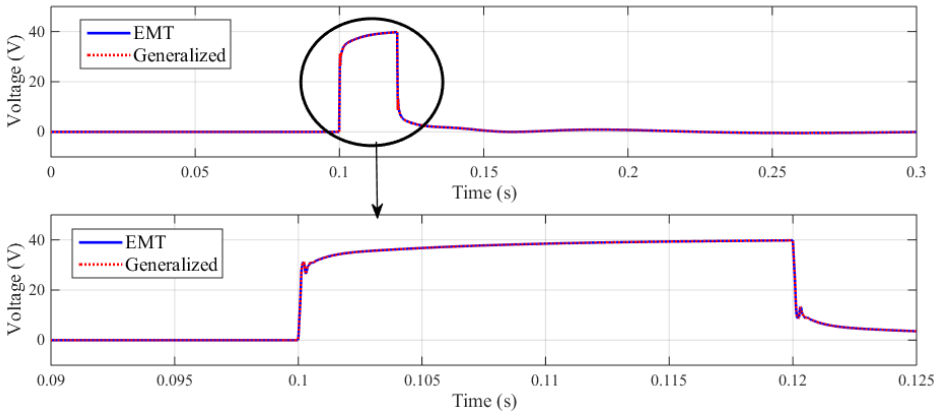


**Figure 5-10 – Sending-end voltage – phase 'b' (Δt=2.5 μs)**

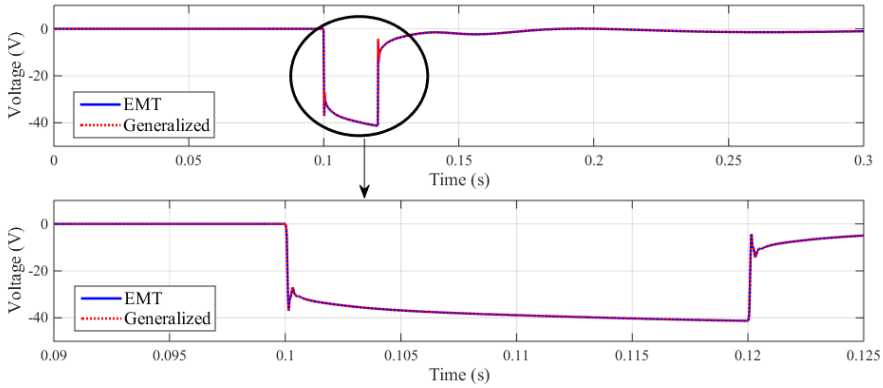


**Figure 5-11 – Receiving-end voltage – phase 'b' (Δt=2.5 μs)**

The results from the generalized time independent model agree well with the EMT results. This is to be expected as the proposed approach degenerates into the conventional EMT model when time-step is less than the minimum propagation delay.

#### 4.4.1.2. Time-step, Δt = 200 μs (greater than the maximum delay)

Sending and receiving end voltages of phase 'b' are compared in Figure 5-12.

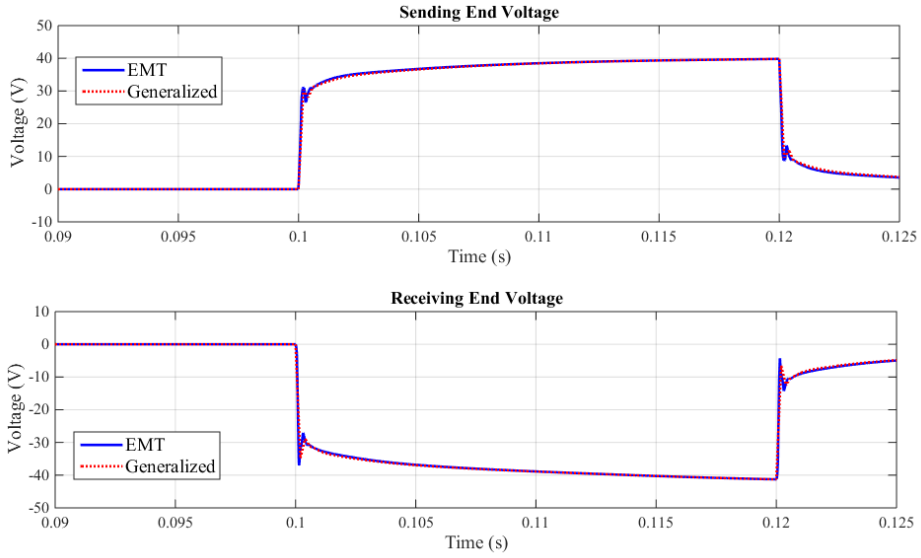


**Figure 5-12– Sending and Receiving end voltages – phase 'b' (Δt=200 μs)**

Results from the generalized time independent model agree well with the EMT results. Slightly high frequency attenuation is observed at 0.1s and 0.12s due to the time-step interpolation.

#### 4.4.1.3. Time-step, Δt = 500 µs (much greater than the maximum delay)

Sending and receiving end voltages of phase 'b' are compared in Figure 5-13 and Figure 5-13.

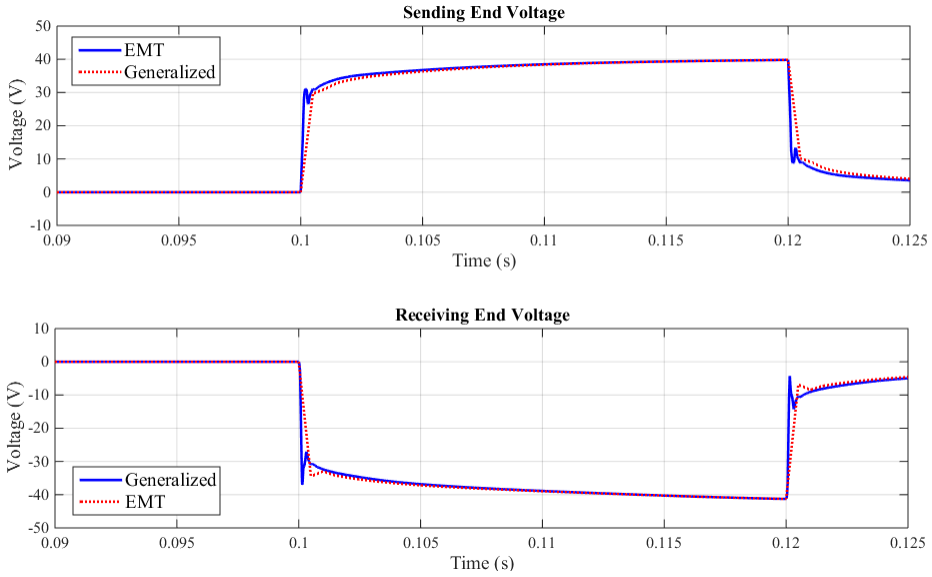


**Figure 5-13 – Sending and receiving end voltage – phase 'b' (Δt=500 µs)**

Although the results agree, it can be seen that the high frequency attenuation is more apparent at 500 µs. This is to be expected as the time-step in this case is approximately 5 times the maximum propagation delay, thus, the interpolation has a heavy impact on higher frequencies. Figure 5-14 and Figure 5-15 compare the above results with those obtained from nominal π-equivalent circuits corresponding to impedances evaluated at 0.01 Hz and 50 Hz.

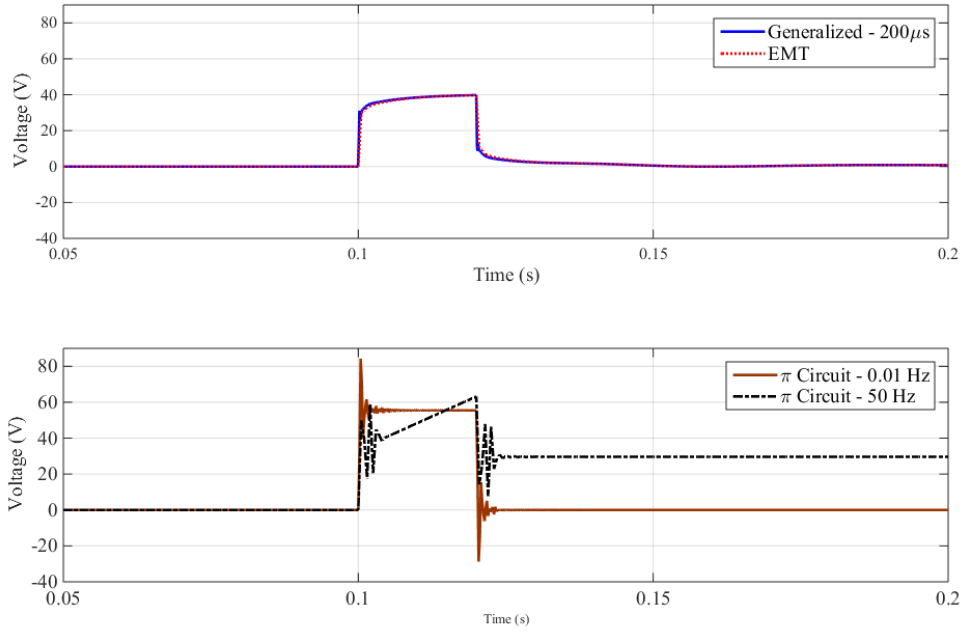


**Figure 5-14 – Sending-end voltage – phase 'b' (Δt=200 µs)**

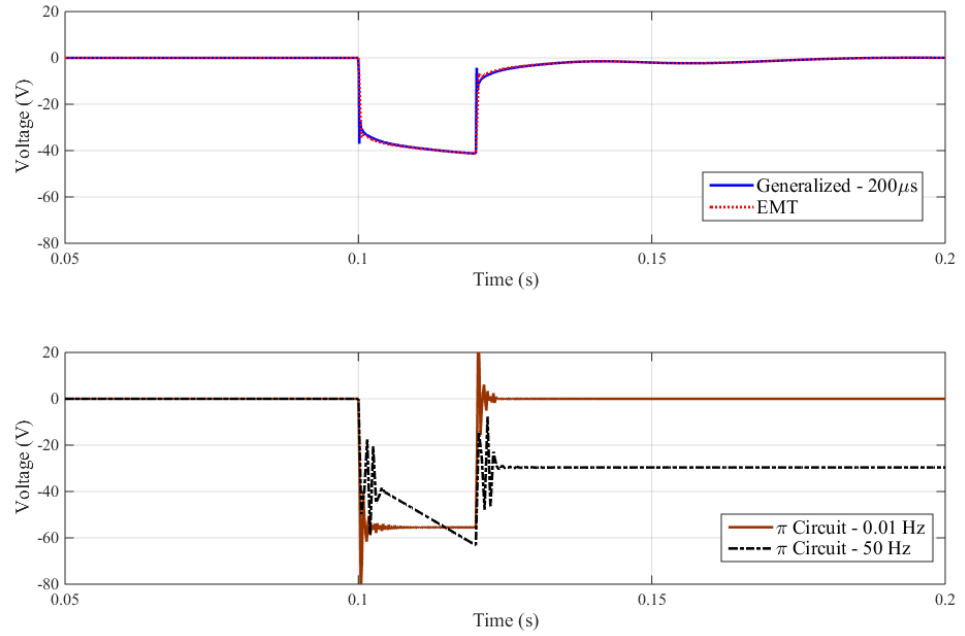


**Figure 5-15 – Receiving-end voltage – phase 'b' (Δt=200 µs)**

It can be seen that none of the π circuits capture the correct behaviour of the waveform. The voltage transient in π circuit evaluated at 50 Hz is closer to the EMT result (however, the peak value is off by about 40%), but the steady state value is highly inaccurate. π circuit evaluated at 0.01 Hz captures the steady state behaviour, however, fails to match the transient waveform (the peak value is twice the EMT result). Both circuit results show spurious oscillations at the start and end on the ramp (at 0.1s and 0.12s respectively).

### 5.4.2 Open circuit termination

Following configuration with open circuit termination (Figure 5-16) is modelled with the generalized model to emphasize the attenuation of high frequencies with large time steps due to time step interpolation. Phase 'a' inner conductor of the cable system is energized at 0.1 s with a current, which ramps from 0 to 1 kA within 200 μs and then saturates.

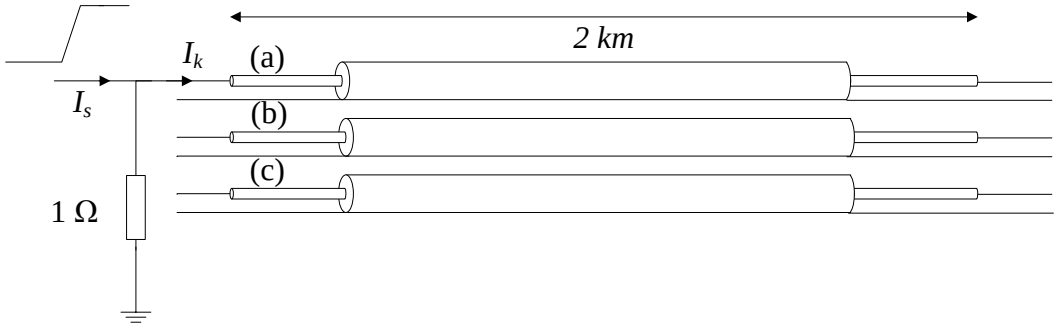


**Figure 5-16 – Cable configuration for open circuit termination**

Receiving-end and sending-end voltages of phase 'b' inner conductor obtained from EMT simulations are plotted in Figure 5-17. A time step of 2.5 µs is used for the EMT simulations. These results are compared with Numerical Inverse Laplace Transform (NILT) [48] of the frequency domain transmission line equation for accurate validation.

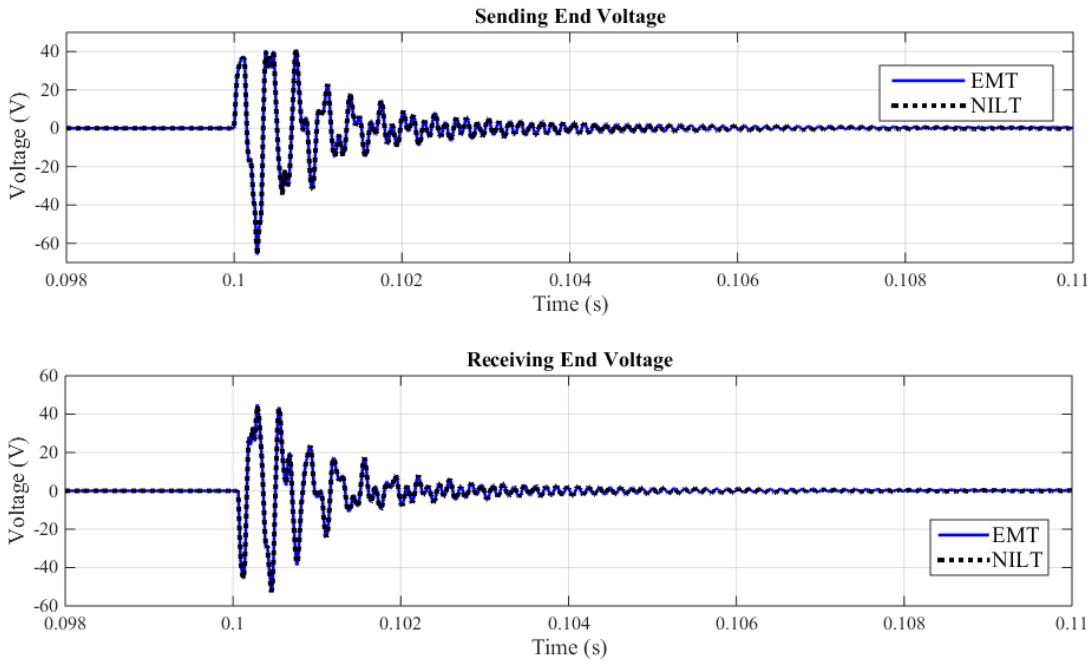


**Figure 5-17 – Sending and Receiving end voltages, phase 'b' – EMT validation**

It can be seen that the EMT results agree well with the frequency domain solution. Therefore, these EMT results are used for the comparisons with the generalized model. Time domain simulations are carried out using the generalized model with the time-steps of 2.5 µs, 20 µs and 200 µs. The maximum and minimum travel times of the cable system are 116.7 µs and

13.5 µs. The induced voltages in the inner conductor of phase 'b' at receiving and sending end are compared with the conventional EMT results in Figure 5-18 and Figure 5-19, respectively.

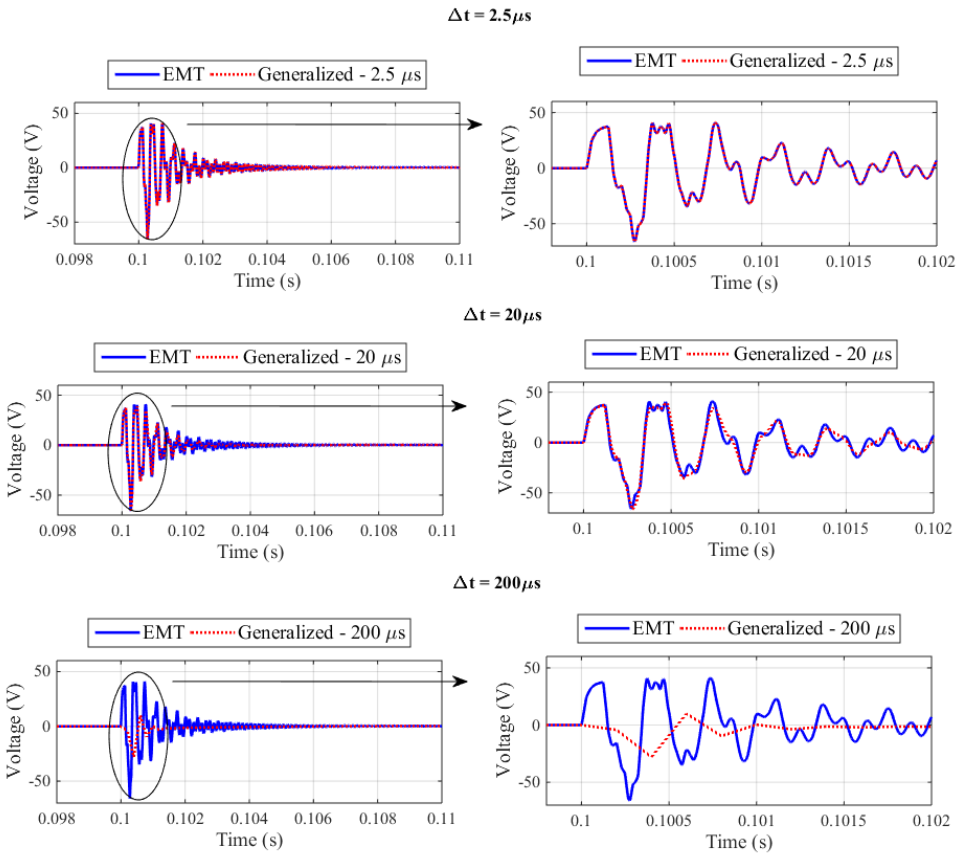


**Figure 5-18 – Sending-end voltage comparison, phase 'b' – at different time steps**

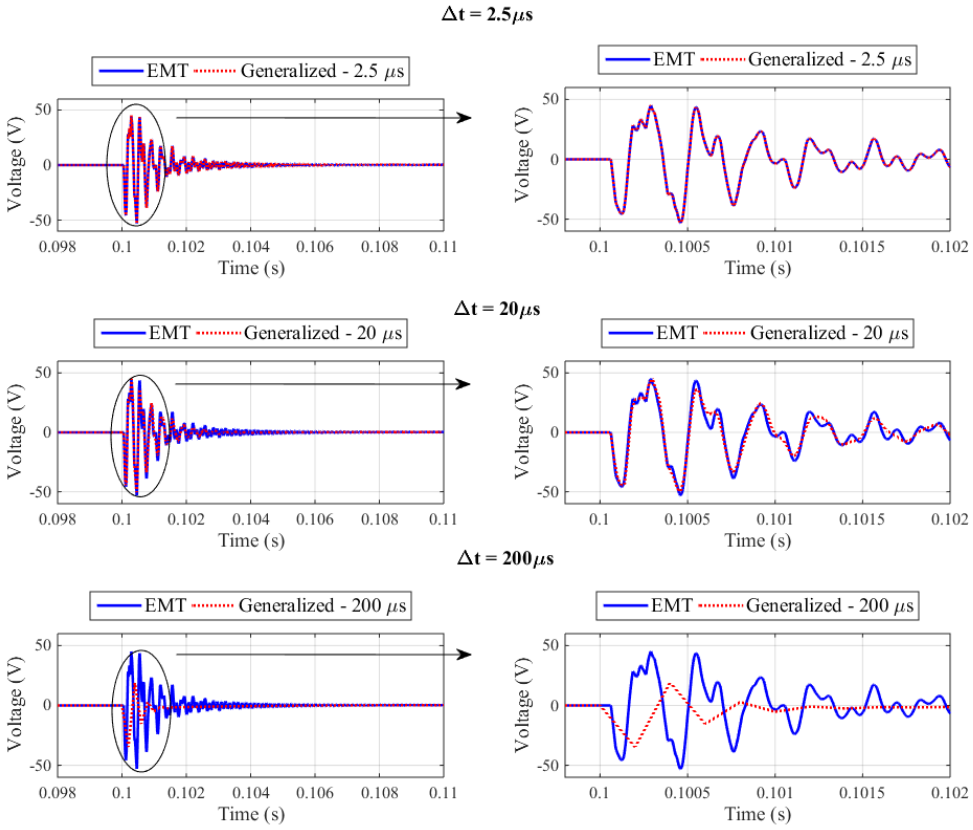


**Figure 5-19 – Receiving-end voltage comparison, phase 'b' – at different time steps**

It can be seen that the generalized model with 2.5 µs yields the same results as the EMT model. When the time step is increased to 20 µs some high frequency attenuation is observed. At 200 µs, heavy attenuation of high frequency transients is observed. Figure 5-20 compares the EMT results with those obtained from nominal π circuits corresponding to impedances evaluated at 0.01 Hz and 5000 Hz. Both π circuit models fail to reach the accuracy of the EMT results or the generalized model at large time steps.

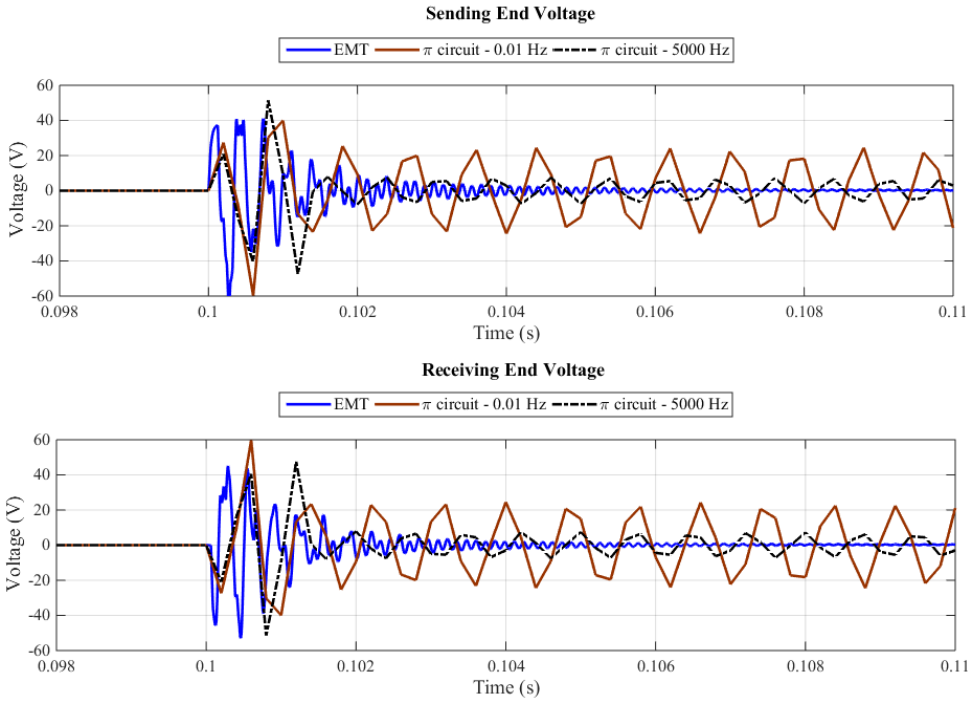


**Figure 5-20 – Receiving and sending end voltage comparison, phase 'b' – with π circuits**

## 5.4.3 Excitation with a harmonic source

The cable geometry given before in Figure 5-6 is used with the configuration shown in Figure 5-21. The system is excited with a harmonic current source generating an imperfect 60 Hz square wave with the harmonic magnitudes given in Table 5-1.

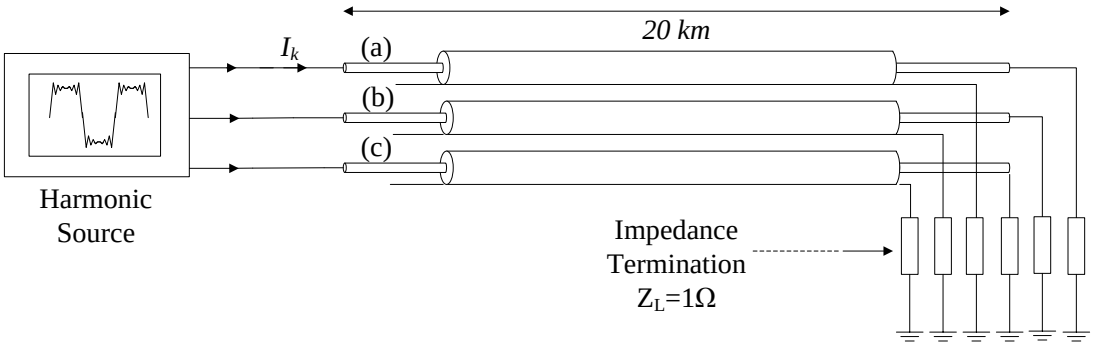


**Figure 5-21 –Cable configuration for impedance termination**

**Table 5-1 – Harmonic magnitudes of the source signal**

| Harmonic Number | Magnitude (A) |
|---|---|
| 1 | 1000.0 |
| 3 | 333.33 |
| 5 | 200.00 |
| 7 | 142.86 |
| 9 | 111.11 |
| 11 | 90.091 |
| 13 | 76.923 |
| 15 | 66.667 |
| 17 | 58.823 |

Inner conductors of all 3 phases are energized with a 60 Hz three phase harmonic source. The source current waveform of phase 'a' is shown in Figure 5-22.

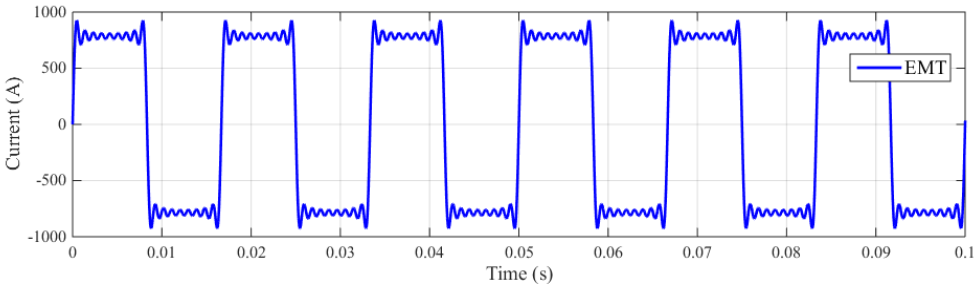


**Figure 5-22 - phase 'a', Source current waveform**

Time domain simulations are carried out using the EMT model, generalized model and the nominal $\pi$-equivalent at 60 Hz. The simulation time step of 2.5 µs is used for EMT model and 200 µs is used for both generalized model and the nominal $\pi$-equivalent. The induced sending-end and receiving-end voltages in the sheath of phase 'a' are shown in Figure 5-23 and Figure 5-24.

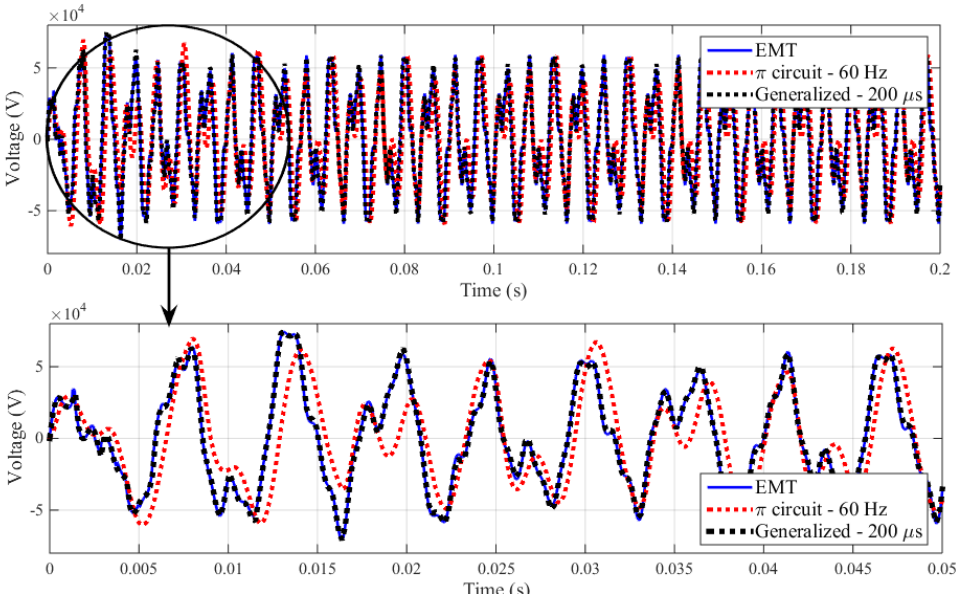


**Figure 5-23 – Sending-end voltage comparison, phase 'a' sheath**

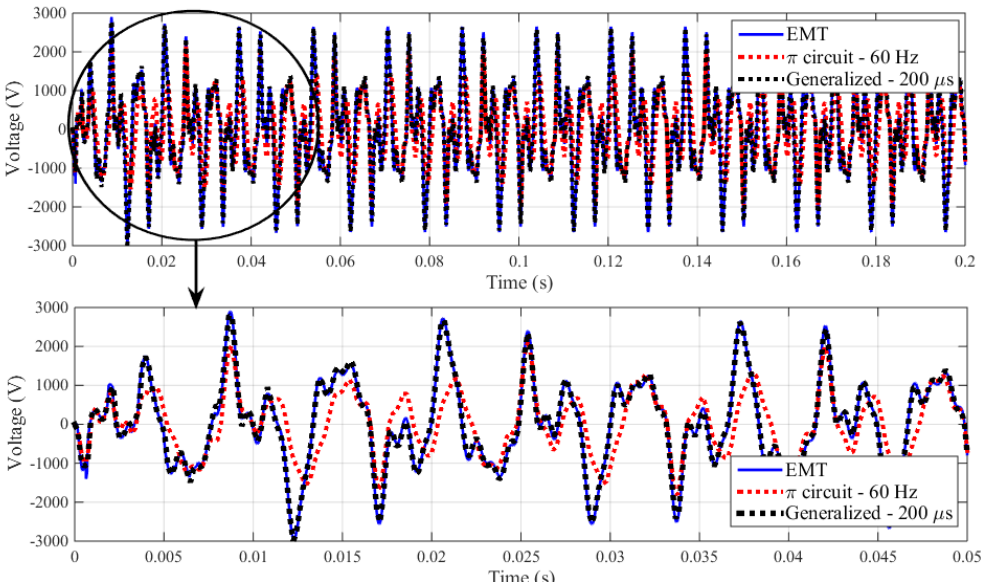


**Figure 5-24 – Receiving-end voltage comparison, phase 'a' sheath**

Results from the generalized time independent model agree well with the EMT results, whereas the results of the nominal $\pi$-equivalent deviates from

the EMT results. This is to be expected as the generalized model considers the frequency dependency of the transmission line and the nominal $\pi$-equivalent is accurate only at 60 Hz. An additional example, which applies a single line-to-ground fault to a cable system, is given in Appendix D.

### 5.4.4 Simulation speed enhancement

The proposed generalized model is implemented as a standalone program (in MATLAB/SIMULINK™) and the previous examples were solved on this program. As seen in Figure 5-25 (a) (simulation time versus time step used), the CPU time decreases with increasing time-step. As seen in Figure 5-25 (b), the speed up ratio being approximately equal to the time-step ratio, i.e. the ratio of CPU time to that required for the smallest time-step used, grows approximately linearly.

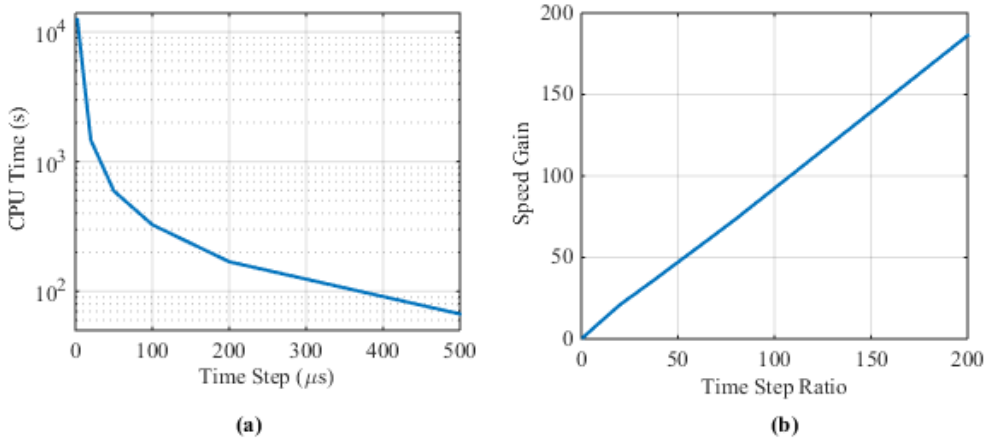


**Figure 5-25 – CPU time and speed gain with different time-steps**

However, ultimately it would be interesting to see how the method would speed up a commercial EMTP type program (e.g., PSCAD/EMTDC™). This way, the speed enhancement due to larger time-step as well as speed reduction due to the loss of network isolation can be properly considered.

This chapter introduces a generalized transmission line model that can accommodate time steps greater than the largest travel time of the line. This model can be used with large time steps in situations when high frequency components are not central to the phenomena being studied. If accurate high frequency transients are studied the proposed model can be used with small time steps. At this point, the model degenerates to the conventional frequency dependent phase model of the transmission line. The general practice requires the use of inaccurate nominal $\pi$ equivalents for large time-step simulations and the detailed frequency dependent model for simulations with high frequency phenomena. The proposed model is highly convenient as the same model can be used for all types of EMT simulations.

# Chapter 6

# Contributions, Conclusions and Recommendations

## 6.1 Contributions and Conclusions

In this section, a summary of the contributions of the thesis is presented. This thesis proposes several techniques to improve the electromagnetic transient modelling and validation of power transmission lines. First, the basic steps of electromagnetic transient modelling theory for transmission lines are discussed. This involves, the estimation of the admittance and propagation matrices (*Yc* and *A*) of the transmission line, conversion of the frequency domain information into time domain and model validation. It is highlighted in the thesis that the following limitations exist in the conventional EMT models of transmission lines.

- The equations to calculate *Yc* and *A* for power cables with circular and annular conductors (e.g. coaxial cables) are available in literature.

However, fast and accurate calculation of *Yc* and *A* for cables with complex conductor shapes such as sector-shaped cables still poses a challenge.

- There are no detailed and accurate techniques available in literature to model cascaded transmission systems in the frequency domain. The existing methods are either numerically inaccurate or simplified methods. Therefore, these are not suitable to validate EMT models of cascaded transmission systems such as transposed overhead lines and cross-bonded cables.
- The simulation time-step used in an EMT study is constrained by the minimum delay of all the transmission lines in the study system. This restriction introduces additional computational burdens to the simulation, particularly, in the presence of short transmission lines.

Based on the above observations, the following major contributions have emerged from this thesis.

- A novel technique is developed to model sector-shaped cables in EMT programs. The introduced parameter calculation method extends the applicability of the elemental sub-conductor technique which is hitherto used for circular conductor shapes. This method is validated with accurate FEM results for a large range of frequencies. The admittance and propagation matrices (*Yc* and *A*) are obtained while also considering

the effect of lossy ground. This technique is then implemented in an EMT type program and the time domain results are validated using NILT method.

- A novel approach is introduced to model cascaded power transmission systems in the frequency domain. The procedure is based on obtaining four composite propagation functions representing the cascaded system. The performance of the technique does not diminish with increased number of cascaded segments as in ABCD parameter method. As this method preserves the intrinsic details of each line segment, it can be used to model cascaded overhead line or cable segments with different characteristic admittances and lengths. It is shown that this model can be used to verify EMT simulations of cascaded transmission lines or underground cables.
- A generalized transmission line model is developed that can accommodate time steps greater than the largest travel time of the line.
    - This model can be used with large time steps in situations when high frequency components are not central to the phenomenon being studied. It is shown that the model accurately captures the low frequency behaviour of the line. If accurate high frequency transients are studied the proposed model can be used with small time steps. If this happens, the model degenerates to the

conventional frequency dependent phase model of the transmission line.

- The present practice requires the use of inaccurate nominal $\pi$ equivalents for large time-step simulations and the detailed frequency dependent model for simulations with high frequency phenomena. The proposed model is highly convenient as the same model can be used for all types of EMT simulations.

## 6.2 Recommendations for Future Research

Some of the proposed approaches in this research can be applied in a broader capacity and therefore, need further investigation. As an extension of this thesis, further research is recommended in the following areas:

- The proposed impedance calculation technique for sector shaped cables can be utilized for other cable types with arbitrarily shaped conductors. The conductors of those cables can be subdivided using elemental sub-conductor technique similar to the procedure detailed in Chapter 3. Then, the frequency dependent impedances can be extracted similar to a sector shaped cable and an EMT model may be developed.
- The proposed frequency domain model in Chapter 4 for cascaded transmission systems can be used to simulate non-uniform transmission lines. A non-homogenous transmission line (e.g. a river

crossing) can be approximated as a cascaded set of homogenous transmission lines. The length of each uniform segment can be varied based on the required accuracy, as the proposed technique can handle cascaded lines of different lengths and parameters. This formation can be readily implemented using the proposed approach.

# Bibliography

[1]. C.R Paul, “Analysis of Multi-conductor Transmission lines,” Wiley Interscience 1994, ISBN 047102080x.

[2]. A. Semlyen and A. Dabuleanu, “Fast and accurate switching transient calculations on transmission lines with ground return using recursive convolutions,” IEEE Trans. Power App. Syst., vol. PAS-94, pp. 561–571, Mar. 1975.

[3]. J. R. Marti, “Accurate modeling of frequency-dependent transmission lines in electromagnetic transient simulations,” IEEE Trans. Power App. Syst., vol. PAS-101, pp. 147–157, Jan. 1982.

[4]. H.V. Nguyen, H.W. Dommel and J.R. Marti, “Direct Phase-Domain Modelling of Frequency-Dependent Overhead Transmission Lines,” IEEE Trans. Power Delivery, Vol. 12, No. 3, pp. 1335–1342, July 1997.

[5]. H.W. Dommel, “Electromagnetic Transients Program (EMTP) Theory Book,” Bonneville Power Administration, Portland, OR, Aug. 1986.

[6]. L.M. Wedepohl and D.J. Wilcox, “Transient pilot-cable induction from underground power-transmission systems,” Proc. IEE, Vol. 126, No 12, December 1979.

[7]. B. Gustavsen and A. Semlyen, “Simulation of transmission line transients using Vector fitting and modal decomposition,” IEEE Trans. Power Delivery, Vol. 13, No 2, pp. 605-614, April 1998.

[8]. A. Ibrahim, S. Henschel, H. Dommel and T. Niimura, "Transmission line model for large step size transient simulations," 1999 IEEE Canadian Conference on Electrical and Computer Engineering, Edmonton, Alberta, Canada, 1999, pp. 1191-1194 vol.2.

[9]. U.S. Gudmundsdottir, C. L. Bak, W. Wiechowski, K. Søgaard and M. R. Knardrupgård, "Measurements for validation of high voltage underground cable modelling,” IPST09 in Kyoto, Japan, paper no. IPST01-15, June 2009.

[10]. S. A. Schelkunoff, “The electromagnetic theory of coaxial transmission line and cylindrical shields,” Bell Syst. Tech. J., vol. 13, pp. 532-579, 1934.

[11]. F. Pollaczek, "Sur le champ produit par un conducteur simple infiniment long parcouru par un courant altematif," Revue Gén. Elec., 29, pp. 851- 867, 1931.

[12]. J.R Carson, “Wave propagation in overhead wires with ground return,” Bell Syst. Tech, Vol 5, pp. 539-554, 1926.

[13]. L. V. Bewley, "Travelling-Waves on Transmission Systems," Wiley, 1951.

[14]. R. Rudenberg, "Transient Performance of Power Systems," McGraw Hill, 1950. (MIT Press, 1969)

[15]. H. W. Dommel, "Digital computer solution of electromagnetic transients in single and multiphase networks," IEEE Trans. Power App. Syst., vol. PAS-88, no. 4, pp.388-399, 1969.

[16]. W. Frey and P. Althammer, "The calculation of electromagnetic transient on lines by means of a digital computer," Brown Boveri Rev., vol. 48, pp. 344, 1961.

[17]. P. E. Lego and T. W. Sze, "A general approach for obtaining transient response by the use of a digital computer," AIEE Trans., vol. 77, Pt. 1. pp. 1031, 1958.

[18]. A. Ametani, "The application of fast Fourier transform to electrical transient phenomena," Inter. J. Elect .Eng. Educ., vol. 10, pp. 277-287, 1972.

[19]. L. M. Wedepohl and A. E. Efthymiadis, "Wave propagation in transmission line over lossy ground-A new complete filed solution," in Proc. Of IEE., vol. 125, no. 6, pp. 505-510, June 1978.

[20]. L. M. Wedepohl and D. J. Wilcox, "Transient analysis of underground power-transmission systems. System-model and wave-propagation characteristics," in Proc. Of IEE, vol. 120, pp. 253-260, Feb. 1973.

[21]. L. Marti, " Simulation of transients in underground cables with frequency dependent modal transformation matrices," IEEE Trans. Power delivery, Vol 03, No 03, pp. 1099 – 1110, July 1998.

[22]. L.M Wedepohl, H.V Nguyen and G.D Irwin, "Frequency Dependent Transformation Matrices for Un-transposed Transmission lines using Newton- Raphson method,", IEEE Trans. Power Systems, Vol 11, No 3, pp. 1538-1546, August 1996.

[23]. B. Gustavsen and A. Semlyen, "Rational approximation of frequency domain responses by vector fitting," IEEE Trans. Power Delivery, vol. 14, no. 3, pp. 1052-1061, July 1999.

[24]. A. Morched, B. Gustavsen and M. Tartibi, "A Universal Model for Accurate Calculation of Electromagnetic Transients on Overhead Lines and Underground cables," IEEE Trans. Power Delivery, Vol 14, No 3, pp. 1032-1038, July 1999.

[25]. D.E. Hedman, "Propagation on Overhead Transmission Lines, I - Theory of Modal Analysis and II – Earth Conduction Effects and Practical Results," IEEE Trans. Power App. and Syst., Vol. 84, No. 3, pp. 200–205, 1965.

[26]. A. Ametani, "A highly efficient method for calculating transmission line transients," IEEE Trans. Power App. and Syst., Vol. PAS-95, No 05, pp. 1545 – 1551, Sept/Oct 1976.

[27]. B. Gustavsen, "Time delay identification for transmission line modeling," Signal Propagation on Interconnects, *2004*. Proceedings. 8th IEEE Workshop, 9-12 May 2004 Page(s): 103 – 106.

[28]. M.Ronald ," Lumped and Distributed Passive networks, A generalized and Advanced Viewpoint," Academic Press, 1969.

[29]. C. Chen , E. Gad, R. Achar, "Passivity Verification in Delay-Based Macromodels of Multi-conductor Electrical Interconnects," IEEE Trans. Circuit and systems, vol. 52, October 2005.

[30]. C. Chen, D. Saraswat, E. Gad, M. Nakhla, R. Achar and M. C. E. Yagoub, "Passivity Enforcement for Method of Characteristics-based Multiconductor Transmission Line Macromodels," 2007 International Symposium on Signals, Systems and Electronics, Montreal, Que., 2007, pp. 25-28.

[31]. A. Chinea, S. Grivet-Talocia, "A Passivity Enforcement Scheme for Delay-Based Transmission Line Macromodels," Microwave and Wireless Components Letters, IEEE Volume 17, Issue 8, Aug. 2007 Page(s):562 – 564.

[32]. H.M.J.S.P. De Silva, "Accuracy and Stability Improvements in Electromagnetic Simulations of Power Transmission Lines and cables," Ph.D. dissertation, Dept. of Elect. & Comp. Eng., University of Manitoba, Canada, 2008.

[33]. S. L. M. Berleze and R. Robert, "Skin and Proximity effects in Nonmagnetic Conductors," IEEE Trans. Education, vol. 46, pp. 368-372, August 2003.

[34]. A. Deri, G. Tevan, A. Semlyen, and A. Castanheira, "The Complex Ground Return Plane: A Simplified Model for Homogeneous and Multi-Layer Earth Return," IEEE Trans. Power App. and Syst., Vol. PAS100, pp. 3686-93, August 1981.

[35]. O. Saad, G. Gaba and M. Giroux, "A Closed-Form Approximation for Ground Return Impedance of Underground Cables," IEEE Trans. Power Delivery, vol. 11, pp. 1536–1545, Jul. 1996.

[36]. G. W. Brown and R. G. Rocamora, "Surge Propagation in Three-Phase Pipe-Type Cables, Part I - Unsaturated Pipe," IEEE Trans. Power App. and Syst., vol. PAS-95, No. 1, pp. 89-95, 1976.

[37]. A. Ametani, "A General Formulation of Impedances and Admittance of Cables," IEEE Trans. Power App. and Syst., vol. PAS-99, No. 3, pp. 902-910, 1980.

[38]. M. Kane, A. Ahmad and P. Auriol, "Multiwire Shielded Cable Parameter Computation," IEEE Trans. Magnetics, vol 31, No. 3, pp. 1646-1649, 1995.

[39]. A. Ametani and K. Fuse, "Approximate method for calculating the impedances of multiconductor cross section of arbitrary shapes," Elect. Eng. Japan, vol. 112, no 2, pp. 117-123, 1992.

[40]. R. Rivas, “Calculation of Frequency-Dependent Parameters of Power Cables with Digital Imaging and Partial Sub-conductors,” Ph.D. dissertation, Dept. of Elect. & Comp. Eng., Univ. British Columbia, July 2001.

[41]. R. A Rivas and J. R. Marti, “Calculation of Frequency-Dependent Parameters of Power Cables: Matrix Partitioning Techniques”, IEEE Trans. Power Delivery, vol. 7, pp. 1085-1092, Oct. 2002.

[42]. Y. Yin, “Calculation of Frequency-Dependent Parameters of Underground Power Cables with Finite Element Method”, Ph.D. dissertation, Dept. of Elect. & Comp. Eng., Univ. British Columbia, September 1990.

[43]. R. Lucas and S. Talukdar, “Advances in finite element techniques for calculating cable resistances and inductances”, IEEE Trans. Power App. and Syst., vol. 3, pp. 875-883, May/June 1978.

[44]. P. de Arizón and H. W. Dommel, “Computation of cable impedances based on subdivision of conductors,” IEEE Trans. Power Delivery, vol. 2, pp. 21–27, Jan. 1987.

[45]. A. Ibrahim, S. Henschel, H. Dommel and T. Niimura, "Transmission line model for large step size transient simulations," 1999 IEEE Canadian Conference on Electrical and Computer Engineering, Edmonton, Alberta, Canada, 1999, pp. 1191-1194 vol.2.

[46]. IEEE Working Group 15.08.09, “Modelling and analysis of system transients using digital programs," IEEE PES Special Publication – 99TP133-0, 1998.

[47]. N. R. Watson and J. Arrillaga, "Power systems electromagnetic transients simulation," Inst. Eng. Technol. Power and Energy, pp.123-124, 2007.

[48]. L.M. Wedepohl and S.E.T. Mohamed, "Transient analysis of multiconductor transmission lines with special reference to nonlinear problems," Proc. IEE, vol. 117, No. 5, Iy'ray 1970.

[49]. R. Nuricumbo-Guillén, P. Gómez, F. P. Espino-Cortés and F. A. Uribe, "Accurate Computation of Transient Profiles Along Multiconductor Transmission Systems by Means of the Numerical Laplace Transform," in IEEE Trans. Power Delivery, vol. 29, no. 5, pp. 2385-2393, Oct. 2014.

[50]. J. S. Savage, W. T. Smith and C. R. Paul, "Moment method calculation of the per-unit-length parameters of cable bundles," IEEE International Symposium on Electromagnetic Compatibility, 1994. Symposium Record. Compatibility in the Loop, Chicago, IL, 1994, pp. 441-446.

[51]. A. Menshov, V. Okhmatovski, H. M. J. S. P. De Silva , K. K. M. A. Kariyawasam, and J. E. Nordstrom, “Modeling of Arbitrary Shaped Cables Using Novel Single Source Integral Equation Formulation,” IPST15 in Cavtat, Croatia, June 2015.

[52]. H. M. J. S. P. De Silva , K. K. M. A. Kariyawasam, A. Gole and J. E. Nordstrom, “Accurate time domain simulation of frequency dependent transmission line models for large timesteps,” IPST13 in Vancouver, Canada, July 2013.

[53]. A.V. Elguera and M.C Tavares, "Influence of Transmission Line Transposition in Electromagnetic Transients Phenomena," in Transmission & Distribution Conference and Exposition: Latin America, 2006. TDC '06. IEEE/PES , vol., no., pp.1-6, 15-18 Aug. 2006

[54]. Cigre Working Group C4.502, "Power System Technical Performance Issues Related to the Application of Long HVAC Cables," in CIGRE Technical Brochure TB556, Oct. 2013

[55]. F. de Leon , M. L. Marques-Asensio and G. Alvarez-Cordero, “Effects of Conductor Counter Transposition on the Positive-Sequence Impedance and Losses of a Cross-bonded Cable,” IEEE Trans. Power Delivery, vol. 26, pp. 2060–2063, No.3, July 2011

[56]. U. S. Gudmundsdottir, B. Gustavsen, C. L. Bak and W. Wiechowski, “Field Test and simulation of a 400-kV Cross-Bonded Cable System”, IEEE Trans. Power Delivery, vol. 26, pp. 1403–1410, No.3, July 2011.

[57]. N. Nagaoka and A Ametani, "Transient Calculations on Crossbonded Cables," IEEE Trans. Power App. and Syst., , vol.PAS-102, no.4, pp.779-787, April 1983.

[58]. A.I. Ramirez, A. Semlyen and R. Iravani, "Modeling nonuniform transmission lines for time domain simulation of electromagnetic transients," IEEE Trans. Power Delivery, vol.18, no.3, pp.968-974, July 2003

[59]. A.R. Chavez, P. Moreno, J.L. Naredo and L. Guardado, "Fast transients analysis of nonuniform multiconductor frequency-dependent transmission lines," IEEE Trans. Power Delivery, vol.21, no.2, pp.809-815, April 2006

[60]. P. de Arisón and H.W. Dommel, “Computation of Cable Impedances Based on Subdivision of Conductors”, IEEE Trans. Power Delivery, vol. PWRD-2, pp. 21-27, Jan. 1987.

[61]. J. Dickinson and P.J. Nicholson, “Calculating the high frequency transmission line parameters of power cables,” ISPCLA ESSEN, Apr. 1997, pp. 127-133.

[62]. S. Habib and B. Kordi, “Calculation of Underground Cables Frequency-Dependent Parameters Using Full-Wave Modal Analysis,” IPST11 in Delft, Netherlands, June 2011.

[63]. A. Morched, B. Gustavsen and M. Tartibi, “A universal model for accurate calculation of electromagnetic transients on overhead lines and underground cables,” IEEE Trans. Power Delivery, vol.14, no.3, pp.1032-1038, Jul 1999.

[64]. IEEE Guide for the Application of Sheath-Bonding Methods for Single Conductor Cables and the Calculation of Induced Voltages and Currents in Cable Sheaths, ANSI/IEEE Std. 575-1988, 1988.

[65]. F. de Leon , M. L. Marques-Asensio and G. Alvarez-Cordero, “Effects of Conductor Counter Transposition on the Positive-Sequence Impedance and Losses of a Cross-bonded Cable,” IEEE Trans. Power Delivery, vol. 26, pp. 2060–2063, No.3, July 2011.

[66]. L.M. Wedepohl and C.S. Indulkar, "Switching Overvoltages in Long Crossbonded Cable Systems Using the Fourier Transform," IEEE Trans. Power App. and Syst., vol.PAS-98, no.4, pp.1476-1480, July 1979

[67]. N. Nagaoka and A Ametani, "Transient Calculations on Crossbonded Cables," IEEE Trans. Power App. and Syst., vol.PAS-102, no.4, pp.779-787, April 1983.

[68]. Yajurveda, "Katha Upanishad", 800 BCE, India.

[69]. Apostle Matthew, Holy Bible, New Testament, *Matthew 15:13-1, circa 80 AD,* Judea

[70]. N.J Higham, "*Functions of matrices: theory and computation"*, Siam, 2008.

[71]. L. Marti, "Simulation of transients in underground cables with frequency-dependent modal transformation matrices," IEEE Trans. Power Delivery, vol.3, no.3, pp.1099-1110, Jul 1988.

[72]. K. K. M. A. Kariyawasam, A. Gole, B. Kordi, and H. M. J. S. P. De Silva, “Accurate Electro-magnetic Transient Modelling of sector shaped cables” IPST11 in Delft, Netherlands, June 2011.

# Appendix A

Cable impedances and admittances

As original equations for cable impedances include Bessel functions and non-analytical integral terms which are numerically inefficient to calculate, the following simplified, yet accurate formulae are commonly used in coaxial power cable calculations.

(1) Internal impedance of solid conductor

The internal impedance of the inner solid conductor is expressed as a division of two modified Bessel functions of the first kind.

$$Z_{\text{int}} = \frac{m\rho I_0(mr)}{2\pi r I_1(mr)}$$

Where,

$m = \sqrt{\frac{j\omega\mu}{\rho}}$, $d_e = \sqrt{\frac{\rho_e}{j\omega\mu_e}}$

$\rho$ is the conductor resistivity and $\mu$ is the conductor permitivity

$\rho_e$ is the ground resistivity and $\mu_e$ is the ground permitivity

$(x_i, y_i)$ and $(x_j, y_j)$ are coordinates of $i^{th}$ and $j^{th}$ conductors

$r$ – radius of the conductor

$d_{ij}$ – distance between conductors

$\omega$ – angular frequency

In the standard notation, $I_n(Z)$ represents the first kind modified Bessel function with order "n" and argument "Z". Similarly, in the text to follow, $K_n(Z)$ denotes the second kind modified Bessel function with order "n" and

argument "Z". The approximation formula for conductor internal impedance $(\Omega/m)$ is given by,

$$Z_{conductor}(\omega) = \frac{\rho m \coth(0.777mr)}{2\pi r} + \frac{0.3565\rho}{\pi r^2}$$

(2) Impedance due to the time varying magnetic field in the i$^{th}$ insulation layer,

$$Z_{insulator}(\omega) = \frac{j\omega\mu_i}{2\pi}\log_e\left(\frac{r_{i+1}}{r_i}\right)$$

Where, for the i$^{th}$ insulation layer

$\mu_i$ = magnetic permeability (H/m).
$r_i$ = inner radius (m) .
$r_{i+1}$ = outer radius (m).

(3) Inner sheath internal impedance

$$Z_{inner\_sheath}(\omega) = \frac{\rho m}{2\pi r_i D}\left[I_0(mr_i)K_1(mr_{i+1}) + K_0(mr_i)I_1(mr_{i+1})\right]$$

Where, for the i$^{th}$ cylindrical sheath

$D$ = $I_1(mr_{i+1})K_1(mr_i) - I_1(mr_i)K_1(mr_{i+1})$
$\rho$ = resistivity of the sheath $(\Omega.\mathrm{m})$
$r_i$ = inner radius $(\mathrm{m})$
$r_{i+1}$ = outer radius $(\mathrm{m})$

The approximate formula developed for inner sheath impedance [15] is,

$$Z_{inner\_sheath}(\omega) = \frac{\rho m}{2\pi r_i}\coth(m\Delta) - \frac{\rho}{2\pi r_i(r_i + r_{i+1})}$$

Where,

$$\Delta = r_{i+1} - r_i$$

(4) Sheath mutual impedance

This impedance is equal to the voltage drop outer surface of the sheath per unit current returning through the inner conductor or vice versa. The exact Bessel function solution and the approximate formula for the sheath mutual impedance are,

$$Z_{sheath\_mutual}(\omega) = \frac{\rho}{2\pi r_i r_{i+1} D}$$

$$Z_{sheath\_mutual}(\omega) = \frac{\rho m}{\pi(r_i + r_{r+1})}\mathrm{cosech}(m\Delta)$$

(5) Outer sheath impedance

This is given as the voltage drop along the outer surface of the sheath as the current returns through the outer conductor. The Bessel function solution and the approximate formula are given by,

$$Z_{outer\_sheath}(\omega) = \frac{\rho m}{2\pi r_{i+1} D}\left[I_0(mr_{i+1})K_1(mr_i) + K_0(mr_{i+1})I_1(mr_i)\right]$$

$$Z_{outer\_sheath}(\omega)=\frac{\rho m}{2\pi r_{i+1}}\coth(m\Delta)+\frac{\rho}{2\pi r_{i+1}(r_i+r_{i+1})}$$

(6) The admittance per unit length between two conducting layers,

$$y_i(\omega)=G_i+\frac{2\pi\varepsilon_i\omega j}{\log_e\left(\frac{r_{i+1}}{r_i}\right)}$$

Where, for the i[th] insulation layer,

$G_i$ = conductivity (S)
$\varepsilon_i$ = permittivity (F/m)
$r_{i+1}$ = outer radius (m)
$r_i$ = inner radius (m)

(7) Mutual earth-return impedance

The mutual earth return impedance between cables i and k is,

$$Z_{earth\_mutual}(\omega)=\frac{\rho m^2}{2\pi}\left[K_0(md)-K_0(mD)+\int_{-\infty}^{\infty}\frac{\exp\left(-(y_1+y_2)\sqrt{\alpha^2+m^2}\right)}{|\alpha|+\sqrt{\alpha^2+m^2}}\exp(j\alpha x)\,d\alpha\right]$$

Where,

$x$ = horizontal distance between cable i and k (m)
$y_i, y_k$ = buried depths of cable i and k respectively (m)
d = direct distance between cables i and k (m)
$=\sqrt{x^2+(y_i-y_k)^2}$
$D$ = distance between cable i and image of cable k (m)
$=\sqrt{x^2+(y_i+y_k)^2}$
$\rho$ = resistivity of earth $(\Omega.m)$
$\mu$ = permeability of earth $(H/m)$
m = reciprocal of complex depth of penitration
$=\sqrt{\frac{j\omega\mu}{\rho}}$

The direct evaluation of the above formula requires computation of Bessel functions using standard methods and the integral term using a numerical technique. A corresponding approximate formula for mutual earth return impedance developed by Wedepohl and Wilcox is,

$$Z_{earth\_mutual}(\omega) = \frac{j\omega\mu}{2\pi}\left[-\log_e\left(\frac{\gamma md}{2}\right) + 0.5 - \frac{2mL}{3}\right]$$

Where,

$\gamma$ = Euler's constant

L = $y_k + y_i$

d = direct distance between cables i and k (m)

Another useful approximate formula developed by Saad, Caba and Ciroax is,

$$Z_{earth\_mutual}(\omega) = \frac{\rho m^2}{2\pi}\left[K_0(md) + \frac{2e^{-(y_i+y_k)m}}{4+m^2x^2}\right]$$

*where,*

$x$ = *h*orizontal distance between cable i and k (m)

The self earth return impedance can be easily derived by substituting $y_k = y_i$ and $x = r$ $(outer\ radius\ of\ cable)$ in the above mutual impedance formulae.

# Appendix B

Calculation of distance $r_1$ for conductor subdivision

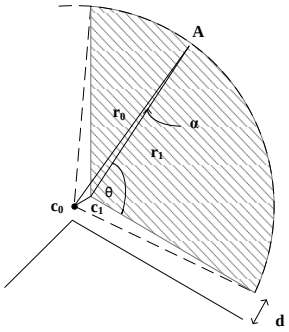


**Figure B- 1 - Conductor shape and geometry of a sector-shaped cable**

Here, we consider finding $r_1$ shown in Figure B- 1 using the known values of $r_0$, d and θ.

a) For $\theta \neq 60^0$

In this case, points A, $C_0$ and $C_1$ form a triangle. Lets denote $C_0\hat{A}C_1$ angle to be $\alpha$.

$$C_0C_1 = \frac{d}{2}\cos\left(30^0\right), \quad \text{as each sector is } 120^0$$

Then, by applying sine law to $C_0AC_1$,

$$\frac{\frac{d}{2}\cos\left(30^0\right)}{\sin(\alpha)} = \frac{r_0}{\sin(120^0+\theta)} = \frac{r_1}{\sin(60^0-\theta-\alpha)} \qquad \text{(B.1)}$$

By solving for α,

$$\alpha = \sin^{-1}\left[\frac{\frac{d}{2}\cos\left(30^0\right)}{r_0}\sin\left(120^0+\theta\right)\right] \tag{B.2}$$

b) For $\theta=60^0$

In this case, points A, $C_0$ and $C_1$ become collinear. Therefore,

$$r_1 = r_0 - C_0C_1 \Rightarrow r_1 = r_0 - \frac{d}{2}\cos\left(30^0\right)$$

Therefore,

$$r_1 = \begin{cases} \dfrac{r_0}{\sin\left(120^0+\theta\right)}\sin\left(60^0-\theta-\alpha\right), \; for\,\theta \neq 60^0 \\ \\ r_0 - \dfrac{d}{2}\cos\left(30^0\right), \; for\,\theta = 60^0 \end{cases} \tag{B.3}$$

# Appendix C

Fast reduction of impedance matrix [43]

Here we consider the problem of reducing the sub-conductor impedance matrix given in equation 3-7 to the conductor impedance matrix given in equation 3-10. The sub-conductor impedance matrix can be written as follows:

$$\begin{bmatrix} \bar{V}^{(1,k-1)} \\ \bar{V}^{(k)} \end{bmatrix} = \begin{bmatrix} Z_{11} & Z_{12} \\ Z_{21} & Z_{22} \end{bmatrix} \cdot \begin{bmatrix} \bar{I}^{(1,k-1)} \\ \bar{I}^{(k)} \end{bmatrix} \qquad \text{(C.1)}$$

Where, $V^{(1,k-1)}$ and $I^{(1,k-1)}$ are the voltage and current vectors of all the sub-conductors in the first *k-1* conductors. $V^{(k)}$ and $I^{(k)}$ are the voltage and current vectors of all the sub-conductors in the last $(k^{th})$ conductor. From equation (C.1),

It can be written,

$$\bar{I}^{(k)} = Z_{22}^{-1} \cdot \left[ \bar{V}^{(k)} - Z_{21} \cdot \bar{I}^{(1,k-1)} \right] \qquad \text{(C.2)}$$

The total current in the $k^{th}$ conductor, $i^{(k)}$ is the summation of all sub-conductor currents in that conductor. Therefore,

$$i^{(k)} = U \cdot \bar{I}^{(k)} \qquad \text{(C.3)}$$

Where, U is a row matrix of size, *1xp*. *p* is the number of sub-conductors in the $k^{th}$ conductor. Similarly, the voltages in all sub-conductor of the $k^{th}$ conductor is equal to the voltage of the $k^{th}$ conductor, $v^{(k)}$,

$$\bar{V}^{(k)} = U^T \cdot v^{(k)} \qquad \text{(C.4)}$$

Where $U^T$ is the transpose of U. Combining (C.2), (C.3) and (C.4) gives,

$$i^{(k)} = U \cdot Z_{22}^{-1} \cdot \left[ U^T \cdot v^{(k)} - Z_{21} \cdot \bar{I}^{(1,k-1)} \right] \qquad \text{(C.5)}$$

By rearranging this,

$$v^{(k)} = \frac{U \cdot Z_{22}^{-1} \cdot Z_{21}}{U \cdot Z_{22}^{-1} \cdot U^T} \cdot \bar{I}^{(1,k-1)} + \frac{i^{(k)}}{U \cdot Z_{22}^{-1} \cdot U^T} \qquad \text{(C.6)}$$

Similarly, first row of (E.1) and (E.5) can be combined as,

$$\bar{V}^{(1,k-1)} = Z_{11} \cdot \bar{I}^{(1,k-1)} + Z_{12} \cdot \left\{ Z_{22}^{-1} \cdot \left[ U^T \cdot v^{(k)} - Z_{21} \cdot \bar{I}^{(1,k-1)} \right] \right\}$$

$v^{(k)}$,is substituted by (C.6),

$$\bar{V}^{(1,k-1)} = Z_{11} \cdot \bar{I}^{(1,k-1)} + Z_{12} \cdot Z_{22}^{-1} \cdot U^T \cdot \left[ \frac{U \cdot Z_{22}^{-1} \cdot Z_{21}}{U \cdot Z_{22}^{-1} \cdot U^T} \cdot \bar{I}^{(1,k-1)} + \frac{i^{(k)}}{U \cdot Z_{22}^{-1} \cdot U^T} \right] - Z_{12} \cdot Z_{22}^{-1} \cdot Z_{21} \cdot \bar{I}^{(1,k-1)}$$

By rearranging,

$$\bar{V}^{(1,k-1)} = \left[ Z_{11} + Z_{12} \cdot Z_{22}^{-1} \cdot U^T \cdot \frac{U \cdot Z_{22}^{-1} \cdot Z_{21}}{U \cdot Z_{22}^{-1} \cdot U^T} - Z_{12} \cdot Z_{22}^{-1} \cdot Z_{21} \right] \cdot \bar{I}^{(1,k-1)} + \frac{Z_{12} \cdot Z_{22}^{-1} \cdot U^T}{U \cdot Z_{22}^{-1} \cdot U^T} \cdot i^{(k)} \qquad \text{(C.7)}$$

(C.6) and (C.7) can be written in matrix form,

$$\begin{bmatrix} \bar{V}^{(1,k-1)} \\ v^{(k)} \end{bmatrix} = \begin{bmatrix} z_{11} & z_{12} \\ z_{21} & z_{22} \end{bmatrix} \cdot \begin{bmatrix} \bar{I}^{(1,k-1)} \\ i^{(k)} \end{bmatrix} \qquad \text{(C.8)}$$

Where,

$$z_{11} = \left[ Z_{11} + Z_{12} \cdot Z_{22}^{-1} \cdot U^T \cdot \frac{U \cdot Z_{22}^{-1} \cdot Z_{21}}{U \cdot Z_{22}^{-1} \cdot U^T} - Z_{12} \cdot Z_{22}^{-1} \cdot Z_{21} \right]$$

$$z_{12} = \frac{Z_{12} \cdot Z_{22}^{-1} \cdot U^T}{U \cdot Z_{22}^{-1} \cdot U^T}$$

$$z_{21} = \frac{U \cdot Z_{22}^{-1} \cdot Z_{21}}{U \cdot Z_{22}^{-1} \cdot U^T} \quad \textit{and}$$

$$z_{22} = \frac{1}{U \cdot Z_{22}^{-1} \cdot U^T}$$

It can be seen that all sub-conductors in the $k^{th}$ conductor are reduced to a single conductor. This procedure can be repeated for all conductors to achieve a reduced matrix of the form given in equation 3-10.

# Appendix D

Single line-to-ground fault example – generalized model

The same cable geometry shown in Chapter 5, Figure 5-6 is used to simulate a single line-to-ground fault. Following termination shown in Figure (a) is modelled with the generalized model to emphasize applicability of the model to switching transient studies.

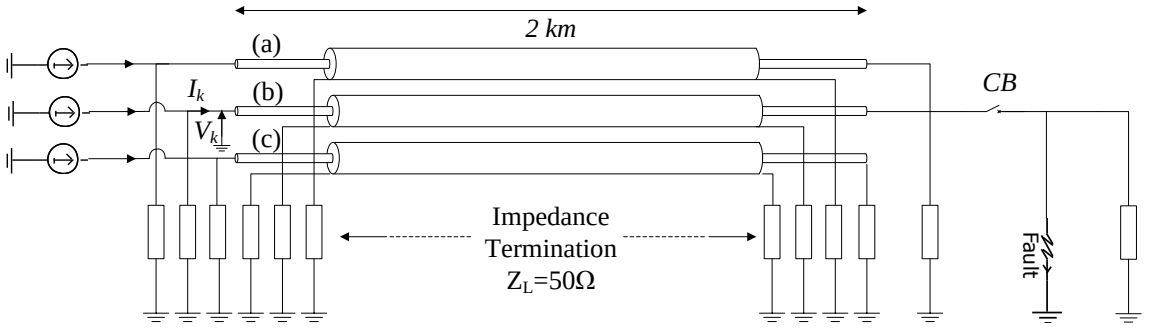


**Figure (a) –Cable configuration for single-line-to-ground fault**

Inner conductors of all 3 phases are energized with a 60 Hz sinusoidal current. A single line-to-ground fault is applied to inner conductor of phase 'b' at 0.1s. The fault is cleared by opening the circuit breaker, CB at 0.15s and the circuit breaker is closed back at 0.21s. Time domain simulations are carried out using the generalized model with the time-steps of 2.5 μs, 20 μs and 200 μs. The sending-end current and voltage in the inner conductor of

phase 'b' are compared with the conventional EMT results in Figure (b) and Figure (c).

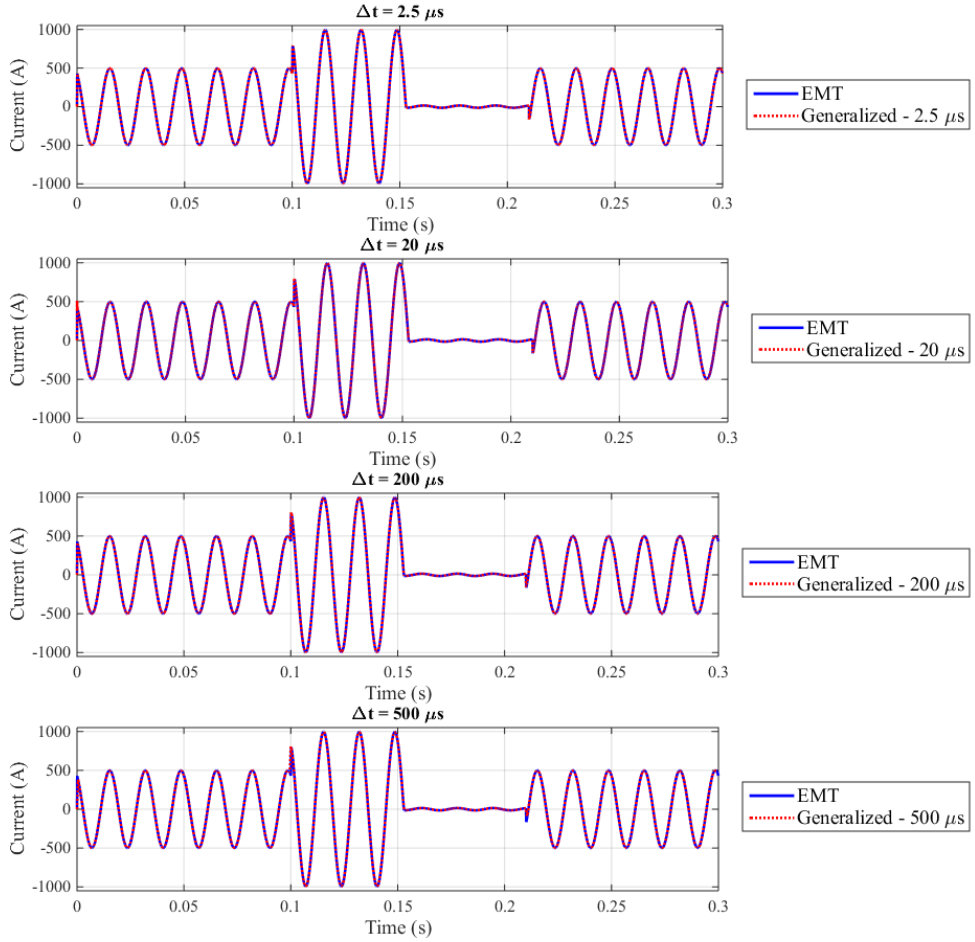


**Figure (b) – Sending-end current comparison, phase 'b' – at different time steps**

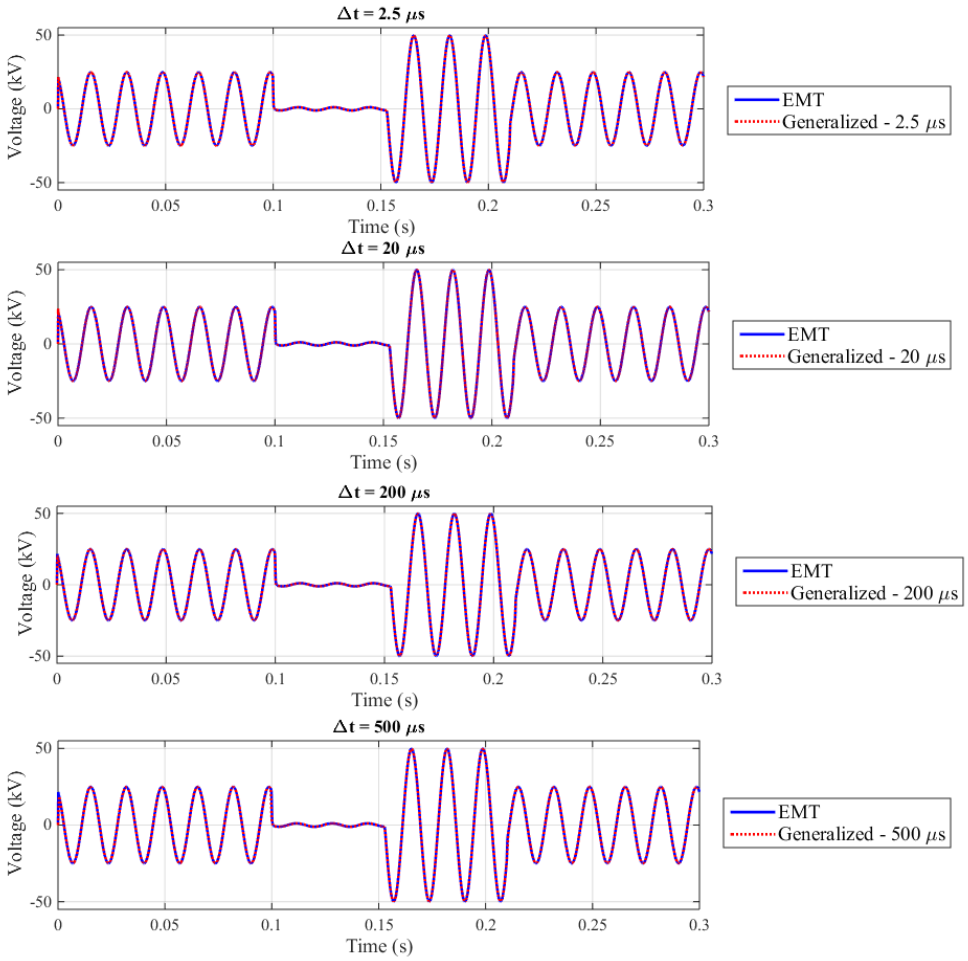


**Figure (c) – Sending-end voltage comparison, phase 'b' – at different time steps**

Results from the generalized time independent model agrees well with the EMT results. This is to be expected as the model shows high accuracy at the low frequency transients observed in fault studies.

# Appendix E

Numerical inverse Laplace transform [48], [49]

A common technique in transforming a known frequency domain function into time domain and vice versa is the Laplace transform method. The Laplace transform and the inverse Laplace transform can be given as follows:

$$H(s)=\int_0^{\infty} h(t)\cdot e^{-st}dt \tag{E.1}$$

$$h(t)=\frac{1}{2\pi j}\int_{c-\infty}^{c+\infty} H(s)\cdot e^{st}ds \tag{E.2}$$

Where, $s=c+j\omega$, is the complex frequency. $H(s)$and $h(t)$ are the frequency domain function and the time domain counterpart. The constant term $c$ is added to the frequency term to ensure that $h(t)$ tends to zero as time tends to infinity. If $H(s)$is available only in discrete form, at a set of frequency samples, numerical methods are used to evaluate the inverse Laplace transform.

When a finite set of frequency samples are available, the upper limit for integration in (E.2) is limited to some $\omega=\Omega$ instead of infinity. With this, inverse Laplace transform can be written as:

$$h(t)=\frac{e^{-ct}}{2\pi}\int_{-\Omega}^{\Omega}H(c+j\omega)\cdot e^{j\omega t}d\omega \qquad \text{(E.3)}$$

This truncation can introduce significant errors and causes oscillations in the time domain solution with an oscillation frequency of $f_g=2\pi/\Omega$, called Gibb's oscillations. This issue can be effectively avoided by using a modified Lanczos filter as follows:

$$h(t)=\frac{e^{-ct}}{2\pi}\int_{-\Omega}^{\Omega}g\cdot H(c+j\omega)\cdot e^{j\omega t}d\omega \qquad \text{(E.4)}$$

Where the modified Lanczos filter is given by,

$$g(\omega)=\frac{\sin\left(\frac{\pi\omega}{\Omega}\right)}{\frac{\pi\omega}{\Omega}}\cdot e^{-\frac{j\pi\omega}{\Omega}}$$

In the numerical evaluation of the integral in (E.4), a finite constant frequency step has to be used between two frequency samples. If the frequecy step is $f_s$ then the time domain solution, $h(t)$ is valid for a period $[0,T]$ where $T$ is called the time of validity. $T$ is given by, $T=\frac{1}{f_0}$.